

THESIS

SNOWMELT RUNOFF ANALYSIS AND MODELING FOR THE UPPER CACHE
LA POUVRE RIVER BASIN, COLORADO

Submitted by

Eric E. Richer

Department of Forest, Rangeland, and Watershed Stewardship

In partial fulfillment of the requirements

For the Degree of Master of Science

Colorado State University

Fort Collins, Colorado

Fall 2009

COLORADO STATE UNIVERSITY

July 27, 2009

WE HEREBY RECOMMEND THAT THE THESIS PREPARED UNDER OUR SUPERVISION BY ERIC E. RICHER ENTITLED SNOWMELT RUNOFF ANALYSIS AND MODELING FOR THE UPPER CACHE LA POUFRE RIVER BASIN, COLORADO BE ACCEPTED AS FULFILING IN PART THE REQUIREMENTS FOR THE DEGREE OF MASTER OF SCIENCE.

Committee on Graduate Work

[Redacted Signature]

Dr. Mazdak Arabi

[Redacted Signature]

Dr. Steven Fassnacht

[Redacted Signature]

Advisor Dr. Stephanie Kampf

[Redacted Signature]

Department Head Dr. Mike Manfredo

ABSTRACT OF THESIS

SNOWMELT RUNOFF ANALYSIS AND MODELING FOR THE UPPER CACHE LA POUUDRE RIVER BASIN, COLORADO

The Cache la Poudre River is a vital water source in Northern Colorado, and it exhibits high variability in annual water yield. This research examines sources of variability in snowmelt runoff as a means of identifying methods that could help improve streamflow prediction for the basin. The objectives of this thesis are to: (1) develop a naturalized flow record for the river and determine the effects of flow modification on the magnitude and timing of discharge; (2) analyze relationships between snow cover distributions and naturalized discharge to identify important areas for runoff production; and (3) evaluate the ability of the Snowmelt Runoff Model (SRM) to simulate seasonal hydrographs. Naturalized flow records were developed by accounting for all diversions from the river, inputs of foreign water via trans-basin diversions, and reservoir operations. Moderate Resolution Imaging Spectroradiometer (MODIS) 8-day snow cover products were obtained for the snowmelt season, mid-March through June, from 2000-2006. Snow cover depletion was analyzed within spatial subsets of sub-basins and elevation zones, and regression analyses were used to compare snow covered area (SCA) to naturalized discharge (Q). To investigate spatial and temporal snow distribution trends, probability of snow cover datasets were derived, which show the frequency of snow cover for different parts of the basin. Using these SCA data, the SRM was then configured to simulate snowmelt runoff hydrographs for the basin using both optimized

and standard sets of model parameters. Daily hydrographs were simulated from March 1 to September 30 for each year in the 2000-2006 study period.

Results show that flow modification delayed hydrograph timing and reduced water yields for all years included in the study period. The naturalized hydrograph displayed a wide range of relationships to SCA depletion patterns in the basin. At low and high elevations in the basin, SCA patterns had poor relationships to naturalized discharge. Snow cover depletion in middle elevations, however, had a much stronger relationship to discharge, with steady snow cover depletion occurring in these areas during hydrograph rise. Snow cover analyses point to strong elevation dependence in runoff generation, with most runoff coming from a small area in the basin above a mid-elevation snow cover transition zone. Snow cover data prove useful for configuring snowmelt runoff simulations, and the SRM simulated seasonal hydrographs with good model performance (Nash-Sutcliffe coefficient of efficiency > 0.9) when calibrated to the naturalized hydrographs for individual years. This suggests that the SRM could be used to generate seasonal streamflow forecasts given appropriate selection of parameter values and input variables. These conclusions all point to the utility of long-term snow cover datasets for improved water resources planning and management in snowmelt dominated mountain basins.

Eric E. Richer
Department of Forest, Rangeland, and Watershed Stewardship
Colorado State University
Fort Collins, CO 80523
Fall 2009

ACKNOWLEDGEMENTS

This project was funded by the Colorado Water Institute with additional contributions from the Cache la Poudre Water Users Association. I acknowledge the support and helpful contributions of Andy Pineda and Katie Melander of Northern Colorado Water Conservancy District; Tom Perkins and Mike Gillespie of the Natural Resources Conservation Service; and George Varra and Mark Simpson of the Colorado Division of Water Resources. I would also like to acknowledge my advisor, Stephanie Kampf, as well as committee members, Steven Fassnacht and Mazdak Arabi, who provided invaluable direction and insight. Special appreciation goes to the National Snow and Ice Data Center for providing public domain snow cover images, as well as Jaroslav Martinec and Albert Rango for development of the open source Snowmelt Runoff Model (SRM).

TABLE OF CONTENTS

| | |
|---|------|
| LIST OF FIGURES..... | viii |
| LIST OF TABLES..... | xi |
| LIST OF ABBREVIATIONS..... | xii |
| CHAPTER 1: INTRODUCTION AND BACKGROUND..... | 1 |
| 1.1 MOTIVATION AND OBJECTIVES..... | 1 |
| 1.2 SITE DESCRIPTION..... | 4 |
| CHAPTER 2: FLOW MODIFICATION..... | 9 |
| 2.1 INTRODUCTION..... | 9 |
| 2.2 METHODS..... | 10 |
| 2.3 RESULTS..... | 12 |
| 2.4 DISCUSSION..... | 19 |
| 2.5 CONCLUSIONS..... | 22 |
| CHAPTER 3: RELATIONSHIPS BETWEEN SNOW COVER AND RUNOFF..... | 23 |
| 3.1 INTRODUCTION..... | 23 |
| 3.2 METHODS..... | 25 |
| 3.2.1 <i>Snow Covered Area Analyses</i> | 25 |
| 3.2.2 <i>Probability of Snow</i> | 29 |
| 3.3 RESULTS..... | 30 |
| 3.4 DISCUSSION..... | 40 |
| 3.5 CONCLUSIONS..... | 44 |
| CHAPTER 4: SNOWMELT RUNOFF MODEL..... | 45 |
| 4.1 INTRODUCTION..... | 45 |
| 4.1.1 <i>Snowmelt Runoff Modeling</i> | 45 |
| 4.1.2 <i>Model Configuration</i> | 48 |
| 4.2 METHODS..... | 50 |
| 4.2.1 <i>Data Processing and Preparation</i> | 50 |
| 4.2.2 <i>Model Parameterization and Calibration</i> | 53 |
| 4.2.3 <i>Model Evaluation</i> | 58 |
| 4.3 RESULTS..... | 58 |
| 4.4 DISCUSSION..... | 61 |
| 4.5 CONCLUSIONS..... | 66 |
| CHAPTER 5: CONCLUSIONS..... | 68 |
| REFERENCES..... | 72 |

| | |
|--|-----|
| APPENDIX A: HYDROLOGIC DATASET..... | 76 |
| APPENDIX B: FLOW MODIFICATION..... | 84 |
| APPENDIX C: SNOW COVERED AREA..... | 99 |
| APPENDIX D: SNOWMELT RUNOFF MODEL..... | 110 |

LIST OF FIGURES

| | |
|---|----|
| Figure 1.1. Naturalized annual water yield and NRCS May forecast error for the Cache la Poudre River at Canyon Mouth: WY 1951-2007..... | 3 |
| Figure 1.2. Location map for Cache la Poudre watershed with hydrometric and meteorological measurement locations, including the forecasting location at the Canyon Mouth..... | 5 |
| Figure 1.3. PRISM derived average annual precipitation and temperature versus elevation within the Cache la Poudre basin above the Canyon Mouth: 1971-2000..... | 6 |
| Figure 1.4. Average monthly precipitation and temperature for the Cache la Poudre basin: 1971-2000..... | 7 |
| Figure 2.1. Observed, natural, and 7-day average natural discharge (Q) for Cache la Poudre River at Canyon Mouth: WY 2000..... | 11 |
| Figure 2.2. Observed and naturalized annual water yields (million m ³) for Cache la Poudre River at Canyon Mouth: WY 2000-2006..... | 13 |
| Figure 2.3. Observed and naturalized water yields (million m ³) for the snowmelt season from May through September 30 for the Cache la Poudre River at Canyon Mouth: WY 2000-2006..... | 13 |
| Figure 2.4. Annual effects of flow modification by type showing total volume (million m ³) of water diverted into (+) and out of (-) the Cache la Poudre River above the Canyon Mouth: WY 2000-2006..... | 15 |
| Figure 2.5. Seasonal (May 1 to September 30) effects of flow modification by type showing total volume (million m ³) of water diverted into (+) and out of (-) the Cache la Poudre River above the Canyon Mouth: WY 2000-2006..... | 15 |
| Figure 2.6. Average monthly totals (million m ³) for flow modification above the Canyon Mouth: WY 2000-2006..... | 17 |

| | |
|---|----|
| Figure 2.7. Naturalized and observed (a) hydrographs and (b) cumulative discharge curves showing timing of Q20, Q50, and Q80 for the Cache la Poudre River at the Canyon Mouth: WY 2001..... | 18 |
| Figure 2.8. Timing of Q20, Qpeak, Q50, and Q80 for observed and naturalized hydrographs at the Canyon Mouth from WY 2000-2006..... | 19 |
| Figure 2.9. Average timing and magnitude of flow modifications above the Canyon Mouth over the study period from WY 2000-2006..... | 20 |
| Figure 3.1. Sub-basin network and elevation zones used in analyses of SCA above the Canyon Mouth..... | 27 |
| Figure 3.2. Variability in (a) snow water equivalent (SWE) at the Joe Wright SNOTEL site (elevation 3085 m), (b) naturalized discharge for the Cache la Poudre River at the Canyon Mouth gauge, and (c) basin-wide snow covered area (SCA) depletion during the snowmelt season for 2000-2006..... | 31 |
| Figure 3.3. Examples of SCA vs. Q regression for the (a) Little South Fork sub-basin and (b) middle elevation band during the snowmelt season of 2006..... | 33 |
| Figure 3.4. Correlation strength (R^2) of the SCA vs. Q relationships during the snowmelt season for the entire basin and sub-basin network above the Canyon Mouth gauge, 2000-2006..... | 34 |
| Figure 3.5. Correlation strength (R^2) of the SCA vs. Q relationships during the snowmelt season for elevation zones above the Canyon Mouth gauge, 2000-2006..... | 34 |
| Figure 3.6. Average probability of snow during snowmelt season for elevation zones: 2000-2006..... | 36 |
| Figure 3.7. Probability of snow time series derived from MODIS 8-day images showing snow depletion for the Cache la Poudre basin during the snowmelt season. For each date, probabilities are calculated using images from 2000-2006..... | 37 |
| Figure 3.8. (a) Probability of snow time series for elevation zones derived from 8-day MODIS images, 2000-2006. (b) Average discharge at the Canyon Mouth gauge and average snow water equivalent (SWE) at the Joe Wright SNOTEL site (elevation 3085 m) for 2000-2006..... | 39 |
| Figure 4.1. Location of elevation zones and meteorological stations used in configuration of the SRM for the Cache la Poudre basin..... | 51 |

Figure 4.2. Degree-day factors (α) used in all trials of the SRM for the Cache la Poudre basin above the Canyon Mouth.....55

Figure 4.3. Envelope line used to obtain initial estimates of x and y -values to determine recession coefficient for the 2000 snowmelt season.....56

Figure 4.4. Range of optimized runoff coefficient values from the initial model trial for 2000-2006 simulations and median values used in the second model trial.....60

Figure 4.5. Optimized recession coefficients (k) used in the first model trial.....60

Figure 4.6. Comparison of observed and simulated hydrographs at the Canyon Mouth for the two model trials during the 2002 snowmelt season.....64

Figure 4.7. Comparison of observed and simulated hydrographs at the Canyon Mouth for the two model trials during the 2005 snowmelt season.....65

LIST OF TABLES

| | |
|---|----|
| Table 2.1. Number of flow modification structures above the Canyon Mouth by type... | 11 |
| Table 2.2. Annual summary statistics for daily observed (Obs) and naturalized (Nat) flow regimes (in m^3s^{-1}) at the Canyon Mouth: WY 2000-2006..... | 14 |
| Table 2.3. May-September summary statistics for daily observed (Obs) and naturalized (Nat) flow regimes (in m^3s^{-1}) at the Canyon Mouth: WY 2000-2006..... | 14 |
| Table 3.1. Elevation range and area for sub-basins within the Cache la Poudre watershed above the Canyon Mouth..... | 27 |
| Table 3.2. Elevation range and area for the seven elevation zones within the Cache la Poudre watershed above the Canyon Mouth..... | 28 |
| Table 4.1. Parameters of the SRM..... | 49 |
| Table 4.2. Elevation range and area for the seven elevation zones used in configuration of the SRM for the Cache la Poudre watershed above the Canyon Mouth..... | 51 |
| Table 4.3. Meteorological stations with daily temperature and precipitation data located within the Cache la Poudre basin used in application of the SRM..... | 52 |
| Table 4.4. Nash-Sutcliffe coefficient of efficiency (NSCE) and percentage difference (D_v) for initial model trials where runoff and recession coefficients were optimized for each year..... | 59 |
| Table 4.5. Values of x and y used to calculate recession coefficients for each year during the initial model trial and resultant median values used in the second model trial..... | 59 |
| Table 4.6. Nash-Sutcliffe coefficient of efficiency (NSCE) and percentage difference (D_v) for secondary model trials using median runoff and recession coefficients from the initial trial..... | 61 |

LIST OF ABBREVIATIONS

CDWR: Colorado Division of Water Resources

CLAFTCO: Cache la Poudre River at Canyon Mouth near Fort Collins, Colorado

COOP: Cooperative Observers

CT: Center of Timing

DEM: Digital Elevation Model

D_v: Percentage Difference

GIS: Geographic Information System

GRG2: Generalized Reduced Gradient

MODIS: Moderate Resolution Imaging Spectroradiometer

NCDC: National Climatic Data Center

NCWCD: Northern Colorado Water Conservancy District

NDSI: Normalized Difference Snow Index

NLCD: National Land Cover Dataset

NOHRSC: National Operational Hydrologic Remote Sensing Center

NRCS: National Resources Conservation Service

NSCE: Nash-Sutcliffe Coefficient of Efficiency

NSIDC: National Snow and Ice Data Center

PRISM: Parameter-elevation Regressions on Independent Slopes Model

Q: Discharge

Q20: 20th percentile on cumulative discharge curve

Q50: 50th percentile on cumulative discharge curve

Q80: 80th percentile on cumulative discharge curve

Qpeak: Maximum daily discharge for a given WY

R²: Coefficient of Determination

RCA: Rainfall Contributing Area

SCA: Snow Covered Area

SNOTEL: Snow Telemetry

SRM: Snowmelt Runoff Model

SSM/I: Special Sensor Microwave/Imager

SWE: Snow Water Equivalent

T_{CRIT}: Critical Temperature

U.S.: United States

USGS: United States Geological Survey

WY: Water Year

CHAPTER 1: INTRODUCTION AND BACKGROUND

1.1 MOTIVATION AND OBJECTIVES

The mountain snowpack in Western North America is key component of the hydrologic cycle, storing winter precipitation that is then released during the spring and summer, when economic, environmental, and recreation water demands are greatest (Ferguson, 1999; Mote et al., 2005; Knowles et al., 2006; Rood et al., 2008). Mountain snowpack and snowmelt are important components and predictors of streamflow and account for 50-80% of the total annual runoff for snowmelt dominated basins (Doesken and Judson, 1996; Stewart et al., 2004). Snow provides the largest component of water storage for most of the Western U.S., making the region vulnerable to the effects of climate variability and warming on snowpack accumulation and melt (Mote et al., 2005). Over the past several decades, climate and streamflow data throughout the mountainous Western U.S. have shown trends of increasing winter minimum temperatures (Knowles et al., 2006; Stewart, 2009), decreasing fractions of snowfall relative to total precipitation (Knowles et al., 2006), decreased spring snow cover and snow depth (Mote et al., 2005; Stewart, 2009), earlier snowmelt runoff (Stewart et al., 2005; Regonda et al., 2005; Rood et al., 2008), and decreasing summer flows (Rood et al., 2008). Changes in snowmelt runoff have been attributed to increased winter and spring temperatures, which cause more precipitation to fall as rain instead of snow, and induce earlier snowmelt runoff (Knowles et al., 2006). However, local runoff responses to these generalized climate

trends are variable, due to possible combinations of geographic location, latitude, elevation, and atmospheric circulation patterns (Stewart, 2009).

The Cache la Poudre River in Northern Colorado is a snowmelt dominated system that is a vital water source for agricultural, municipal, and industrial users in the region. The river has been utilized as a water source since settlers first arrived in the area during the 1850s, and it is modified by an extensive network of diversions and impoundments to meet regional water needs. It is the only river in Colorado classified as both a Wild and Scenic River and a National Heritage River. Current water users are concerned that the flow regime has been altered because forecasts have overestimated seasonal water yields in recent years. Seasonal forecasts of May to September runoff for the river at the Canyon Mouth are currently issued by both the Northern Colorado Water Conservancy District (NCWCD) and the National Resource Conservation Service (NRCS). Methods used to forecast streamflow for the Cache la Poudre River have changed through the years and have produced variable and inconsistent results (Figure 1.1) Historical forecasts by the NRCS were most accurate in years with average annual water yields. In dry years, flow forecasts tended to overestimate water yield, whereas runoff tended to be underestimated in wet years. Accurate forecasts are challenging to produce because they must rely primarily on ground observations that leave much of the hydrologic cycle under-sampled in both time and space (Bales et al., 2006).

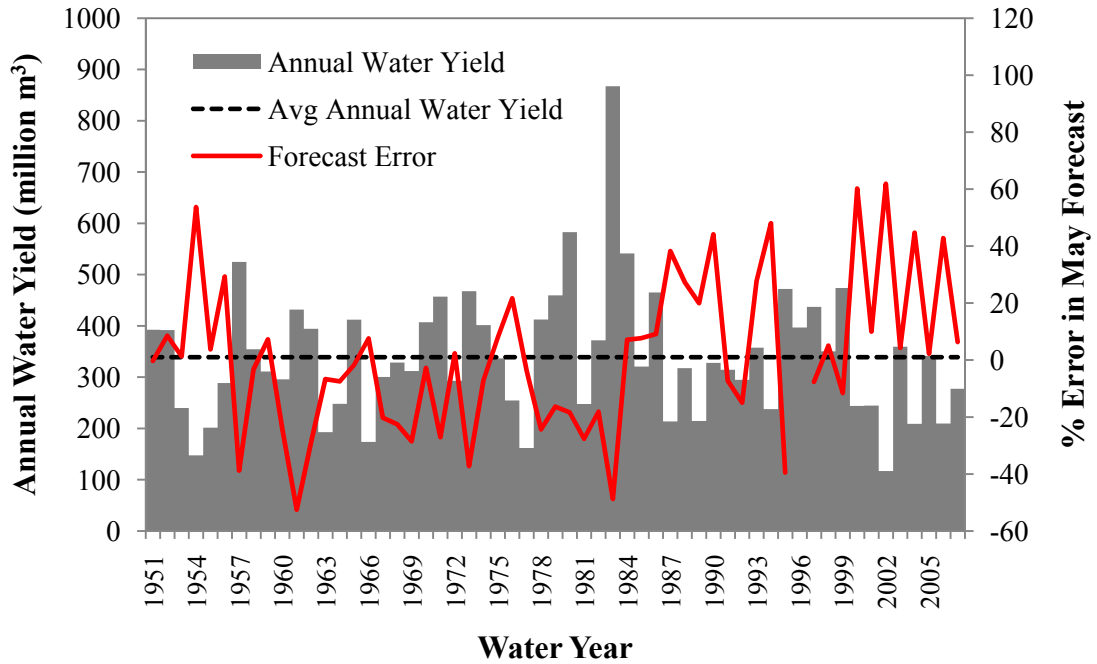


Figure 1.1. Naturalized annual water yield and NRCS May forecast error for the Cache la Poudre River at Canyon Mouth: WY 1951-2007.

The primary motivation for this research is to identify possible strategies for improving snowmelt runoff prediction for the Cache la Poudre River. An integrated approach to hydrologic monitoring and modeling that incorporates both ground and satellite derived observations could help characterize hydrologic processes in parts of the basin that generate runoff but are currently not monitored. Several factors could affect the consistency of runoff generation in the Cache la Poudre basin, including changes in the timing and quantity of precipitation, temperature, and land cover. This study focuses on the effects of climate on runoff generation with an emphasis on identifying where and when runoff is generated and developing appropriate methods for simulating snowmelt runoff. To accomplish this goal, the objectives of this thesis are to:

- 1) Develop a naturalized flow record for the Cache la Poudre River and determine the effects of flow modification on the magnitude and timing of discharge.
- 2) Analyze relationships between snow cover distributions and naturalized discharge to identify important areas for runoff production.
- 3) Evaluate the ability of the Snowmelt Runoff Model (SRM) to simulate seasonal hydrographs at a daily time step for the Cache la Poudre River.

This thesis first provides a site description for the Cache la Poudre basin. The effects of flow modification on the flow regime, relationships between snow cover distributions and naturalized discharge, and application of the SRM are addressed in individual chapters. The concluding chapter synthesizes results and implications of the research.

1.2 SITE DESCRIPTION

The Cache la Poudre watershed is located in Northern Colorado with a small area in Southeastern Wyoming (Figure 1.2). The headwaters of the river are located in Rocky Mountain National Park. After flowing approximately 130 km through the Poudre Canyon, the river passes through the municipalities of Fort Collins and Greeley before reaching its confluence with the South Platte River. The basin covers an area of 4824 km² and ranges in elevation from 1406 to 4125 m, with an average elevation of 2167 m. Land cover in the basin includes tundra at high elevations, subalpine and montane coniferous forests at middle elevations, and grasslands at low elevations. Land cover, elevation, and distributed precipitation are presented in Appendix A. All analyses included in this thesis

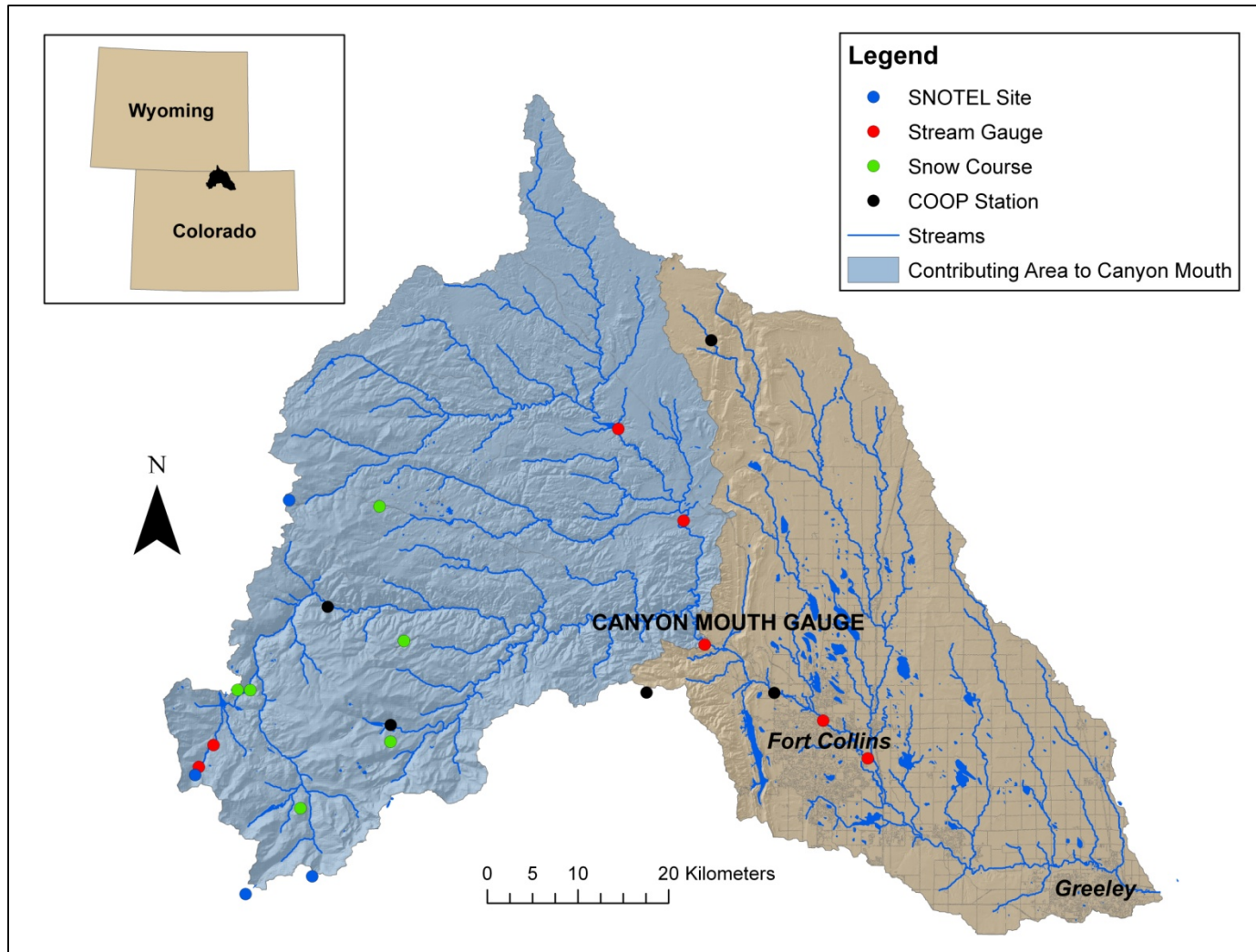


Figure 1.2. Location map for Cache la Poudre watershed with hydrometric and meteorological measurement locations, including the forecasting location at the Canyon Mouth.

will focus on the portion of the basin above the Colorado Division of Water Resources (CDWR) stream gauge at the Canyon Mouth (Cache la Poudre River at Canyon Mouth near Fort Collins (CLAFTCCO)), which is the forecasting location for the Cache la Poudre River. The portion of the basin above the Canyon Mouth covers an area of 2730 km² (Figure 1.2) and ranges in elevation from 1590 to 4125 m, with an average elevation of 2560 m.

Precipitation generally increases while temperature decreases with elevation, which contributes to significant spatial variability in climate throughout the basin (Figure 1.3). From 1971-2000, average annual precipitation for the basin ranged from 330 mm at

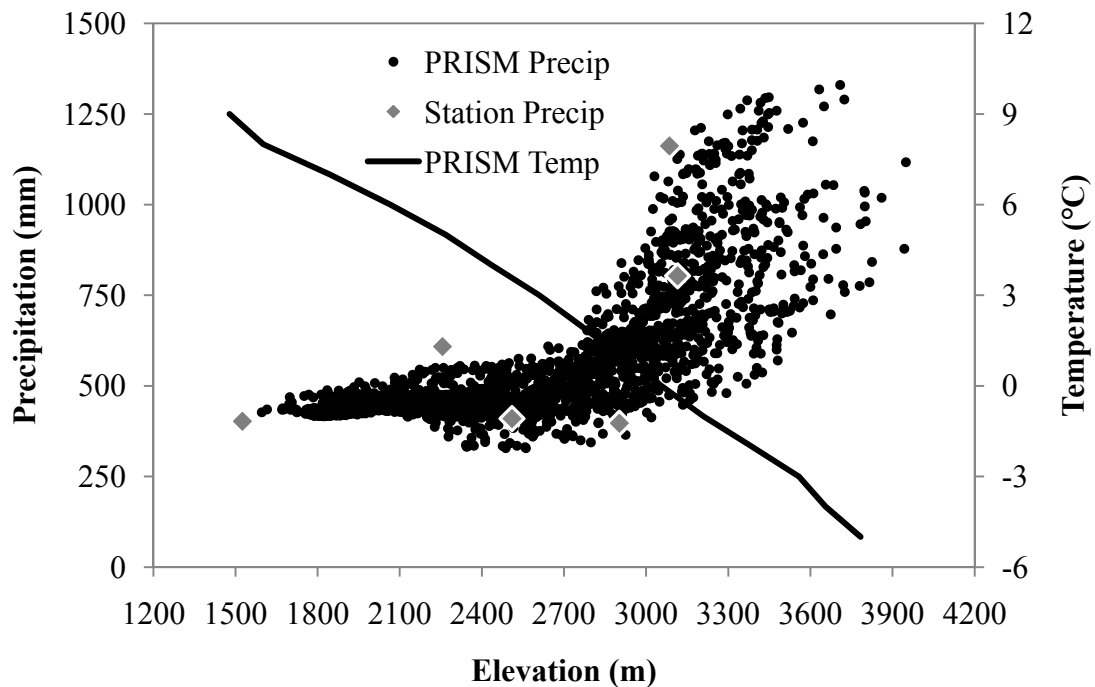


Figure 1.3. PRISM derived average annual precipitation and temperature versus elevation within the Cache la Poudre basin above the Canyon Mouth from 1971- 2000 (PRISM, Oregon State University, www.prismclimate.org). Grey diamonds indicate average annual precipitation for weather stations within the basin over each station's period of record between 1971 and 2000. For weather stations, the period of record between 1971 and 2000 ranged from 11 to 30 years.

lower elevations to 1350 mm near the headwaters, with a basin-wide average of 540 mm. Precipitation increases only gradually to an elevation of about 2800 m, above which the amount and variability of precipitation increases substantially (Figure 1.3). Basin average precipitation is generally low during winter months then increases during the spring, ranging from 27 mm in February to 70 mm in May (Figure 1.4). Average monthly temperature ranges from a low of -7°C in January to a high of 15°C in July (Figure 1.4). This spatial and temporal variability in both precipitation and temperature lead to high variability in runoff generation across the basin. From 1951 to 2006, naturalized annual discharge for the Cache la Poudre River at the Canyon Mouth ranged from 117 to 867 million m³, with an average of 339 million m³. The snowmelt hydrograph at the Canyon

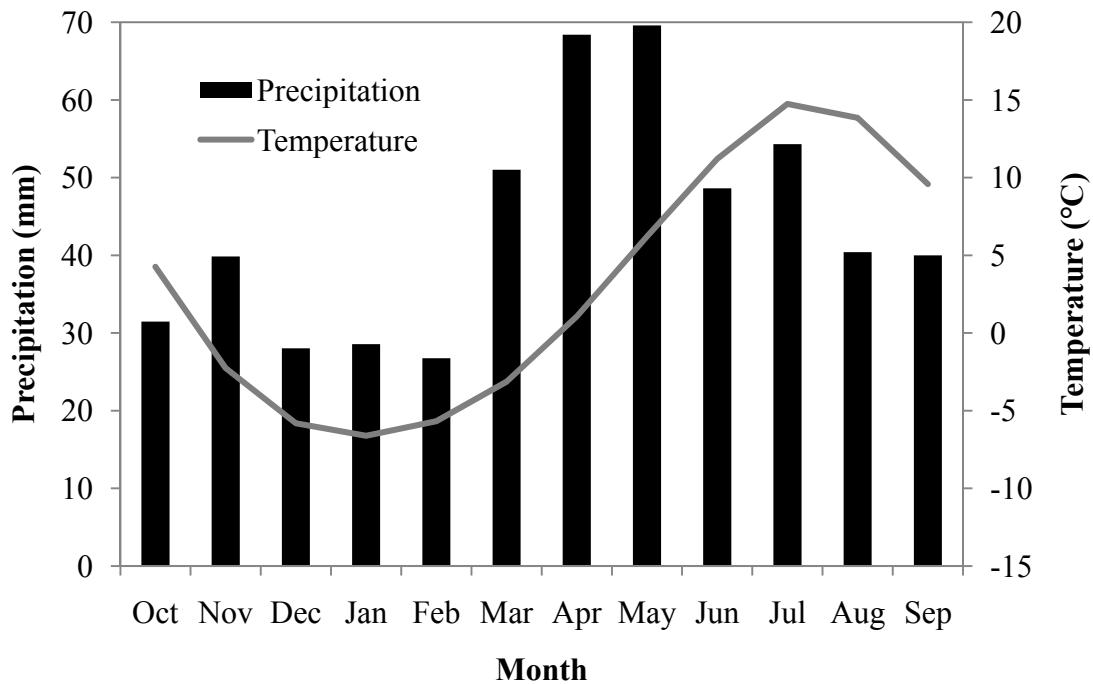


Figure 1.4. Average monthly precipitation and temperature for the Cache la Poudre basin: 1971-2000. Derived from PRISM, Oregon State University, www.prismclimate.org.

Mouth generally starts to rise subtly around April 1st, while the onset of peak flow does not begin until early to mid-May. Peak flow usually occurs between the end of May and beginning of June, after which flows recede through summer and fall until reaching winter baseflow levels in October.

CHAPTER 2: FLOW MODIFICATION

2.1 INTRODUCTION

The Cache la Poudre River is modified by an extensive network of diversions and impoundments. This chapter describes the effects of flow modifications on the timing and magnitude of discharge for the Cache la Poudre River at the Canyon Mouth by investigating the timing and magnitude of diversions, foreign water inputs, and changes in reservoir storage. Diversions take water from the river for consumptive use throughout the year. Foreign water is diverted into the Cache la Poudre drainage network from outside the basin (i.e., trans-basin diversions) causing flows to be higher than natural conditions. The main channel of the Cache la Poudre River has never been impounded, although numerous tributary impoundments and off-channel reservoirs have been constructed to store snowmelt runoff. Water diversions into and releases from these reservoirs modify the flow regime. To determine river flow response to snowmelt runoff alone, effects of these modifications must be removed from the flow records. Naturalized hydrographs will be used for all subsequent analyses in the following chapters of this thesis.

2.2 METHODS

Naturalized, or un-depleted, discharge for the Cache la Poudre River can be estimated by accounting for all diversions, foreign water, and changes in reservoir storage. A basic accounting method can estimate naturalized flow by adding or subtracting diversions, foreign water, and changes in reservoir storage (Equation 2.1):

(2.1)

$$\textit{Naturalized flow} = \textit{Observed flow} + \textit{Diversions} - \textit{Foreign water} \pm \Delta\textit{Storage}$$

The number and type of flow modification structures above the Canyon Mouth is shown in Table 2.1, and a comprehensive list is provided in Appendix B. For this study, naturalized flows, diversions, and foreign water inputs were provided by the CDWR at a daily time step for 2000-2006. These data were then used to calculate change in reservoir storage with Equation 2.1. Reservoir releases are not routed through the drainage network in this accounting method. Therefore, the travel times these releases take to reach the Canyon Mouth are not included in the naturalized flow estimates, producing unrealistic changes in daily flow. To minimize this routing signature on the naturalized hydrograph, the naturalized daily flows were smoothed using a 7-day moving average (Figure 2.1). Most of the larger diversions and reservoirs are monitored continuously, while smaller structures are monitored weekly. Some flow modification structures are not monitored and therefore were not accounted for in estimation of naturalized flows. This contributes to additional uncertainty in daily naturalized flow calculations, which highlights another reason for using 7-day average natural discharge instead of the daily un-depleted flow

data. All analyses that follow in this thesis therefore use 7-day average un-depleted discharge at the Canyon Mouth.

Table 2.1. Number of flow modification structures above the Canyon Mouth by type.

| | Diversions | Foreign Water | Reservoirs |
|----------------------|-------------------|----------------------|-------------------|
| Number of structures | 24 | 10 | 42 |

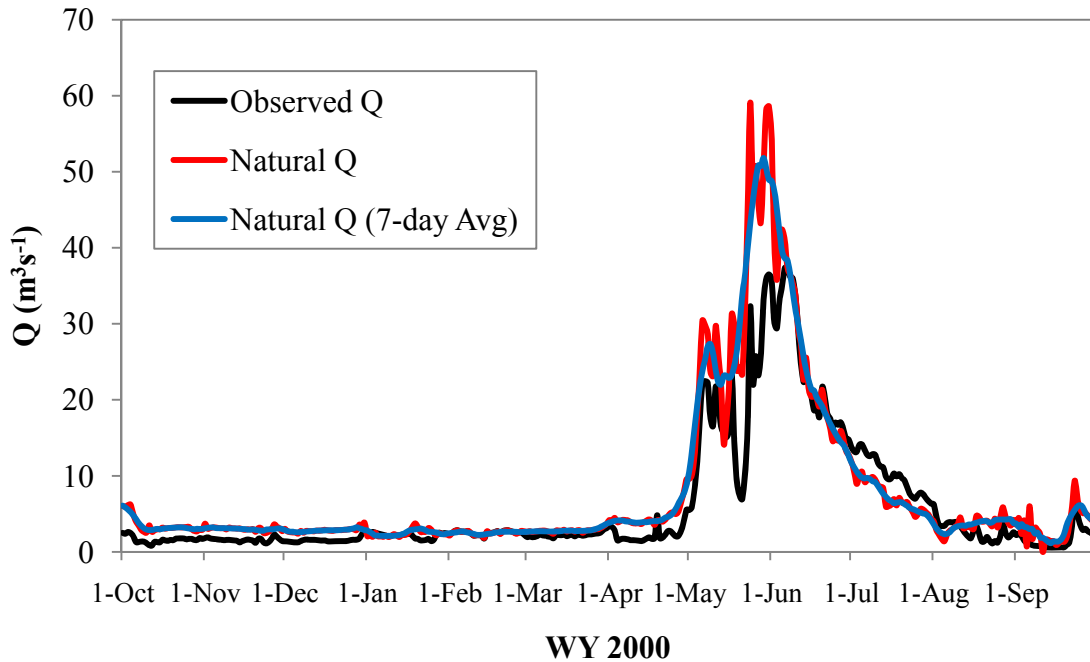


Figure 2.1. Observed, natural, and 7-day average natural discharge (Q) for Cache la Poudre River at Canyon Mouth: WY 2000.

To characterize the difference in magnitude between naturalized and observed flows at the Canyon Mouth, summary statistics were computed for annual and seasonal (May 1 to September 30) time scales. Summary statistics for each type of flow modification were also analyzed at monthly, seasonal, and annual timescales. Annual calculations are based on the water year (WY), which begins on October 1 and ends on September 30. To determine the effects of flow modification on the timing of runoff, dates of peak flow and timing of inflection points in the cumulative discharge curves were compared for the observed and naturalized hydrographs. The inflection points

approximate the beginning, middle, and end of snowmelt (Moore et al., 2007), and correspond approximately to the 20th, 50th, and 80th percentiles on the cumulative discharge curve. The 50th percentile represents the center of timing (CT), which is the day of the year on which one-half of the total annual water flow has occurred (Barnett et al., 2008). The day-of-year for the 20th, 50th, and 80th percentiles were used to compare the timing of observed and naturalized flows at the Canyon Mouth for all WYs, and these percentiles are hereafter referred to as Q20, Q50, and Q80, respectively.

2.3 RESULTS

Naturalized discharge was generally greater than observed discharge at both the annual time scale (Figure 2.2) and during the snowmelt season (Figure 2.3). For the 2000-2006 study period, the net effect of flow modification was a reduction in annual observed discharge at the Canyon Mouth by 56 million m³ or 23% on average. Annual naturalized flows were greater than observed flows for all years (Figure 2.2), and seasonal naturalized flows were greater than observed flows in all years except 2004 (Figure 2.3). Annual and seasonal summary statistics for observed and naturalized daily flows are presented in Table 2.2 and 2.3, respectively. For the seven observed hydrographs included in the study period, peak daily flow ranged from 19.4 to 85.2 m³s⁻¹ (Table 2.2). Naturalized peak flows ranged from 24.1 to 101.3 m³s⁻¹ (Table 2.2) and were higher than observed peak flows for all years except 2004. Minimum daily flows were also higher for the naturalized than for the observed flow regimes in all years at both annual (Table 2.2) and seasonal (Table 2.3) time scales.

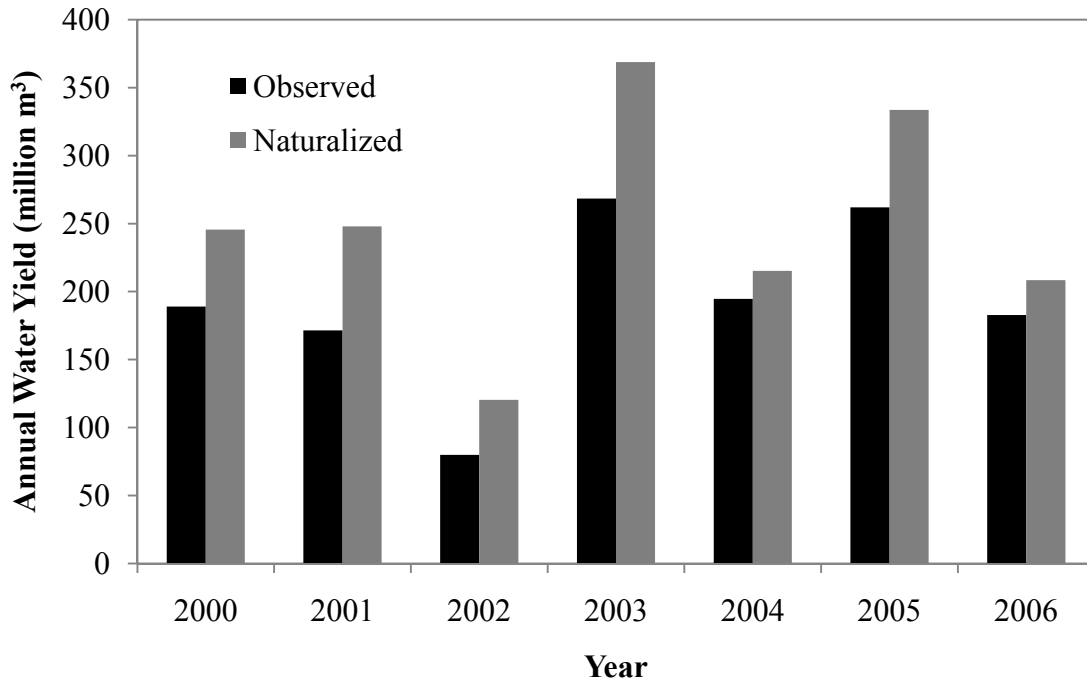


Figure 2.2. Observed and naturalized annual water yields (million m³) for Cache la Poudre River at Canyon Mouth: WY 2000-2006.

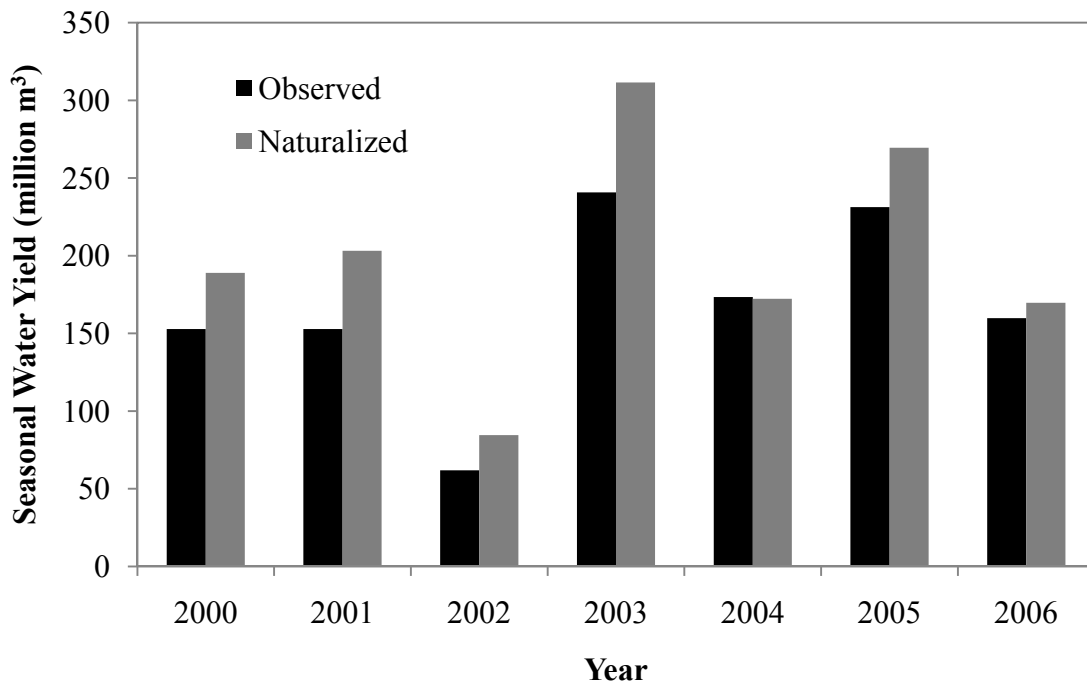


Figure 2.3. Observed and naturalized water yields (million m³) for the snowmelt season from May through September 30 for the Cache la Poudre River at Canyon Mouth: WY 2000-2006.

Table 2.2. Annual summary statistics for daily observed (Obs) and naturalized (Nat) flow regimes (in m^3s^{-1}) at the Canyon Mouth: WY 2000-2006.

| Regime | Stats | 2000 | 2001 | 2002 | 2003 | 2004 | 2005 | 2006 |
|---------------|--------------|-------------|-------------|-------------|-------------|-------------|-------------|-------------|
| Obs | Max | 37.4 | 43.6 | 19.4 | 85.2 | 35.4 | 56.9 | 45.6 |
| Obs | Mean | 5.99 | 5.44 | 2.53 | 8.51 | 6.17 | 8.31 | 5.80 |
| Obs | Min | 0.566 | 0.425 | 0.311 | 0.045 | 0.340 | 0.538 | 0.368 |
| Obs | SD | 8.18 | 8.61 | 3.42 | 14.6 | 8.02 | 13.5 | 9.98 |
| Nat | Max | 51.8 | 46.3 | 24.1 | 101 | 26.2 | 62.7 | 46.3 |
| Nat | Mean | 7.79 | 7.86 | 3.82 | 11.7 | 6.84 | 10.6 | 6.61 |
| Nat | Min | 1.15 | 1.16 | 0.969 | 0.894 | 0.568 | 1.45 | 1.27 |
| Nat | SD | 10.6 | 11.3 | 4.55 | 19.3 | 7.13 | 15.4 | 9.93 |

Table 2.3. May-September summary statistics for daily observed (Obs) and naturalized (Nat) flow regimes (in m^3s^{-1}) at the Canyon Mouth: WY 2000-2006.

| Regime | Stats | 2000 | 2001 | 2002 | 2003 | 2004 | 2005 | 2006 |
|---------------|--------------|-------------|-------------|-------------|-------------|-------------|-------------|-------------|
| Obs | Max | 37.4 | 43.6 | 19.4 | 85.2 | 35.4 | 56.9 | 45.6 |
| Obs | Mean | 11.6 | 11.6 | 4.68 | 18.2 | 13.1 | 17.5 | 12.1 |
| Obs | Min | 0.566 | 0.566 | 0.311 | 1.330 | 1.953 | 0.623 | 0.538 |
| Obs | SD | 10.3 | 10.6 | 4.45 | 18.3 | 8.38 | 17.1 | 13.0 |
| Nat | Max | 51.8 | 46.3 | 24.1 | 101 | 26.2 | 62.7 | 46.3 |
| Nat | Mean | 14.3 | 15.3 | 6.4 | 23.4 | 13.0 | 20.4 | 12.8 |
| Nat | Min | 1.15 | 2.41 | 1.16 | 1.53 | 3.62 | 1.45 | 2.10 |
| Nat | SD | 14.0 | 14.4 | 6.13 | 25.1 | 7.31 | 19.9 | 13.0 |

For all types of flow modification, diversions had the greatest effect on discharge at the Canyon Mouth for both annual (Figure 2.4) and seasonal time scales (Figure 2.5). The amount of water diverted from the river was over twice the amount of foreign water brought into the basin via trans-basin diversions (Figures 2.4 and 2.5). Diversions decreased annual discharge by 68 to 143 million m^3 with an average reduction of 104 million m^3 for the study period, while trans-basin diversions increased annual water yields by 27 to 61 million m^3 , with an average of 42 million m^3 (Figure 2.4). For the study period, 78% of diversions from the river occurred between May 1 and September

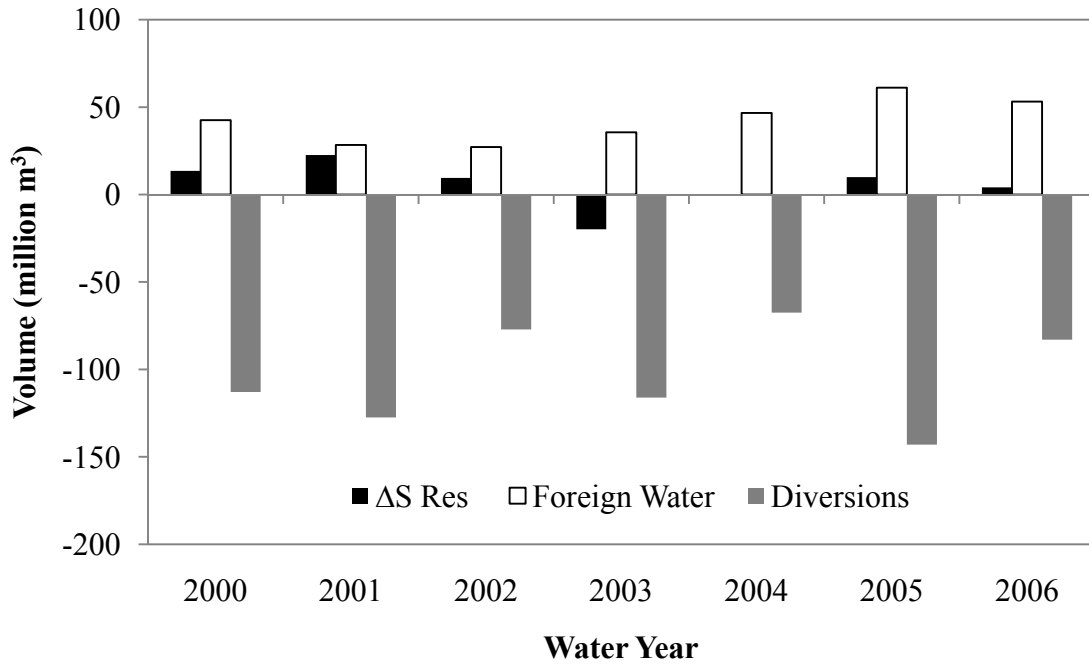


Figure 2.4. Annual effects of flow modification by type showing total volume (million m³) of water diverted into (+) and out of (-) the Cache la Poudre River above the Canyon Mouth: WY 2000-2006.

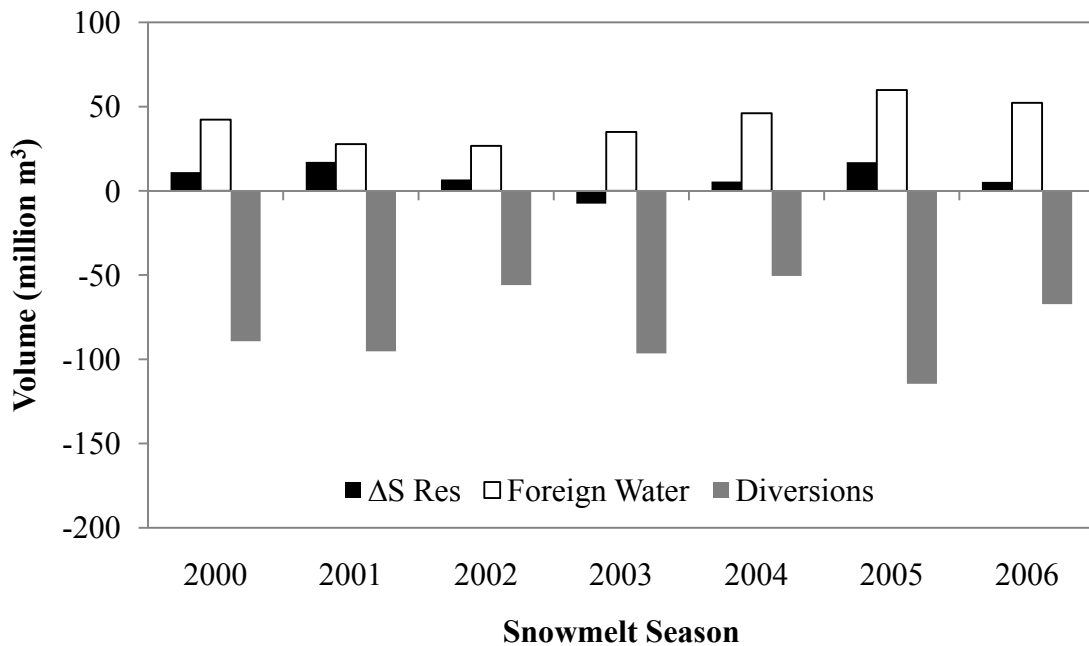


Figure 2.5. Seasonal (May 1 to September 30) effects of flow modification by type showing total volume (million m³) of water diverted into (+) and out of (-) the Cache la Poudre River above the Canyon Mouth: WY 2000-2006.

30, while 99% of the foreign water inputs to the drainage network occurred from May 1 to September 30. The net effect of reservoir operations (i.e., diversions into and releases from reservoirs) at annual and seasonal time scales was less significant than the effects of diversions and foreign water (Figures 2.4 and 2.5). For the study period, reservoir operations increased flows at the Canyon Mouth by 23 million m³ per year on average, with the exception of 2003 when reservoir operations led to net decrease in flows at the Canyon Mouth (Figure 2.4 and 2.5).

Diversions from the river were generally small during winter months when flows were low and then increased with snowmelt runoff during the spring. Diversions peaked in May and June, before receding through late-summer into fall (Figure 2.6). Foreign water inputs were almost negligible during winter, but then increased substantially during May, peaked in the month of June, and receded to winter levels by October (Figure 2.6). Of all types of flow modification, reservoir operations exhibited the highest variability throughout the year. During 2000-2006, water was usually diverted into reservoirs during winter and spring months, which reduced discharge at the Canyon Mouth (Figure 2.6). Reservoir operations reduced flow most substantially during May, but shifted to releasing water from storage in July through October (Figure 2.6). The net effects of flow modification on discharge were greatest from May through September, although the interaction of diversions, foreign water inputs, and reservoir operations varied on a daily basis producing sudden changes in observed flows at the Canyon Mouth (Appendix B).

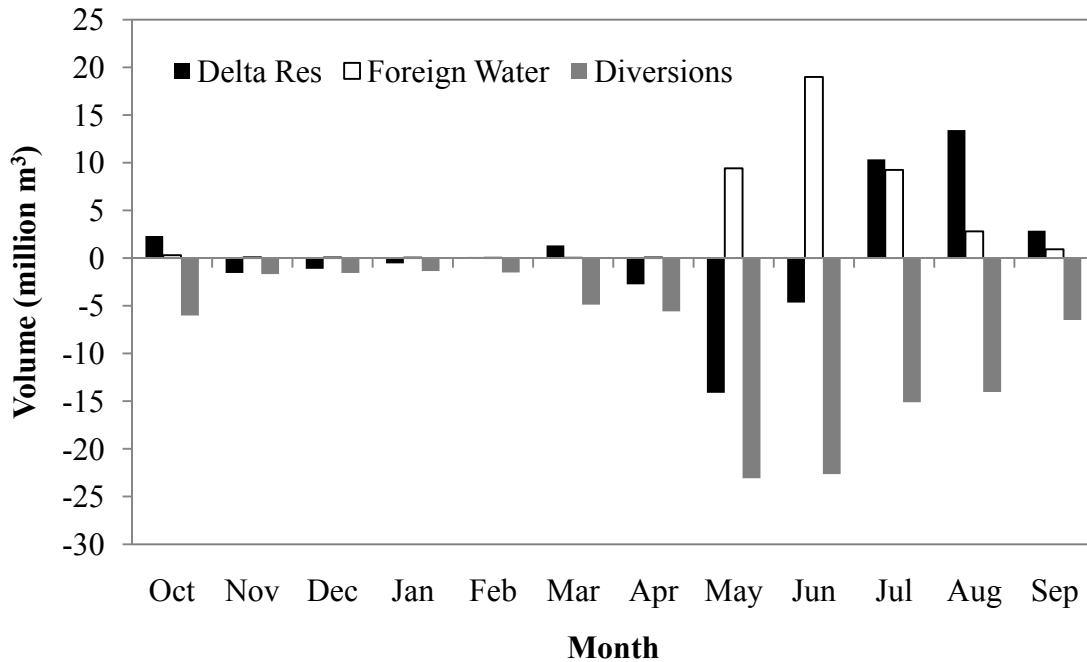


Figure 2.6. Average monthly totals (million m³) for flow modification above the Canyon Mouth: WY 2000-2006.

Analysis of hydrograph timing showed that flow modification delayed occurrence of Q20, Q50, and Q80 for all years (Appendix B). An example of this timing delay is shown in Figure 2.7. Naturalized Q20 was the timing metric most affected by flow modification, occurring 19 days earlier than the observed Q20 on average. Naturalized Q20 also showed the greatest variability of all timing metrics for both the observed and naturalized flow regimes (Figure 2.8). The CT (Q50) for the observed flow regime occurred eight days later than the naturalized regime on average, and exhibited little variability between years. The difference in timing between regimes for Q80 was greater than Q50 but less than Q20. When averaged for the study period, flow modification delayed occurrence of Q80 by 11 days.

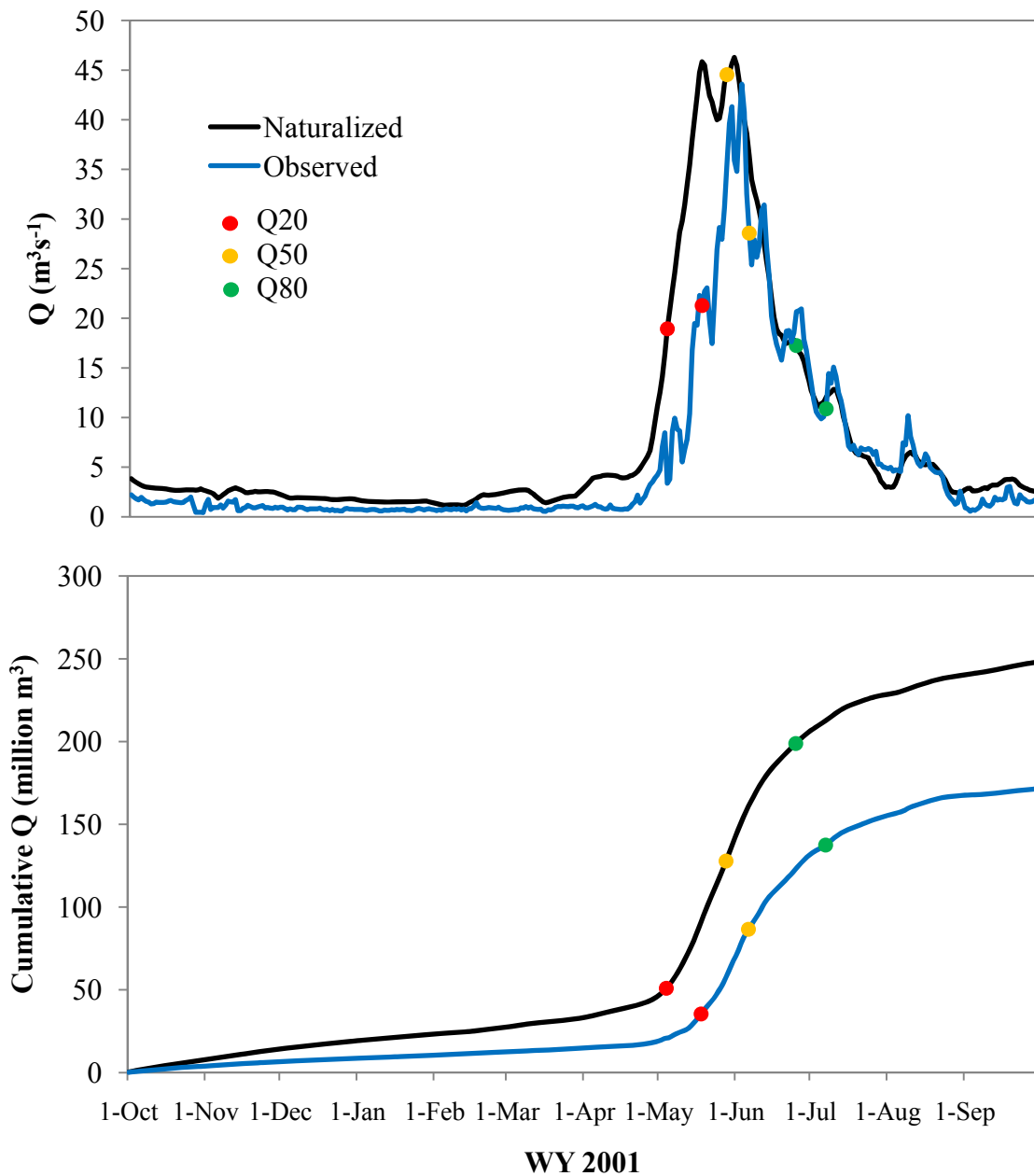


Figure 2.7. Naturalized and observed (a) hydrographs and (b) cumulative discharge curves showing timing of Q20, Q50, and Q80 for the Cache la Poudre River at the Canyon Mouth: WY 2001.

The timing of Q_{peak} and Q_{50} were generally similar (Figure 2.8). For the study period, the timing of Q_{peak} and Q_{50} differed by only 6 days on average for both the naturalized and observed hydrographs. For the study period, observed hydrographs

peaked 3 days later than naturalized hydrographs on average. The only instance where flow modification advanced the timing of flow metrics occurred for Qpeak in 2001, when the observed hydrograph peaked 10 days earlier than the naturalized hydrograph. The timing and magnitude of daily flow modification for each year during the study period are presented in Appendix B as Figures B.1 to B.7.

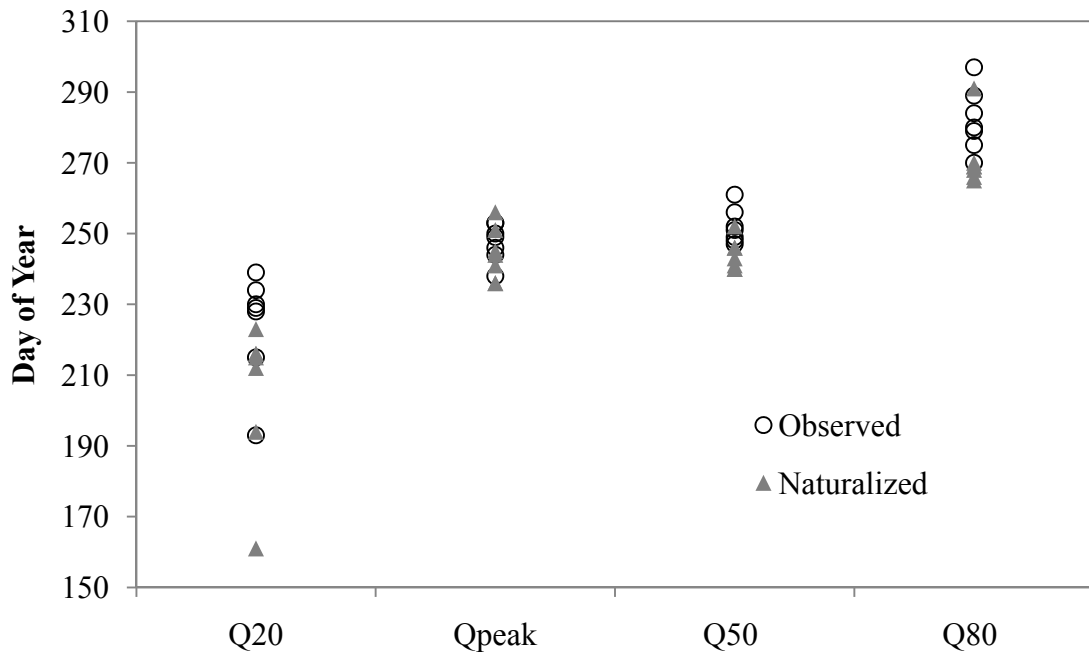


Figure 2.8. Timing of Q20, Qpeak, Q50, and Q80 for observed and naturalized hydrographs at the Canyon Mouth from 2000-2006.

2.4 DISCUSSION

The most noticeable effects of the modified flow regime were delayed hydrograph rise, decreased peak flows, and lower winter baseflows at the Canyon Mouth (Figures 2.1 and 2.7). The timing and magnitude of flow modifications varied seasonally. Foreign water inputs are driven by snowmelt runoff and generally peaked around June 1st before receding throughout the remainder of the summer (Figure 2.9). As irrigation demands

increased during the spring so did diversions from the river. Water diversions generally peaked around June 1st and then receded gradually throughout the summer.

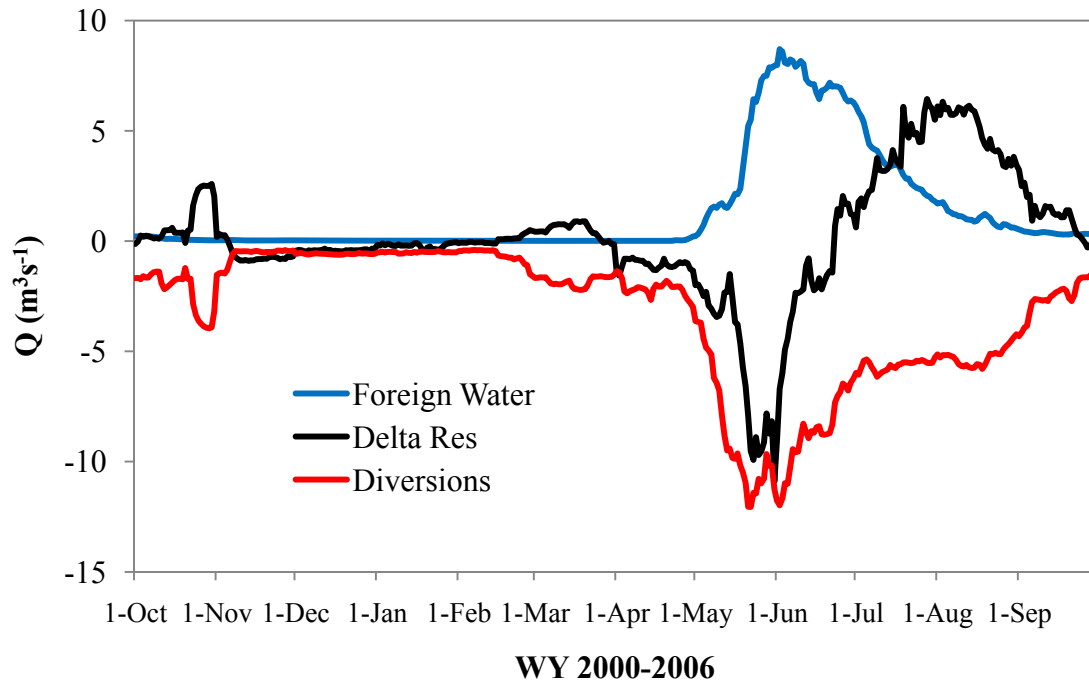


Figure 2.9. Average timing and magnitude of flow modifications above the Canyon Mouth over the study period from WY 2000-2006. Positive values indicate addition of water to the river and negative values the removal of water from the river.

Reservoirs generally released water prior to snowmelt runoff to increase storage capacity for potential spring flooding. As the snowmelt hydrograph rose, water was diverted into reservoirs and stored for release during the later summer months when irrigation demands were greatest. The net effect of reservoir operations shifted from negative (increasing storage) to positive (releasing storage) towards the end of June (Figure 2.9). During winter and spring months, water was periodically released from upstream reservoirs and then diverted for consumptive use farther downstream. These symmetrical signals often appeared during the months of October, November, and March (Figure 2.9 and Figures B.1 to B.7).

In addition to these average flow modifications for 2000-2006, water management in the river also responded to inter-annual trends in water availability. Water yields in 2002 were the lowest ever recorded at the Canyon Mouth, which led to substantial reservoir drawdown to meet water demands. The drought year of 2002 was followed by an average year for runoff in 2003. To return reservoirs to ideal levels, the amount of water that was diverted into reservoirs was above average in 2003, which led to reduced flows at the Canyon Mouth (Figure 2.4 and 2.5). Another dry year occurred in 2004, where calls for reservoir releases caused seasonal observed flows to be slightly higher than naturalized flows (Figure 2.3).

Flow modification generally delayed the onset of the snowmelt hydrograph, according to the quantile-based method of evaluating flow timing. Although observed and naturalized hydrographs had different magnitudes of runoff, Q20, Q50 and Q80 approximated the inflection points on cumulative discharge curves for both the observed and naturalized hydrographs during the study period (Figures B.8 to B.14), which suggests these timing metrics provided an objective means to analyze differences in hydrograph timing. Water was diverted into reservoirs and irrigation ditches during hydrograph rise, as demonstrated by Q20, which shifted 19 days later on average during the study period due to flow modification. On the other hand, peak discharge appears to be a strong enough signal in the hydrograph that timing of Q_{peak} was less affected by flow modification. As the hydrograph receded, water was released from reservoirs to supplement irrigation demands, which tended to shift the recession limb later in time and delayed observation of Q80 by 11 days on average for the study period.

The timing and magnitude of snowmelt hydrographs are both key indicators of hydrologic response to climate. The hydrograph shifts observed between naturalized and modified flow regimes in the Cache la Poudre highlight the importance of naturalized flow calculations for monitoring hydro-climate responses.

2.5 CONCLUSIONS

The net effect of flow modification was to reduce discharge at the Canyon Mouth of the Cache al Poudre River during 2000-2006. The amount of water diverted from the river was over double the amount of foreign water inputs from trans-basin diversions. The net effect of reservoir operations on discharge varied seasonally and both increased and decreased flow at the Canyon Mouth. Reservoir operations generally reduced flow during hydrograph rise and supplemented flow during hydrograph recession. The combined effects of diversions, foreign water, and reservoir operations generally led to a shift in the timing of the snowmelt hydrograph, delaying the onset of the hydrograph rise and recession. Flow modification resulted in the delayed occurrence of all hydrograph timing metrics. In developed basins where drainage networks are modified by diversions and impoundments, the shift in hydrograph timing due to flow modification is significant enough that it could mask changes in the response of snowmelt runoff to climate.

CHAPTER 3: RELATIONSHIPS BETWEEN SNOW COVER AND RUNOFF

3.1 INTRODUCTION

Snow covered area (SCA) has been cited as an important variable for understanding, modeling, and predicting atmospheric, hydrological, and ecological processes in snowmelt-dominated regions (Ferguson, 1999; Jain and Lall, 2000; Tekeli et al., 2005; Zhou et al., 2005). Because SCA can be observed over large spatial areas, monitoring of seasonal SCA is a useful means of tracking spatial and temporal patterns in snowpack across variable mountain terrain. SCA is one of the three fundamental features, along with snow water equivalent (SWE) distribution and melt rate, required to describe the spatial evolution of snow cover from the end of accumulation through melt (Liston, 1999). In mountainous regions, however, data limitations have inhibited detailed understanding of the variability of snow cover and melt. *In situ* snowpack measurements are sparsely distributed relative to snowpack heterogeneity leaving much of the hydrologic cycle under-sampled in both time and space (Bales et al., 2006).

In the Western United States, the primary forms of *in situ* monitoring are SWE measurements recorded continuously at NRCS Snow Telemetry (SNOTEL) sites and monthly snow surveys at snow course sites. In Colorado, these point measurements are generally located at elevations above 3000 m with an average elevation of 3060 m. These discrete points provide little information on the spatial distribution of water stored as

snow (Balk and Elder, 2000). Because mountain regions are heterogeneous and exhibit strong gradients in precipitation over space, characterizing the spatial distribution of snow is an important step in understanding snowmelt runoff generation, particularly in areas without *in situ* measurements. Estimates of SWE spatial distributions have been derived indirectly from passive microwave remote sensing using a variety of algorithms (Rees, 2006), but the footprint size of passive microwave data from satellite remote sensing is large (~25 km pixels for SSM/I), making it difficult to verify the accuracy of SWE retrieval algorithms. In mountain regions, studies estimating spatial SWE have therefore used combinations of image data and snow melt modeling (e.g., Cline et al., 1998; Balk and Elder, 2000; Molotch and Margulis, 2008) or spatial interpolation (Fassnacht et al., 2003). In contrast to SWE, the spatial distribution of SCA is easier to derive from remote sensing (Balk and Elder, 2000; Maurer et al., 2003; Fassnacht et al., 2003; Nagler et al., 2008), making SCA a useful snow variable for spatial monitoring.

To supplement ground measurement networks, remotely derived images of SCA have been recognized as providing useful information for runoff prediction during the snowmelt season (Maurer et al., 2003; Tekeli et al., 2005; Zhou et al., 2005; Dressler et al., 2006). In most cases, these runoff prediction studies incorporate SCA into pre-existing simulation models that relate snow distributions to snowmelt runoff generation. SCA has been used as a direct input to the Snowmelt Runoff Model (e.g., Martinec, 1975; Gómez-Landesa and Rango, 2002; Lee et al., 2005; Tekeli et al., 2005) or as a means of updating hydrologic model snowpack simulations (e.g., Andreadis and Lettenmaier, 2006; Clark et al., 2006; Dressler et al., 2006; McGuire et al., 2006). Although SCA products from satellite sensors are now widely available (Dozier and

Painter, 2004; Seidel and Martinec, 2004), and snow cover depletion is important for predicting snowmelt runoff, SCA data are not currently used in most flow forecasting applications.

This study uses SCA to characterize how snow spatial variability relates to snowmelt runoff generation across a large range of elevations in the Cache la Poudre basin. In contrast to model-based studies, relationships between SCA and snowmelt runoff are examined directly, without assuming *a priori* any defined relationship between these variables. In this sense, this study is data-based, with the overall objective of assessing how SCA images can best be incorporated into long-term hydro-climate monitoring of mountain watersheds. To this end, the specific objectives of the chapter are to (1) identify spatial and temporal patterns of SCA and (2) identify relationships between SCA distribution and runoff production for the Cache la Poudre River.

3.2 METHODS

3.2.1 Snow Covered Area Analyses

All analyses of SCA use the Moderate Resolution Imaging Spectroradiometer (MODIS)/Terra 8-day 500 m snow-cover products, downloaded from the National Snow and Ice Data Center (NSIDC) (<http://nsidc.org/data/modis/index.html>). The MODIS SCA product is derived using a snow mapping algorithm that employs a Normalized Difference Snow Index (NDSI) and other criteria tests (Hall et al., 2006). The MODIS product was selected due to its accessibility and available time range. MODIS SCA has also been found to have superior snow classification ability over the National Weather

Service National Operational Hydrologic Remote Sensing Center (NOHRSC) snow cover products in the presence of cloud in topographically complex and forested snow-dominated areas (Maurer et al., 2003). MODIS SCA products are available at either daily time intervals or as 8-day composites that give the maximum snow cover extent over an 8-day time period. Due to substantial cloud impairment in daily images, 8-day composite images, which were less affected by cloud, were used for all analyses in this study. All MODIS images were obtained for the Cache la Poudre basin from 2000 to 2006 for the snowmelt season, which is defined as occurring from mid-March until less than 1.0% of the entire basin was snow covered. The date of 1.0% snow cover ranged from June 10 to July 4 for the 2000-2006 study period. The number of images analyzed per year depended on snow persistence and ranged from 11 in 2000 to 15 in 2004 (Appendix C).

To characterize spatial and temporal patterns in SCA, images were analyzed both in the basin as a whole and in spatial subsets of sub-basins and elevation zones (Figure 3.1). The first subdivision separates the basin into four sub-basins representing the three major tributaries and the canyon that connects them. These sub-basins cover areas ranging from 332 to 1464 km² and elevation ranges of 1562 to 2016 m (Table 3.1). The North Fork and Canyon sub-basins include large areas of lower elevations (Figure 3.1 and Table 3.1) where snow accumulation and runoff generation are relatively low. The second spatial subdivision separates the basin into elevation zones, which include seven zones that each cover an elevation range of approximately 360 m (Table 3.2). The area of elevation zones ranges from 7 to 896 km², with the uppermost elevation zone covering a significantly smaller portion of the basin than all other zones (Table 3.2).

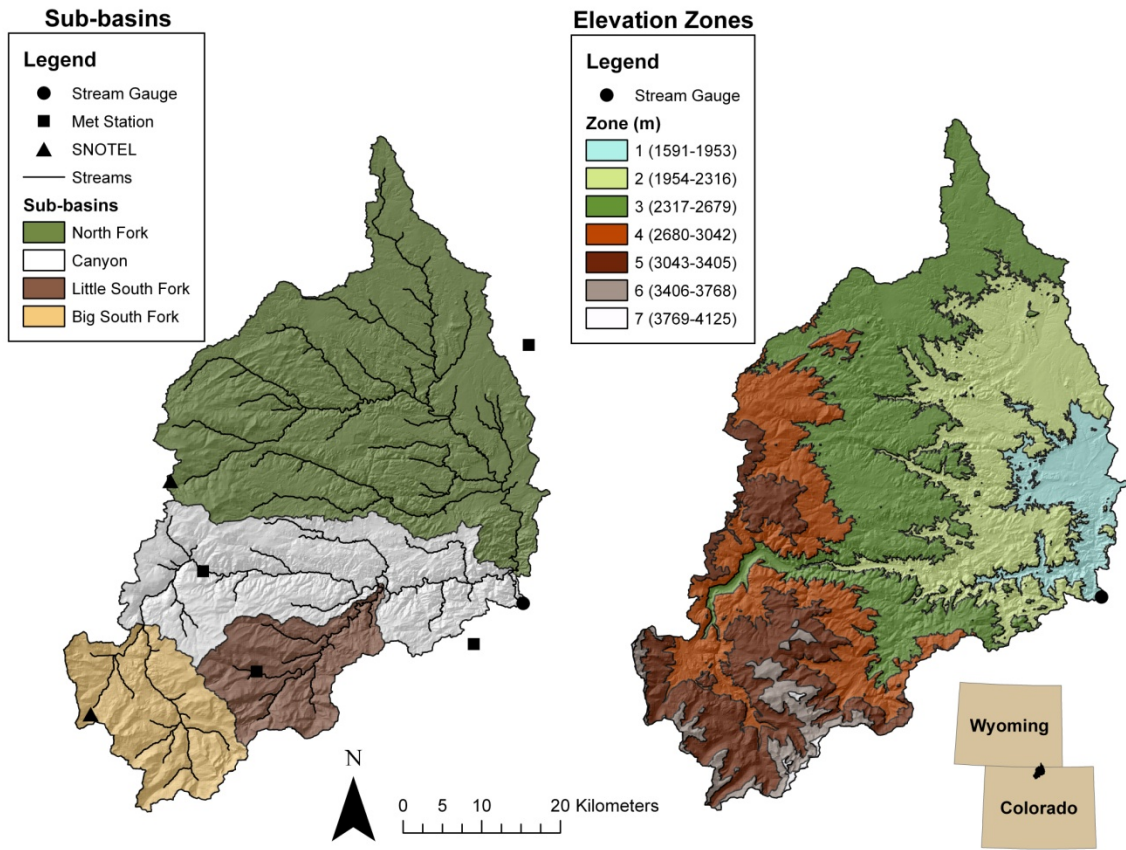


Figure 3.1. Sub-basin network and elevation zones used in analyses of SCA above the Canyon Mouth.

Table 3.1. Elevation range and area for sub-basins within the Cache la Poudre watershed above the Canyon Mouth.

| Sub-basin | Elevation (m) | | | Area (km ²) |
|-------------------|---------------|------|---------|-------------------------|
| | Min | Max | Average | |
| North Fork | 1632 | 3472 | 2357 | 1464 |
| Canyon | 1591 | 3508 | 2529 | 664 |
| Little South Fork | 1998 | 4014 | 2945 | 267 |
| Big South Fork | 2563 | 4125 | 3238 | 332 |

Table 3.2. Elevation range and area for the seven elevation zones within the Cache la Poudre watershed above the Canyon Mouth.

| Elevation zone | Elevation (m) | | | Area (km ²) |
|----------------|---------------|------|---------|-------------------------|
| | Min | Max | Average | |
| 1 | 1591 | 1953 | 1851 | 196 |
| 2 | 1954 | 2316 | 2150 | 671 |
| 3 | 2317 | 2679 | 2480 | 896 |
| 4 | 2680 | 3042 | 2861 | 471 |
| 5 | 3043 | 3405 | 3196 | 384 |
| 6 | 3406 | 3768 | 3522 | 104 |
| 7 | 3769 | 4125 | 3860 | 7 |

The spatial subdivisions form the basis for analyzing relationships between SCA and discharge (Q). These two variables were compared using a combination of regression analyses and spatial patterns of snow cover probabilities. Regression analyses compare SCA within each spatial subset to the 7-day moving average naturalized discharge at the Canyon Mouth gauge. Separate regressions compare SCA vs. Q at the Canyon Mouth during the snowmelt season of each year (2000-2006), giving a total of seven yearly regressions per spatial subset of the basin. The strength of each regression relationship was evaluated by selecting the linear or non-linear (i.e., exponential, logarithmic, polynomial, or power) regression equation that resulted in the greatest coefficient of determination (R^2) (Equation 3.1).

(3.1)

$$R^2 = \frac{\sum_{i=1}^n (M_i - \bar{M})^2}{\sum_{i=1}^n (O_i - \bar{O})^2}$$

where M is the simulated value, \bar{M} is the average of simulated values, O is the observed value, and \bar{O} is the average of observed values. These coefficients provide a first

indication of whether the spatial extent of snow cover in the basin correlates directly to discharge at the basin outlet.

3.2.2 Probability of Snow

To investigate spatial snow distribution in the watershed, spatial patterns of snow occurrence were derived during the melt season, hereafter called “probability of snow” distributions. Probability of snow was defined for a given 500-m pixel as the fraction of MODIS images from 2000-2006 that were snow-covered. Probability of snow distributions were calculated using the 8-day MODIS SCA images, each of which have pixel classifications of snow, no snow, cloud, and lake. SCA images were reclassified such that snow or cloud observations were equal to one, and all other attributes were equal to zero. “Probability of snow” was then calculated as:

(3.2)

$$P_s = \frac{\sum_{i=1}^n S}{n - \sum_{i=1}^n C}$$

where S is observations of snow, C is observations of cloud, an n is total observations. Similarly, “probabilities of cloud” were calculated to determine the extent of cloud impairment in the MODIS dataset.

Distributed snow probabilities were derived over multiple image subsets. First, probabilities were calculated for the entire MODIS SCA database, which included ninety total images from the snowmelt seasons of 2000-2006 (Appendix C). Next, to determine inter-annual variability in snow cover over the basin, probability of snow was calculated for all images included in analyses for a given year (Appendix C). Finally, to determine general snow depletion patterns, a time series of snow probability at 8-day intervals was

calculated during the snowmelt season using MODIS images across the seven years. Because probabilities of snow are calculated for each MODIS pixel, they can be examined within any spatial subsets of the basin. For all sub-basins and elevation zones (Tables 3.1 and 3.2), the range and average probabilities of snow were calculated.

3.3 RESULTS

Analyses using the MODIS 8-day SCA product were generally un-impaired by cloud throughout the basin for the study time period. Maximum probability of cloud was less than 16% per grid cell for the entire dataset of ninety MODIS images over the seven years. For all MODIS images, cloud cover ranged from 0% to 54% of the basin, with an average of 3% for the entire MODIS dataset. For the ninety MODIS images used in analyses, eight images had more than 10% cloud cover, three images had more than 25% cloud cover, and only one image had more than 50% cloud cover for the area above the Canyon Mouth. Cloud cover increased with elevation across the basin, ranging from an average cloud cover of 2% in the lowest elevation zone to 10% in the highest elevation zone for the entire MODIS dataset, with a distinct increase in cloud cover above approximately 3000 m. For individual years, average cloud cover ranged from 1% of the basin area for 2006 to 7% for 2000 (Appendix C).

Figure 3.2 shows how MODIS-derived SCA compares to naturalized discharge and high elevation SWE during the snowmelt season. In each year, SCA gradually decreases throughout the spring, but spring snow storms often result in temporary increases in snow cover percent. These increases typically last for only one 8-day period.

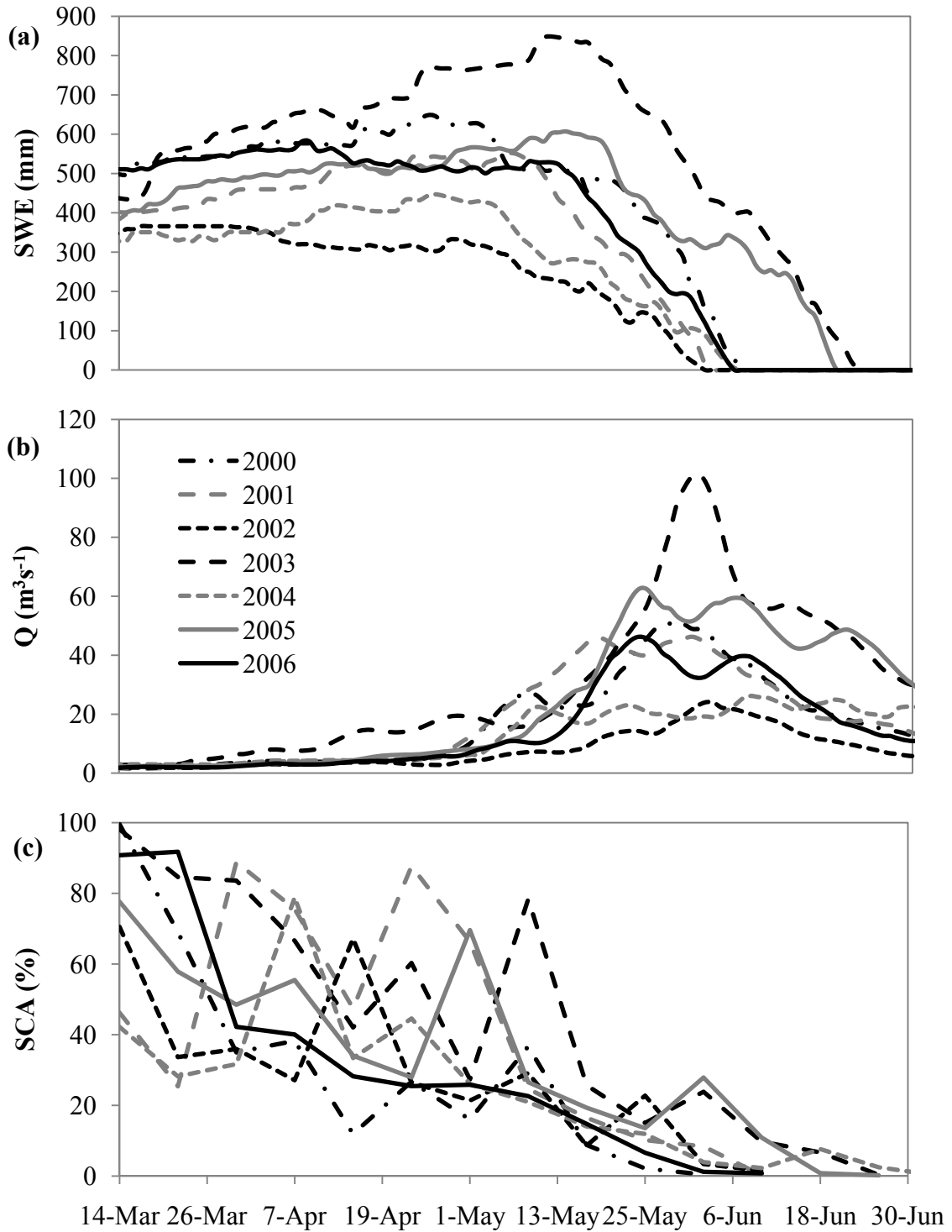


Figure 3.2. Variability in (a) snow water equivalent (SWE) at the Joe Wright SNOTEL site (elevation 3085 m), (b) naturalized discharge for the Cache la Poudre River at the Canyon Mouth gauge, and (c) basin-wide snow covered area (SCA) depletion during the snowmelt season for 2000-2006.

High elevation SWE either stays relatively constant or increases during early spring (mid-March to Mid-April). Depletion of high elevation SWE begins early to mid-May, and in most years, SCA is less than 50% of the basin area by the time SWE starts to decrease at the high elevation SNOTEL site. In almost all years, discharge at the Canyon Mouth does not begin to increase above winter baseflow levels until mid-April. Peak snowmelt runoff occurred between mid-May and early June for all the study years. SCA, Q, and SWE all show substantial inter-annual variability.

Regressions between SCA and discharge during the snowmelt season exhibit a wide range of correlation strength ($0.00 < R^2 < 0.92$) across different years and spatial subsets of the basin. Examples of regressions with high correlation strength are shown in Figure 3.3. These regressions show a non-linear increase in discharge as SCA depletes. In these two examples, the highest scatter in the SCA vs. Q relationship occurs for the highest discharge rates. In contrast to these examples, most SCA vs. Q regressions have relatively poor correlations. Figures 3.4 and 3.5 show the range of correlation strength for regressions comparing SCA in each spatial subdivision to discharge at the Canyon Mouth. When the basin was subdivided into sub-basins, the strongest correlations between SCA and streamflow were for the Little South Fork sub-basin ($0.59 < R^2 < 0.92$) (Figure 3.4). SCA over the entire basin and within the Canyon sub-basin produced slightly lower average correlations than the Little South Fork, while the lowest correlations between SCA and discharge occurred for the North Fork and Big South Fork sub-basins, which have the lowest and highest elevations, respectively. The Big South Fork exhibited the largest range in correlation strength for sub-basins ($0.12 < R^2 < 0.82$),

whereas SCA within the entire basin had the smallest range of R^2 -values ($0.55 < R^2 < 0.79$) for all spatial subsets.

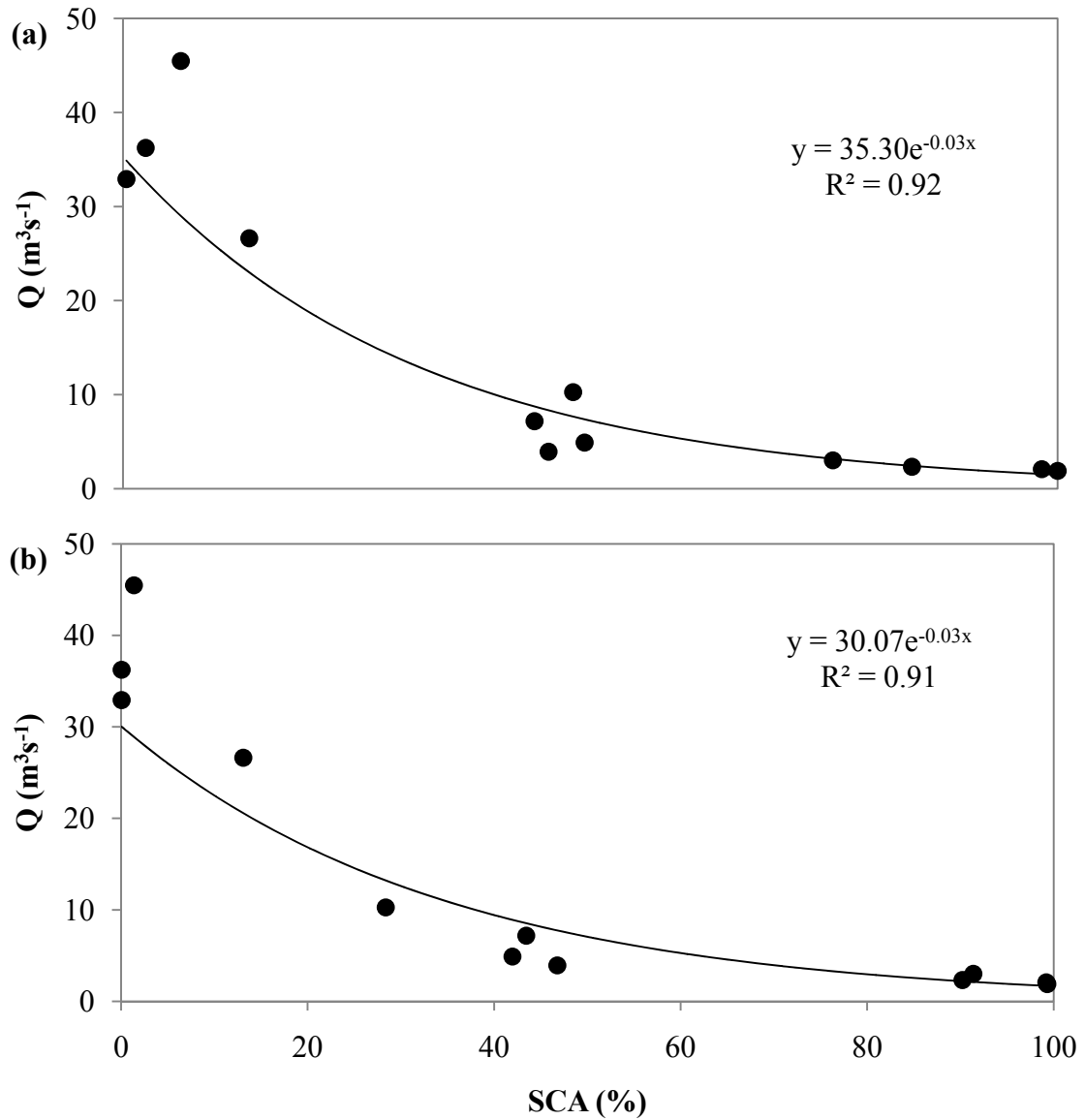


Figure 3.3. Examples of SCA vs. Q regression for the (a) Little South Fork sub-basin and (b) middle elevation band during the snowmelt season of 2006.

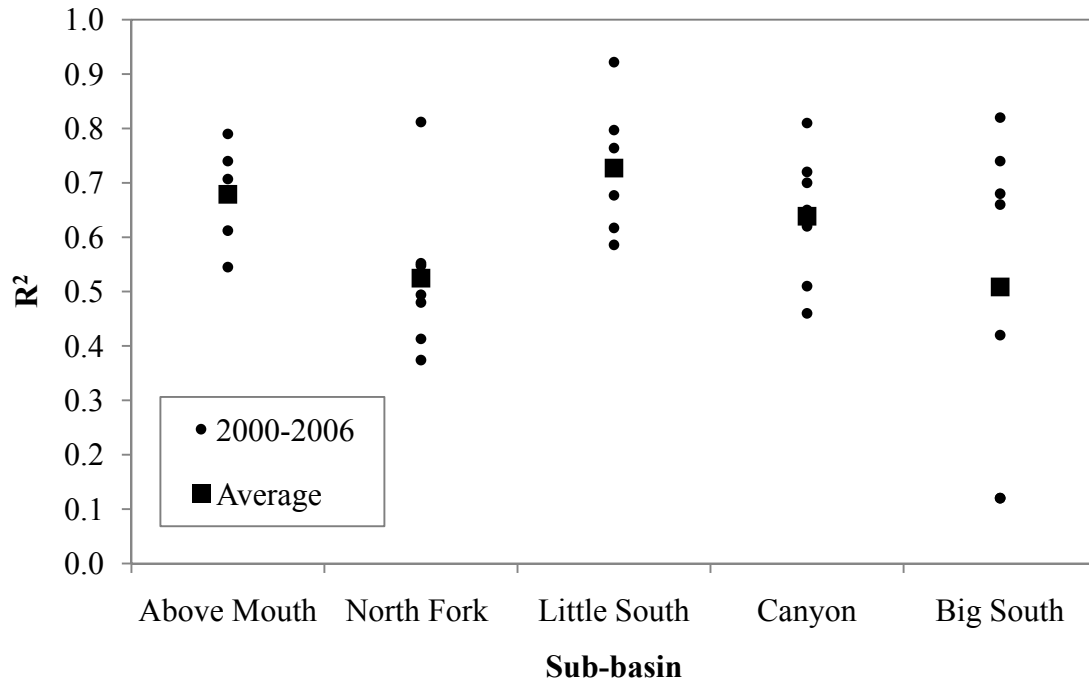


Figure 3.4. Correlation strength (R^2) of the SCA vs. Q relationships during the snowmelt season for the entire basin and sub-basin network above the Canyon Mouth gauge, 2000-2006.

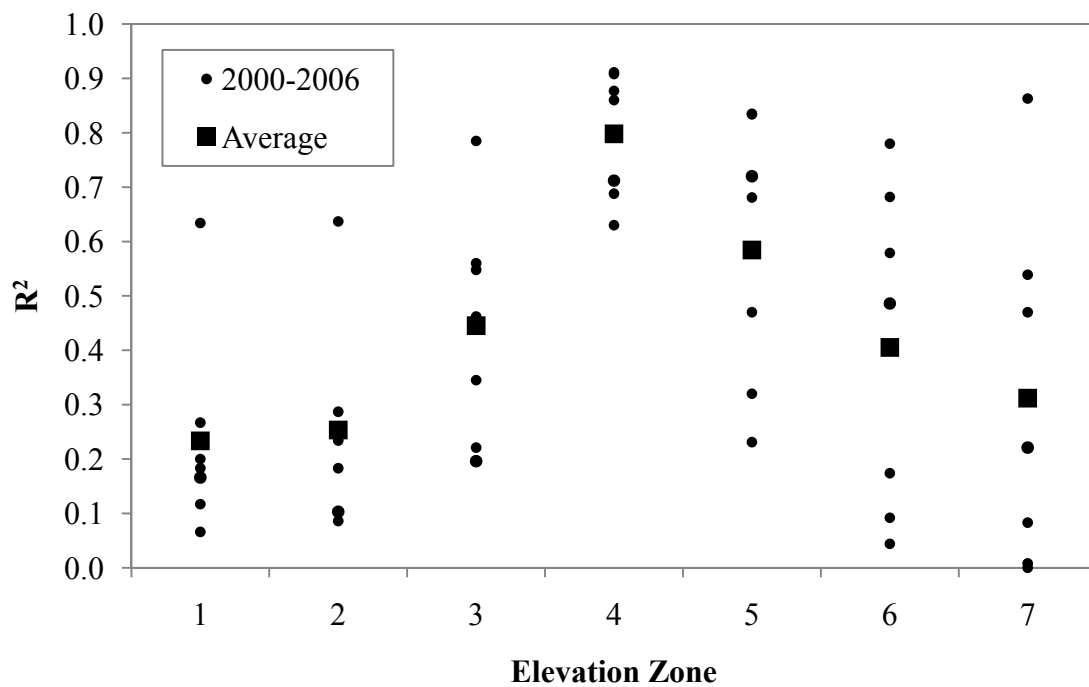


Figure 3.5. Correlation strength (R^2) of the SCA vs. Q relationships during the snowmelt season for elevation zones above the Canyon Mouth gauge, 2000-2006.

For elevation zone subsets, correlations between SCA and discharge were poorest (maximum $R^2 < 0.3$) for the lower elevations zones 1 and 2. Correlation strength increased with elevation reaching maximum values ($0.63 < R^2 < 0.91$) in the middle elevation zone 4 which extends from 2680 to 3042 m (Figure 3.5). This middle elevation zone also had the least variability in correlation strength of all elevation zones. Above the middle elevation zone, correlations between SCA and discharge again decrease, with a moderate average correlation ($R^2 = 0.58$) in elevation zone 5 and relatively poor correlations (average $R^2 < 0.41$) for the highest two elevation zones. Variability in correlation strength was similar for the three lowest elevation zones, while the highest variability in correlation strength occurred for the two highest elevation zones (Figure 3.5). The average R^2 -values across the seven years shows a clear pattern of correlation between SCA and discharge increasing with elevation until peaking in the middle elevation zone and then decreasing with elevation above zone 4.

Probabilities of snow calculated from the MODIS images shows both high spatial and temporal variability in snow cover. These probabilities were calculated over multiple image subsets that show variability between years, within the snowmelt season, and between spatial subsets of the basin. Calculated over the entire snowmelt season, probabilities of snow increase with elevation through elevation zone 5, with the greatest increase between zone 3 and 5 (Figure 3.6). From elevation zones 5 to 7, snow cover probabilities increase with elevation during some years but decrease during others. The highest inter-annual variability in snow cover probability over the study period occurs for elevation zone 3 (Figure 3.6), whereas all other elevation zones have similar ranges of variability.

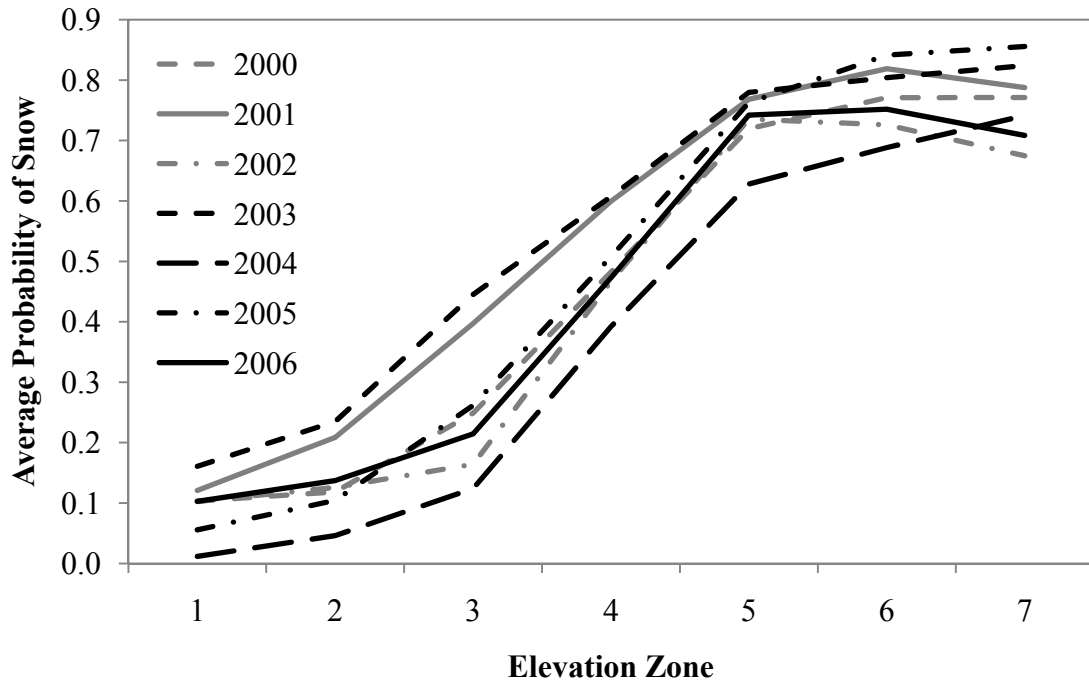


Figure 3.6. Average probability of snow during snowmelt season for elevation zones: 2000-2006.

Figure 3.7 shows the temporal evolution of snow probabilities across the basin during the snowmelt season. Probability of snow values were calculated on a pixel by pixel basis at eight-day intervals from March 14 to June 10 using the binary SCA images from each year during the 2000-2006 study period. The highest probability of snow during the snowmelt season, 90-100%, occurred above 3000 m (Figure 3.7), where snow accumulation is high and temperatures are low (Figure 1.3). At these high elevations, the probability of snow changes relatively little until mid-May, when the high elevation snowpack begins to melt. Below elevation zone 4, snow cover gradually decreases throughout the snowmelt season, as indicated by the steady changes in probability of snow. The lowest elevations on the east side of the basin have consistently low probabilities of snow from April through the duration of the snowmelt season. By May,

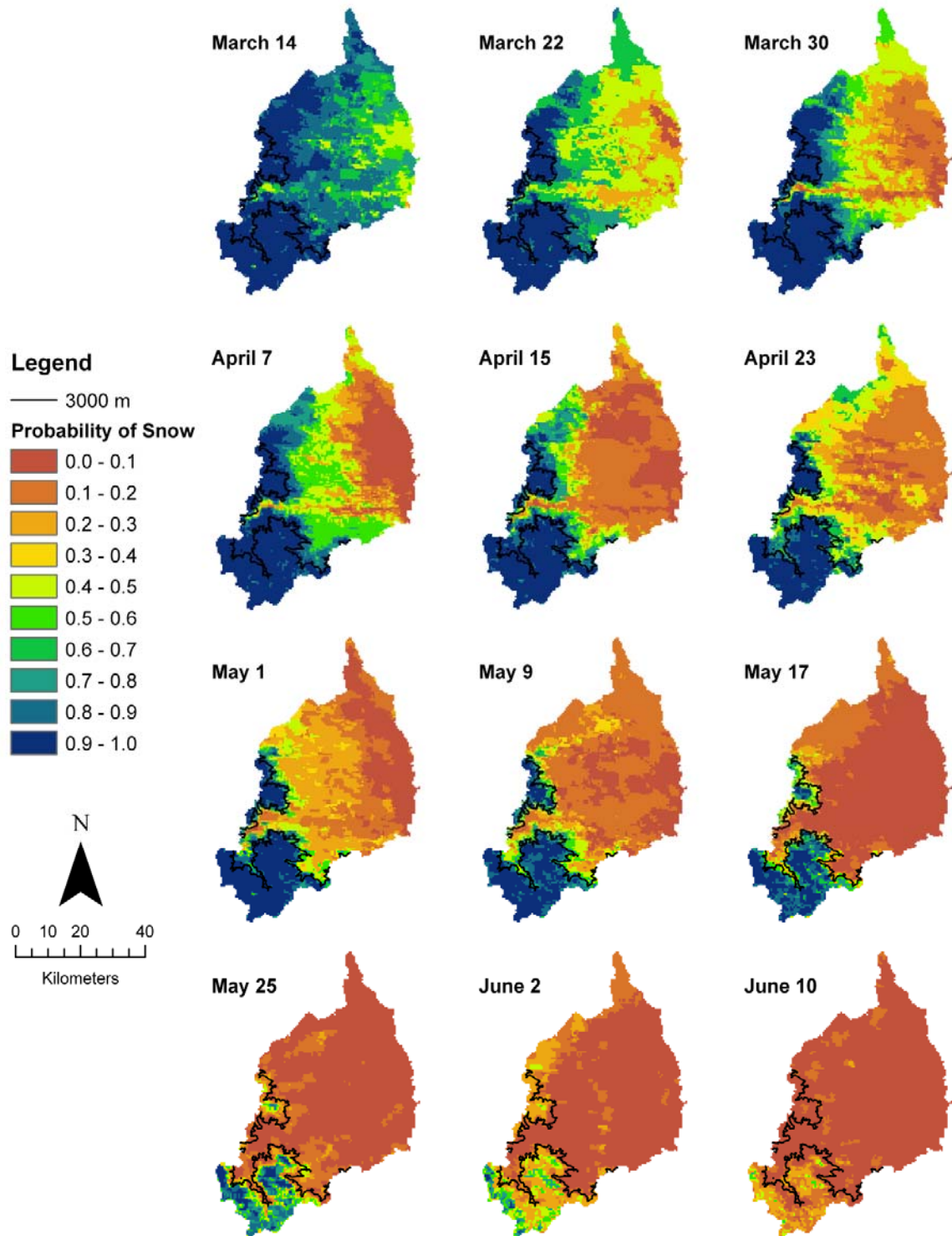


Figure 3.7. Probability of snow time series derived from MODIS 8-day images showing snow depletion for the Cache la Poudre basin during the snowmelt season. For each date, probabilities are calculated using images from 2000-2006.

low snow probabilities (<0.3) at lower elevations meet a sharp interface with high snow probabilities (>0.9) around 3000 m elevation (Figure 3.7).

The spatial distributions and evolution of snow cover probabilities during the snowmelt season can also be analyzed for elevation zones within basin (Figure 3.8). Within these elevation zones, the distinction between snow cover probabilities at low elevations (i.e., elevation zone 1 and 2) and high elevations (i.e., elevation zones 6 and 7) are also quite evident. For lower elevations, the average probability of snow is relatively high (0.6-0.7) in mid-March, and then decreases rapidly through late-March to reach low snow probabilities (<0.2) by April. At these lower elevations, the slight increase in snow probability that occurs in late April is due to spring snow storms that occurred during some years. Snow cover generally ablates by late-May for the two lowest elevation zones. At middle elevations (i.e., elevation zones 3 and 4), snow cover depletes steadily during the snowmelt season (Figure 3.8). The three elevation zones above 3000 m (i.e., elevation zones 5, 6, and 7) show consistently high snow cover probabilities until May, at which point probability of snow decreases steadily for the duration of the snowmelt season. The three highest elevation zones all show similar temporal patterns of snow depletion, with the two highest elevation zones exhibiting nearly identical trajectories for probability of snow.

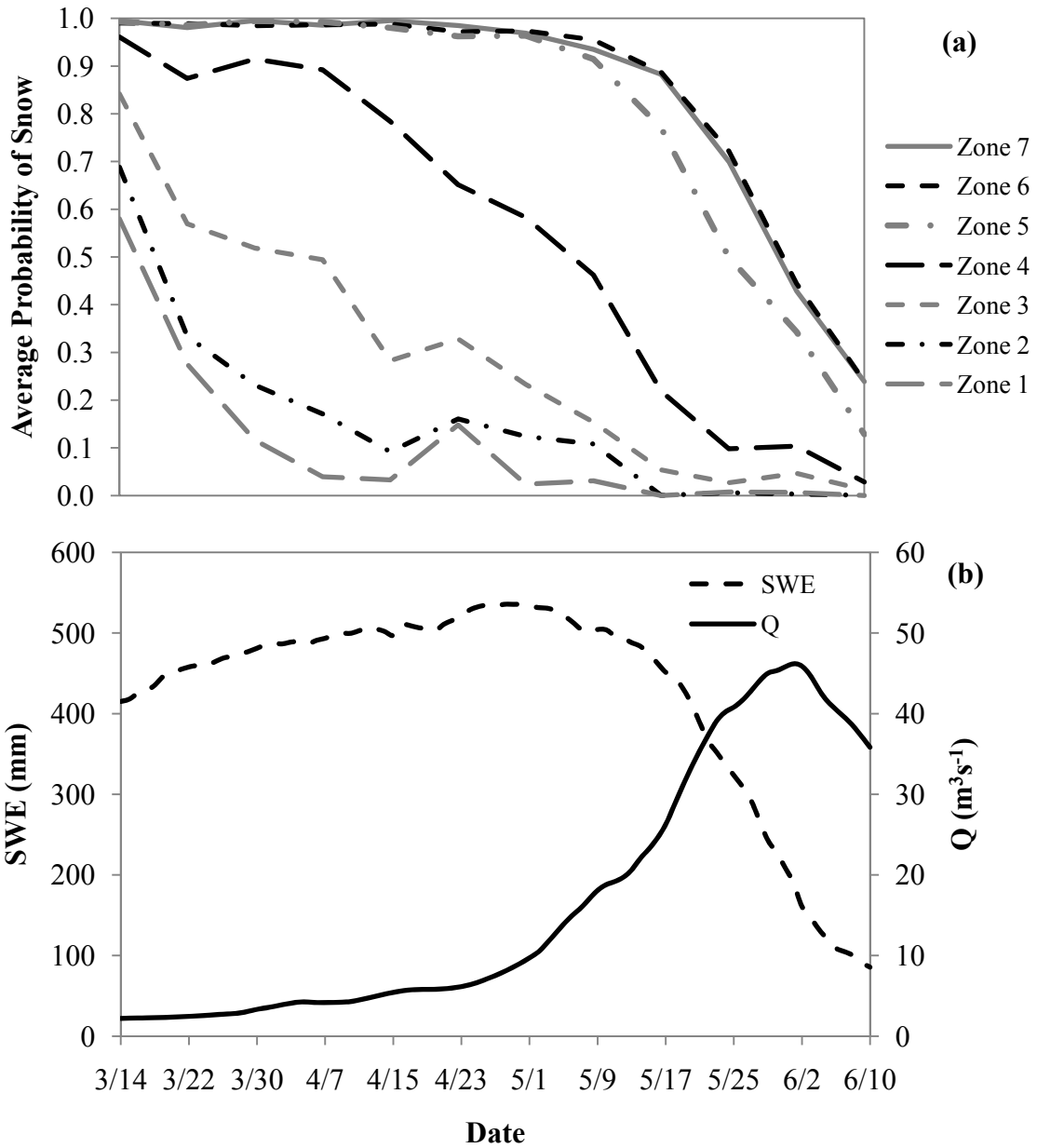


Figure 3.8. (a) Probability of snow time series for elevation zones derived from 8-day MODIS images, 2000-2006. (b) Average discharge at the Canyon Mouth gauge and average snow water equivalent (SWE) at the Joe Wright SNOTEL site (elevation 3085 m) for 2000-2006.

3.4 DISCUSSION

Analyses of SCA patterns show clear distinctions with elevation in SCA vs. Q relationships and snow probabilities, with evidence of transitional snow cover behavior within the middle elevation zone 4. Several lines of evidence point to the existence of this mid-elevation snow cover transition zone. First, analyses of SCA vs. Q relationships within spatial subsets show much clearer distinctions between elevation zones than between sub-basins. For elevation zones, SCA vs. Q correlation strength (Figure 3.5) peaks at the middle elevation zone (2680-3042 m), which also exhibited much lower variability in relationships between SCA and discharge during the snowmelt season than all other elevation zones (Figure 3.5). Both below and above this middle elevation transition zone, correlations between SCA and Q tend to decrease in strength and increase in variability. For sub-basins, SCA vs. Q correlation strength also appears to relate primarily to the elevation ranges of sub-basins, with the highest elevation sub-basin (Big South Fork; 3238 m average elevation) exhibiting the lowest average correlation and highest variability in correlation strength, similar to the uppermost elevation zones. The sub-basin with the highest correlation between SCA and discharge is the Little South Fork sub-basin (Figure 3.4), which has an average elevation of 2944 m, ranging from 1998 to 4002 m. This average elevation is similar to that of the middle elevation zone, 2861 m, where the correlations between SCA and Q are strongest. These two spatial subsets also exhibit similar relationships between snow cover depletion and discharge during the snowmelt season (Figure 3.3). Correlations between SCA and discharge were less variable for sub-basins (Figure 3.4) than elevation zones (Figure 3.5). Sub-basins

cover a wider range of elevations than elevation zones (Table 3.1 and 3.2), which explains the lower variability in correlation strength.

This apparent elevation-dependency of the SCA vs. Q relationships points to the presence of a snow transition zone within the basin at middle elevations. In this zone, both high correlation strength and lower variability in SCA vs. Q relationships suggest that the timing of snow cover depletion within that middle elevation zone generally coincides with the rise of the snowmelt hydrograph. Elevations below this transition zone, particularly the lowest elevation zones, have little persistent snow cover during the spring. In these areas little to no snow cover remains at the time when the snowmelt hydrograph begins to rise. Because April and May are the most important months for basin-wide precipitation (Figure 1.4), spring snow storms can cause large increases in SCA at lower elevations, but discharge generally does not increase when snow cover melts in these low elevation areas (Figure 3.8). Therefore, these storms tend to result in increased noise and reduced correlation between SCA and Q. Conversely, at high elevations SCA is not usually impacted by spring snow storms because snow cover persists well into the spring. Although the onset of peak discharge follows SWE depletion at high elevations (Figure 3.2), high elevation snow cover changes relatively little until after the onset of hydrograph rise (Figure 3.8). Even though snow may be melting in the high elevation zones and contributing to discharge, melting of the deep snowpack above elevation zone 4 does not lead to a substantial change in SCA until later in the snowmelt season (Figure 3.8), which can lead to poor correlations between SCA and discharge for the high elevation zones.

Probability of snow distributions also point to the presence of a mid-elevation snow cover transition zone. The spatial subsets from the SCA vs. Q analyses that had the highest average correlation strength both had average elevations near 2900 m and average probabilities of snow near 50% during the snowmelt season across the seven years. These areas are transitional between the persistent snow pack at high elevations, where probabilities of snow are greater, and the minimal snow cover at lower elevations where snow cover depletes relatively early in the spring. The transition in snow cover behavior becomes particularly evident when examining how probabilities of snow vary through the melt season for different elevation zones (Figure 3.8). At low elevations, spring snow cover depletes rapidly, reaching very low probabilities before the onset of the hydrograph rise. At high elevations, snow probability stays constant and high well into April then rapidly declines through May and early June. By the time snow probabilities drop significantly at high elevations the onset of peak discharge is already occurring, with the average peak discharge timing corresponding to snow probabilities of 50% in the two uppermost elevation zones (Figure 3.8). In contrast, the probability of snow decreases steadily at middle elevations throughout the snowmelt season. This continuous decline in snow probability corresponds with the rising snowmelt hydrograph, explaining the stronger correlations between SCA and Q for the middle elevation zone. Therefore, this zone where snow transitions to a more persistent snowpack at high elevations may be a key region to monitor, as it represents an important threshold in snowpack persistence and may be useful for snowmelt runoff prediction.

These elevation, snow cover, and discharge relationships indicate that the majority of snowmelt runoff for the Cache la Poudre River is generated from the portion

of the watershed at and above the middle elevation zone (i.e., approximately 3000 m), an area that comprises only 20% of the entire basin area above the Canyon Mouth. The location of this runoff-generating area is important because it is the portion of the watershed that generates peak flows and has the greatest potential influence on downstream flow (Smith et al., 2008). The strong increase in probability of snow across the middle elevations that form the lower boundary of this runoff generation zone corresponds well with the precipitation distribution generated by the PRISM model, which shows a similar increase in precipitation across middle elevations (Figure 1.3). Although these analyses show high inter-annual variability in snowpack characteristics across the basin, they also reveal characteristic behaviors in which the snowpack at high elevations behaves very differently from the snowpack through and below the mid-elevation transition zone. Our results suggest that monitoring the snowpack along elevation gradients that encompass both the high snow accumulation areas and the transitional zones at middle elevation could be useful for snowmelt runoff prediction.

Although SCA does not indicate the quantity of snow over space, our analyses show that SCA is useful for identifying spatial gradients in snow pack characteristics that are important for runoff generation. Spatial probabilities of snow calculated over multiple years reveal characteristic behaviors in the snowpack that would be difficult to discern from analyses of SCA for individual years alone. These spatial probabilities are integrative variables that could be useful large-scale indices of snowpack and snowmelt behavior over time. Characteristic behaviors derived from the SCA analyses also highlight important regions for *in situ* snow monitoring, particularly the mid-elevation snowpack transition zone.

3.5 CONCLUSIONS

Point location snow monitoring at high elevations with persistent snow cover may be insufficient for determining climate-induced snowpack changes in mountain regions, as spatial patterns of snow accumulation and melt are also important controls on snowmelt runoff generation. SCA is a spatial snow variable that can be derived directly from image data and is observable at a range of spatial scales. This makes it a useful addition to long-term hydro-climate monitoring networks, as it can supplement sparsely distributed point-scale snow measurements. In the Cache la Poudre basin, middle elevations (2680 to 3042 m) exhibited the strongest correlation between snow depletion and hydrograph rise. The two spatial subsets with the highest correlation between SCA and discharge, the Little South Fork sub-basin and middle elevation zone, had average elevations near 2900 m and average probabilities of snow near 50% during the snowmelt season. The elevation-dependency of SCA vs. Q relationships and probability of snow distributions point to a mid-elevation snow cover transition zone. Analysis of snow cover probability and PRISM datasets confirm that a small portion of the watershed above this transition zone generates the majority of snowmelt runoff for the Cache la Poudre River. Due to the influence of elevation on precipitation and snowmelt in mountainous regions, snow measurements should be collected along elevation gradients that include both high elevations with deep snowpack and transitional zones at middle elevations to improve runoff prediction in snowmelt dominated basins. The spatial variability in snowmelt response could be further elucidated by analyzing relationships between snow cover and discharge at multiple gauges within the basin, which would help characterize the

streamflow response to snowmelt at different elevations and identify important areas for runoff production above the mid-elevation snow transition zone.

CHAPTER 4: SNOWMELT RUNOFF MODEL

4.1 INTRODUCTION

4.1.1 Snowmelt Runoff Modeling

Watershed models are employed to understand dynamic interactions between climate and land-surface hydrology, and they are fundamental to water resources assessment, development, and management (Singh and Woolhiser, 2002). Runoff models transform incoming precipitation into discharge, taking account of losses to the atmosphere, groundwater storage, and the runoff processes by which water is routed to the channel (Ferguson, 1999). Snowmelt runoff models can range from simple regression equations (i.e., black-box approaches), through conceptually-based models, to the more detailed physically-based models. Black-box models are usually lumped, meaning the basin is treated as a single spatial unit, whereas physically-based models are often distributed, meaning the basin is divided into zones or grid cells (Ferguson, 1999). Conceptual models can be either lumped or distributed.

Snowpack accumulation occurs when precipitation falls as snow and temperatures are not warm enough to induce snowmelt. When temperatures warm, and the snowpack melts, melt water travels to the channel via the same hydrologic pathways as rainfall. Therefore, most snowmelt models are rainfall runoff models that account for the storage and melt of snow (Ferguson, 1999). Snowmelt runoff models have to achieve three

specific operations at each time step: (1) extrapolate available meteorological data to the snowpack, (2) calculate snowmelt rates, and (3) integrate snowmelt over the stream contributing area to estimate the total volume of new meltwater (Ferguson, 1999). This meltwater is then routed to the basin outlet.

The Snowmelt Runoff Model (SRM) is the most widely used model for simulating and forecasting snowmelt runoff (Rango and van Katwijk, 1990; Ferguson, 1999; Tekeli et al., 2005; Martinec et al., 2007). The SRM is a conceptual, deterministic, degree-day hydrologic model that is designed to simulate and forecast daily runoff from snowmelt and rainfall in mountainous environments (van Katwijk et al., 1993; Tekeli et al., 2005; Martinec et al., 2007). The model uses an empirically based temperature-index approach to simulate melt, analogous to degree-day models that estimate snowmelt as a linear function of average air temperature for time periods of a day or longer (Rango and Martinec, 1995; Dingman, 2002; Soncini-Sessa and Volta, 2005). SRM has been applied in mountain basins of almost any elevation range or size, and it can be used for three purposes: (1) simulation of daily flows in a snowmelt season, year, or sequences of years; (2) short term and seasonal runoff forecasts; and (3) evaluating the potential effects of climate change on seasonal snow cover and runoff (Martinec et al., 2007). The SRM has been successfully applied elsewhere in mountain basins with similar areas and elevation ranges to that of the Cache la Poudre (Ferguson, 1999; Tekeli et al., 2005).

The objective of this chapter is to evaluate the ability of the SRM to simulate seasonal (March 1 to September 30) runoff for the Cache la Poudre River at the Canyon Mouth. SRM was chosen to simulate snowmelt runoff in the Cache la Poudre because the basin does not have a sufficient density of meteorological data to merit fully distributed

physically-based modeling. SRM is instead driven primarily by snow-cover depletion, and analyses of MODIS SCA data in Chapter 3 showed that snow cover characteristics do relate to runoff production in the Cache la Poudre basin for some elevation zones. SRM can be configured using SCA data for the same elevation zones used in hydrologic analyses for Chapter 3.

4.1.2 Model Configuration

The SRM divides a basin into elevation zones, and requires daily temperature, precipitation, and SCA as input variables for each zone. For each day, SRM computes the water produced from snowmelt and rainfall, superimposes that runoff on the calculated recession flow, and transforms this into daily discharge from the basin (Equation 4.1):

$$Q_{n+1} = [C_{Sn}\alpha_n(T_n + \Delta T_n)S_n + C_{Rn}P_n] \frac{A \cdot 10000}{86400} (1 - k_{n+1}) + Q_n k_{n+1} \quad (4.1)$$

where Q = average daily discharge [$\text{m}^3 \text{s}^{-1}$]; C_S and C_R = runoff coefficients for snowmelt and rain [cm cm^{-1}]; α = degree-day factor [$\text{cm } ^\circ\text{C}^{-1} \text{ d}^{-1}$] indicating the snowmelt depth from one degree-day; T = number of degree-days [$^\circ\text{C d}$]; ΔT = the adjustment by temperature lapse rate when extrapolating the temperature from the station to the average hypsometric elevation of the basin or zone [$^\circ\text{C d}$]; S = ratio of SCA to total area of the basin or zone; P = precipitation contribution to runoff [cm]; A = area of the basin or zone [km^2]; k = recession coefficient representing the decline in discharge during a period without snowmelt or rainfall; n = sequence of days during the discharge computation period; and $10000/86400$ = conversion from $\text{cm} \cdot \text{km}^2 \text{d}^{-1}$ to $\text{m}^3 \text{s}^{-1}$ (Martinec et al., 2007). Equation 4.1 is written for a lag time of 18 hours between the daily temperature

cycle and resulting discharge cycle. In this case, the number of degree-days measured on the n^{th} day corresponds to discharge on the $n+1$ day.

SRM has eight model parameters (Table 4.1). These parameters can either be derived from measurement or estimated by hydrological judgment taking the basin characteristics, physical laws, and theoretical relations or empirical regression relations into account (Martinec and Rango, 1986). Many of the parameters are dynamic, evolving through both time and space (Hawkins, 2006; Martinec et al., 2007), which indicates that a single group of parameter values may not be applicable for all years.

Table 4.1. Parameters of the SRM (adapted from van Katwijk et al., 1993).

| Parameter | Symbol | Description |
|----------------------------|-------------------|---|
| Snow Runoff Coefficient | C_S | Coefficient representative of losses from snowmelt runoff |
| Rain Runoff Coefficient | C_R | Coefficient representative of the losses from rainfall runoff |
| Degree-Day Factor | α | Coefficient [$\text{cm } ^\circ\text{C}^{-1} \text{ d}^{-1}$] that converts the number of degree-days [$^\circ\text{C d}$] into the daily melt depth [cm] |
| Lapse Rate | γ | Factor that represents the change of temperature with elevation [$^\circ\text{C}/100\text{m}$]. |
| Critical Temperature | T_{CRIT} | Air temperature that is used to determine whether the measured or forecasted precipitation event is rain or snow. |
| Rainfall Contributing Area | RCA | Portion of the basin where the snowpack is considered ripe and will transmit rainfall through the snowpack on a given day. |
| Recession Coefficient | k | Coefficient representative of the decline in discharge during a period without snowmelt or rainfall. |
| Lag Time | L | Time before melt water appears as runoff |

4.2 METHODS

The SRM was used to simulate hydrographs at the Canyon Mouth from March 1 to September 30 for 2000-2006. Two model trials were used to assess model performance and application potential for streamflow forecasting. For the first trial, two model parameters were optimized for each year. To evaluate parameter variability and model sensitivity, the second trial used median parameter values from the initial trial. The model's ability to simulate observed hydrographs with a standard set of parameters across multiple years will help determine the feasibility of generating seasonal streamflow forecasts for the Cache la Poudre River with the SRM.

4.2.1 Data Processing and Preparation

For application of the SRM in the Cache la Poudre basin, the basin was divided into seven elevation zones of approximately 360 m (Figure 4.1). Characteristics of each zone are shown in Table 4.2. For each elevation zone, daily temperature, precipitation, and SCA were required as model inputs. Temperature and precipitation data were obtained from the NCDC Cooperative Observers (COOP) and NRCS SNOTEL networks for stations within or adjacent to the basin. Meteorological stations used to generate input data for the model are shown in Figure 4.1 and Table 4.3.

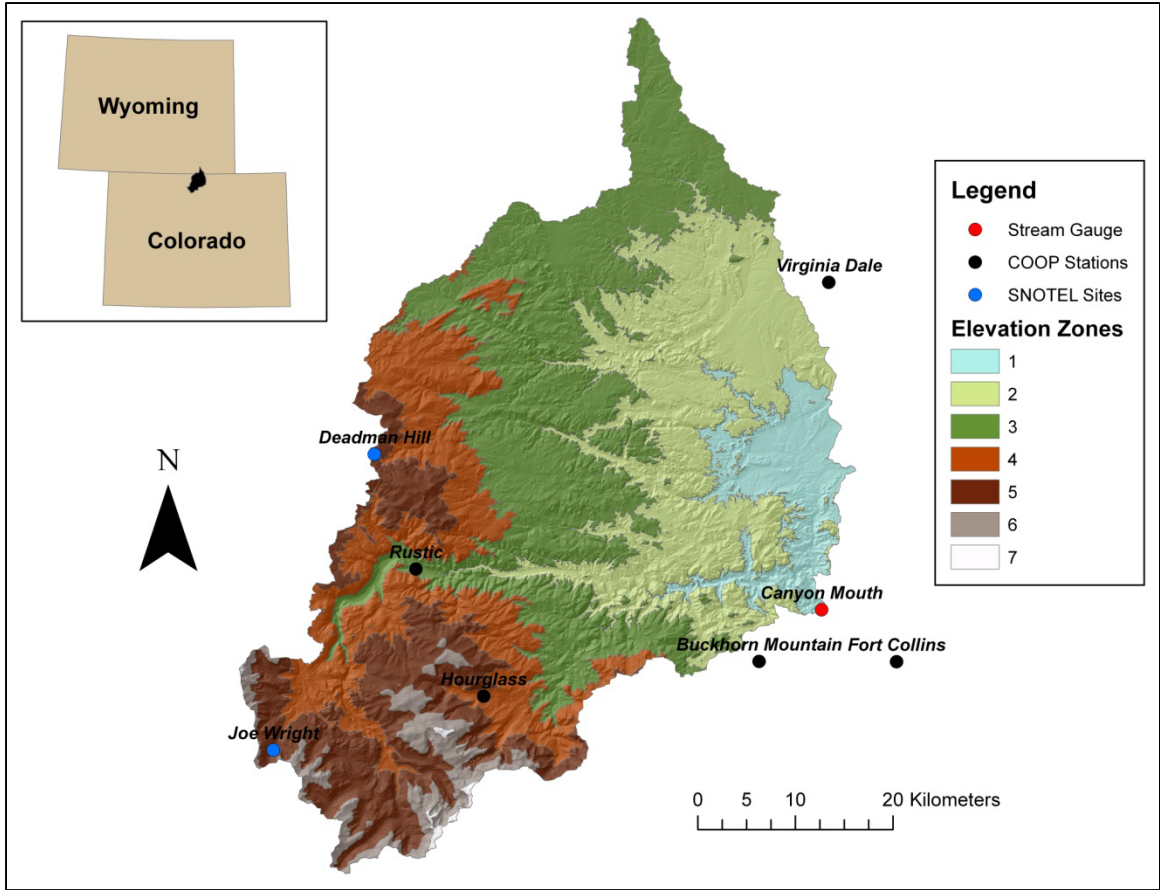


Figure 4.1. Location of elevation zones and meteorological stations used in configuration of the SRM for the Cache la Poudre basin.

Table 4.2. Elevation range and area for the seven elevation zones used in configuration of the SRM for the Cache la Poudre watershed above the Canyon Mouth.

| Elevation zone | Elevation (m) | | | Average | Area (km ²) |
|----------------|---------------|------|-------|---------|-------------------------|
| | Min | Max | Range | | |
| 1 | 1591 | 1953 | 362 | 1851 | 196 |
| 2 | 1954 | 2316 | 362 | 2150 | 671 |
| 3 | 2317 | 2679 | 362 | 2480 | 896 |
| 4 | 2680 | 3042 | 362 | 2861 | 471 |
| 5 | 3043 | 3405 | 362 | 3196 | 384 |
| 6 | 3406 | 3768 | 362 | 3522 | 104 |
| 7 | 3769 | 4125 | 356 | 3860 | 7 |

Table 4.3. Meteorological stations with daily temperature and precipitation data located within the Cache la Poudre basin used in application of the SRM.

| Name | ID | Type | Elevation (m) | Elevation Zone |
|-------------------|-----------|-------------|----------------------|-----------------------|
| Fort Collins | 53005 | COOP | 1525 | 1 |
| Virginia Dale | 58690 | COOP | 2138 | 2 |
| Buckhorn Mountain | 51060 | COOP | 2256 | 2 |
| Rustic | 57296 | COOP | 2347 | 3 |
| Hourglass | 54135 | COOP | 2902 | 4 |
| Joe Wright | 05J37S | SNOTEL | 3085 | 5 |
| Deadman Hill | 05J06S | SNOTEL | 3115 | 5 |

Daily temperature values for each elevation zone were calculated by averaging the daily temperature records for each meteorological station within a particular zone. Before averaging temperature values for all stations within an elevation zone, the individual station records were lapsed to the hypsometric mean elevation of the zone. To interpolate station temperatures to the hypsometric mean elevation of each zone, a lapse rate of 0.65°C per 100 m was applied as suggested in Martinec et al. (2007). Lapsing station temperatures to the mean elevation of each zone prior to model trials removes the ΔT term from Equation 4.1. For elevation zones with only one station (e.g., zones 1, 3, and 4), the lapsed daily temperature records for the individual station were used to represent temperature for the elevation zone. No temperature data were available for zones 6 and 7 due to an absence of meteorological stations within these high elevation zones. Therefore, temperatures were lapsed from zone 5 to generate temperature records for the two highest elevation zones.

Precipitation data for each elevation zone were estimated as the average of daily precipitation records for all meteorological stations within a zone. For zones with only

one meteorological station, data from the single station were used directly to represent precipitation for the elevation zone. For zones 6 and 7, where no precipitation data were available, daily precipitation values were estimated by multiplying precipitation data from the zone below by 1.035, or 3.5% (Hawkins, 2006; Martinec et al., 2007). This method was also used to estimate missing precipitation data for all elevation zones.

MODIS/Terra 8-day SCA images were used to generate snow cover depletion curves for each elevation zone. To minimize impairment of SCA observations due to cloud cover, SCA values were estimated for cloud-covered times and locations. If the images preceding and following a cloud impaired image were 100% snow covered for a given elevation zone, then SCA data for that zone were changed to 100%. If images preceding and following the cloud-impaired image were not 100% snow covered, then SCA values were estimated using linear interpolation between values for the preceding and following images. After adjusting SCA images for cloud impairment, daily SCA values for each zone were then derived using linear interpolation between the 8-day MODIS observations.

4.2.2 Model Parameterization and Calibration

Two trials were used to (1) generate parameter values through calibration and (2) investigate model sensitivity to parameter variability. For initial parameterization of the SRM, several assumptions were made to simplify configuration and application of the model. First, runoff coefficients for rain (C_R) and snowmelt (C_S) were assumed to be equal (Hawkins, 2006). This composite runoff coefficient (C) was held spatially constant for all elevation zones, but it was allowed to change through model optimization at 14-

day time intervals. The runoff coefficient accounts for melt water or rain that does not appear as runoff and is the primary candidate for adjustment if a runoff simulation is not successful (Martinec et al., 2007). For the initial model trial, runoff coefficients (C) were optimized by maximizing the Nash-Sutcliffe coefficient of efficiency (NSCE) for each seasonal simulation.

The degree-day factor (α) [$\text{cm } ^\circ\text{C}^{-1} \text{ d}^{-1}$] converts the number of degree-days (T) [$^\circ\text{C d}$] into the daily snowmelt depth (M) [cm] according to Equation 4.3 (Martinec et al., 2007).

(4.3)

$$M = \alpha \cdot T$$

Degree-day ratios generally increase during the snowmelt season (Martinec et al., 2007), and were evaluated by comparing degree-day values with the daily decrease in SWE at the Joe Wright SNOTEL site. Daily SWE and temperature records used for this procedure were averaged from 2000-2006. Daily melt (M) was estimated by relating the change in SWE to temperature and deriving the degree-day factor (Equation 4.3). The resultant degree-day values were smoothed using a 5-day moving average to minimize noise. The smoothed degree-day values were then averaged over the same 14-day periods used to vary runoff coefficients, resulting in a change in the degree-day factor every 14 days. Degree-day values used for all model trials are shown in Figure 4.2.

The recession coefficient (k) represents the decline in discharge during a period without snowmelt or rainfall (Martinec et al., 2007). The SRM model is particularly sensitive to this parameter as $(1 - k)$ is the proportion of daily meltwater that immediately

appears as runoff (Equation 4.1). The coefficient is not constant, but increases with decreasing discharge according to Equation 4.4 (Martinec et al., 2007).

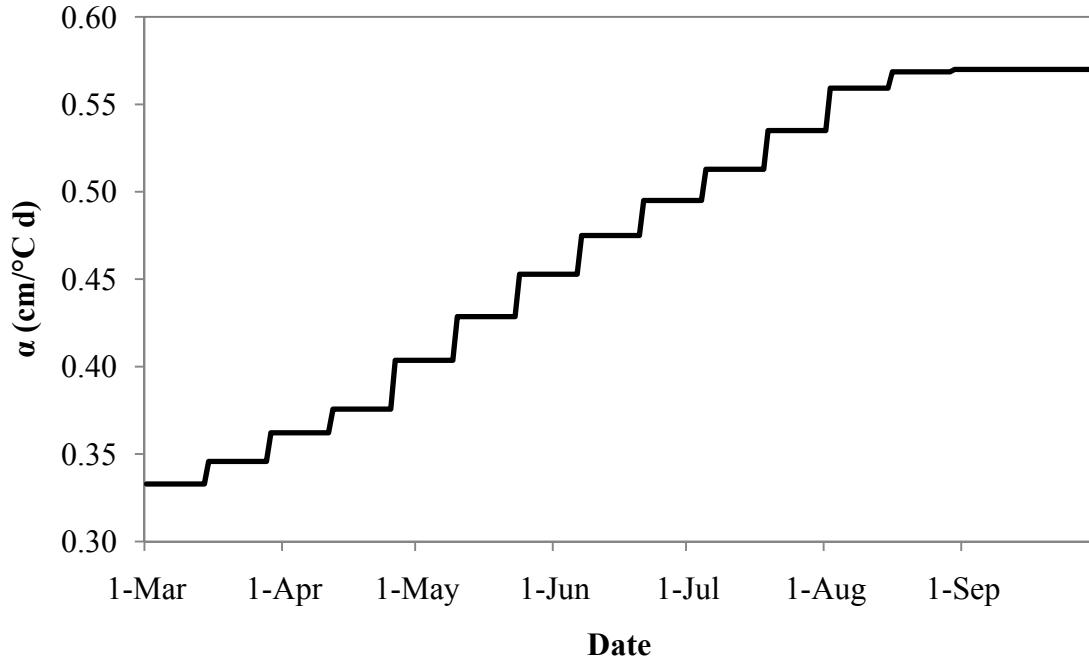


Figure 4.2. Degree-day factors (α) used in all trials of the SRM for the Cache la Poudre basin above the Canyon Mouth.

(4.4)

$$k_{n+1} = x \cdot Q_n^{-y}$$

where n refers to the time step, and x and y are constants. The constants, x and y , must be determined for the basin by solving the equations:

$$k_1 = x \cdot Q_1^{-y}$$

$$k_2 = x \cdot Q_2^{-y}$$

$$\log k_1 = \log x - y \cdot \log Q_1$$

$$\log k_2 = \log x - y \cdot \log Q_2$$

Analysis of historical data was used to obtain preliminary estimates of the recession coefficient. By plotting Q_{n+1} over Q_n , the envelope line and values of x and y were

derived for the basin to obtain preliminary estimates of the runoff coefficient (Figure 4.3) (Martinec and Rango, 1986). Following calibration of runoff coefficients, the preliminary x and y -values were adjusted with a separate optimization trial by again maximizing the NSCE for each seasonal simulation.

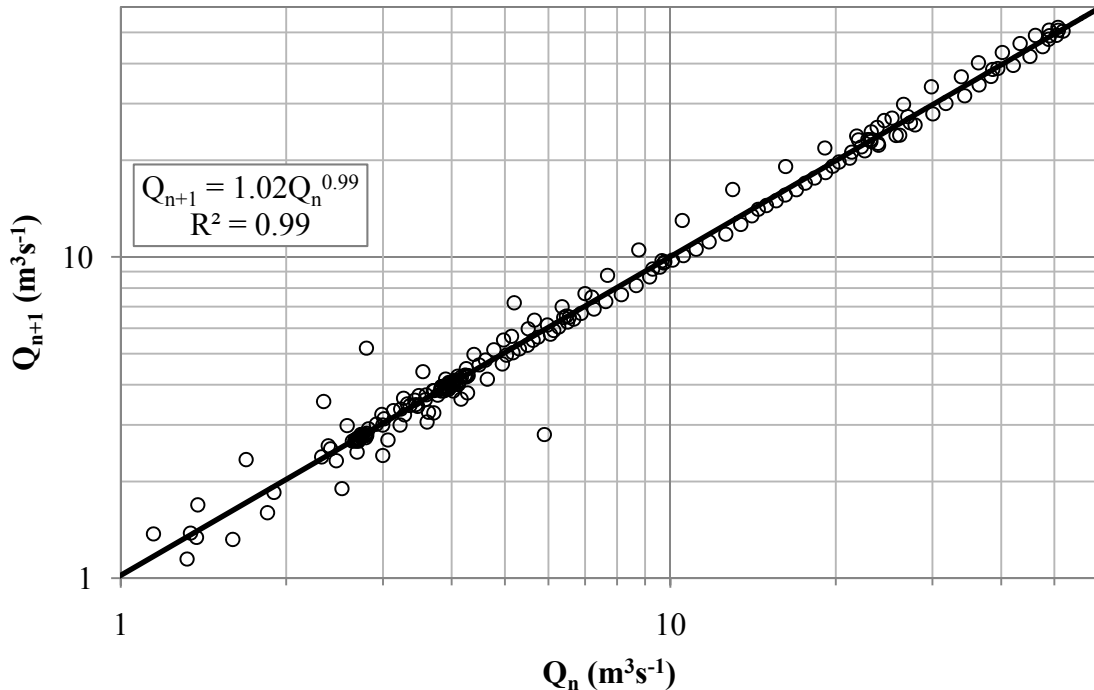


Figure 4.3. Envelope line used to obtain initial estimates of x and y -values to determine recession coefficient for the 2000 snowmelt season.

The remaining parameters, including lapse rate, critical temperature, rainfall contributing area, and lag time, were estimated with a series of assumptions and not used in model calibrations. The critical temperature (T_{CRIT}) is defined as the air temperature that is used to determine whether the measured or forecasted precipitation event is rain or snow (Martinec et al., 2007). T_{CRIT} is not included in Equation 4.1 and was not used in this initial application of the SRM, meaning that precipitation was not separated into rain and snow. However, T_{CRIT} was effectively set to 0°C by only totaling positive values of meltwater and rainfall output from individual elevations zones on a given day. The

rainfall contributing area (RCA) represents the portion of the basin where the snowpack is considered ripe and will transmit rainfall through the snowpack on a given day (Martinec et al., 2007). Similar to Hawkins (2006), this binary parameter was assumed to be 1 for all zones, meaning that all precipitation that fell during the simulation period was immediately transformed into runoff and not stored in the snowpack. Although lag-time can be estimated for a particular basin, the standard lag-time of 18 hours was used in application of the SRM for the Cache la Poudre basin.

Of the parameters described above, lapse rate, TCRIT, RCA, and lag time were assigned fixed values for all simulations. Degree-day factors were changed every 14 days, determined from historical data prior to model calibration, and did not vary between simulations or trials. Runoff coefficients were determined in the first model trial through model calibration at a 14-day time step. Recession coefficients were also determined through model calibration and calculated for each day in a simulation. Runoff and recession coefficients were determined, respectively, by optimizing the NSCE for each simulation in the initial trial with Microsoft Excel Solver which uses a Generalized Reduced Gradient (GRG2) algorithm for optimizing nonlinear problems (Microsoft, 2009). As a preliminary test of model sensitivity to parameter variability, the median values for runoff and recession coefficients generated during the initial trial were used as a standard set of parameters for all simulations in the second trial. Median values of x and y from the initial trial were used to derive recession coefficients for all simulations in the second model trial.

4.2.3 Model Evaluation

Two measures of model performance, the Nash-Sutcliffe coefficient of efficiency (NSCE) (Equation 4.5) and percentage difference (D_v) (Equation 4.6), were used to evaluate simulation results from both model trials.

(4.5)

$$NSCE = 1 - \frac{\sum_{i=1}^n (Q_i - Q'_i)^2}{\sum_{i=1}^n (Q_i - \bar{Q})^2}$$

where Q_i is observed daily discharge, Q'_i is modeled daily discharge, \bar{Q} is average daily discharge, and n is the number of daily discharge values.

(4.6)

$$D_v = \frac{V_R - V'_R}{V_R}$$

where V_R is the total measured runoff volume and V'_R is simulated runoff volume.

4.3 RESULTS

Initial simulations for the Cache la Poudre River at the Canyon Mouth were run for the snowmelt season (March 1 to September 30) by calibrating runoff and recession coefficients for each year in the study period. Results from the initial trial demonstrate good model performance when the model was calibrated independently for each snowmelt season (Table 4.4). For the initial trial, NSCE values were greater than 0.90 for all years, and D_v was less than 10% in all years but 2002.

Table 4.4. Nash-Sutcliffe coefficient of efficiency (NSCE) and percentage difference (D_v) for initial model trials where runoff and recession coefficients were optimized for each year.

| | 2000 | 2001 | 2002 | 2003 | 2004 | 2005 | 2006 |
|-------|------|------|------|------|------|------|------|
| NSCE | 0.96 | 0.97 | 0.93 | 0.90 | 0.94 | 0.97 | 0.96 |
| D_v | 6.1 | -0.1 | 13.2 | -0.6 | 1.7 | 1.0 | 2.6 |

The runoff coefficient was changed every fourteen days, and it was the first parameter to be calibrated during the initial model trial. Runoff coefficients generated from the initial model trial and median values used in the second model trial are shown in Figure 4.4. Median parameter values were selected for the second trial because average values produced biased estimates of runoff coefficients due to outliers on 1-March, 15-March, and 5-July (Figure 4.4). Conversely, the median value for 21-June may have underrepresented runoff coefficient values on this date. The recession coefficient was the second parameter to be calibrated during the initial model trial. The values of x and y used to determine recession coefficients for each year in the initial trial and median values used to calculate recession coefficients in the second trial are presented in Table 4.5. The resultant k -values from initial model simulations are shown in Figure 4.5.

Table 4.5. Values of x and y used to calculate recession coefficients for each year during the initial model trial and resultant median values used in the second model trial.

| Year | 2000 | 2001 | 2002 | 2003 | 2004 | 2005 | 2006 | Median |
|------|-------|-------|-------|-------|-------|-------|-------|--------|
| x | 1.00 | 1.00 | 1.00 | 1.00 | 0.98 | 0.99 | 0.97 | 1.00 |
| y | 0.013 | 0.013 | 0.015 | 0.015 | 0.007 | 0.008 | 0.004 | 0.013 |

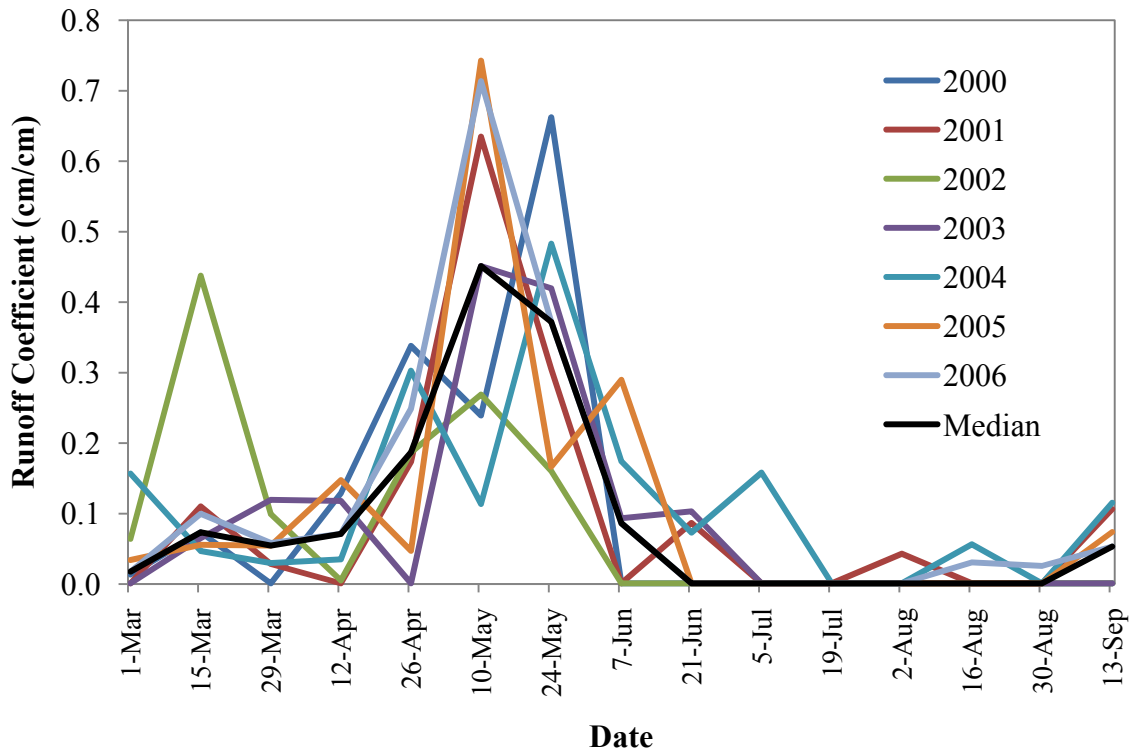


Figure 4.4. Range of optimized runoff coefficient values from the initial model trial for 2000-2006 simulations and median values used in the second model trial.

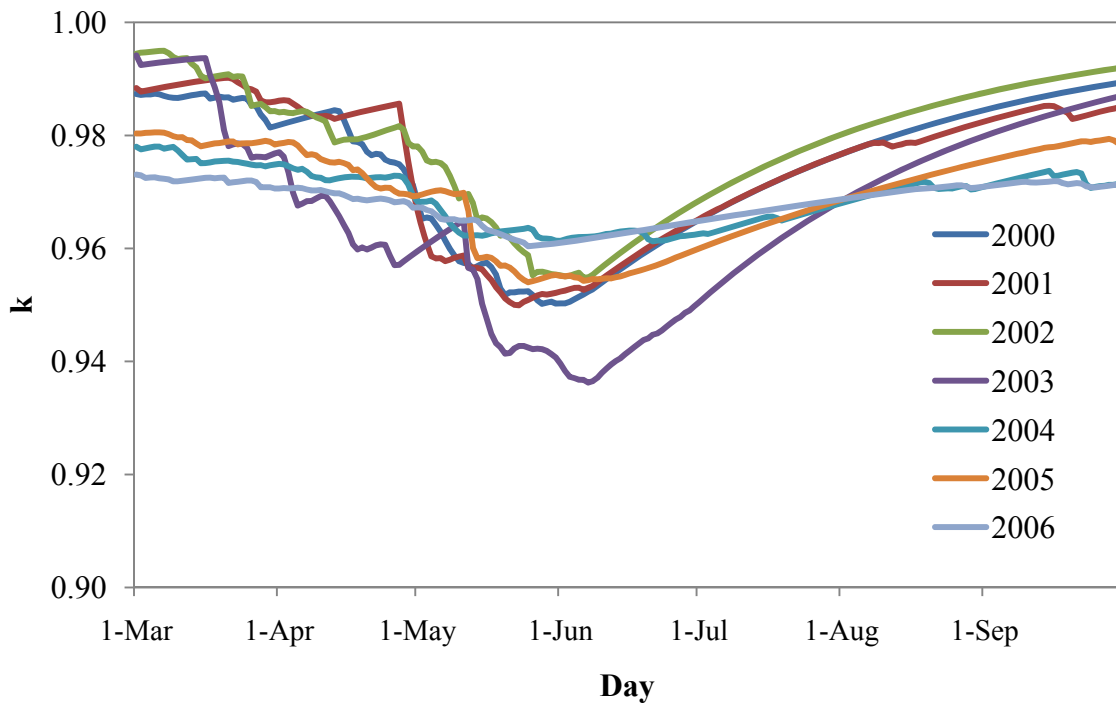


Figure 4.5. Optimized recession coefficients (k) used in the first model trial.

Compared to the first trial, model performance decreased for all simulations in the second trial (Table 4.6). For all years but 2002, the SRM still had a fair performance (NSCE > 0.7) using the standard parameter values. Percentage difference was less than 10% for five of the seven years in the second trial. Seasonal runoff was substantially overestimated in 2002 leading to volumetric overestimation of 77.1% and NSCE of -0.58 (Table 4.6). Results from the initial and second model trials are compared graphically in Appendix D.

Table 4.6. Nash-Sutcliffe coefficient of efficiency (NSCE) and percentage difference (D_v) for secondary model trials using median runoff and recession coefficients from the initial trial.

| | 2000 | 2001 | 2002 | 2003 | 2004 | 2005 | 2006 |
|-------|------|------|-------|------|------|------|-------|
| NSCE | 0.87 | 0.91 | -0.58 | 0.87 | 0.70 | 0.88 | 0.75 |
| D_v | 9.3 | 7.0 | 77.1 | 1.5 | -8.4 | -0.4 | -29.9 |

4.4 DISCUSSION

Runoff coefficients taken directly from the literature produced very poor simulations for the Cache la Poudre River. Therefore, runoff coefficients were generated through model calibration. While published values of runoff coefficients generally range between 0.6-1.0 and decrease throughout the snowmelt season (Martinec and Rango, 1986), optimized values of runoff coefficients for the first model trial ranged from 0.01-0.74, began to increase in mid-April, and peaked around the middle of May (Figure 4.4). This temporal trend resembled the rising limb of the hydrograph, although the hydrograph generally peaked around the beginning of June. From mid-May to mid-June, runoff coefficients decreased which again resembled the shape of the hydrograph except that the decrease in runoff coefficients preceded the receding limb of the hydrograph,

which generally extended from early June into August. The temporal variability in calibrated runoff coefficients was similar to results reported by Hawkins (2006) for the Salt-Verde system, Arizona, although the magnitude of runoff coefficients was greater for the Cache la Poudre system than those reported for the Salt-Verde system.

When the SRM was calibrated using spatially uniform parameter values, more runoff was simulated from middle elevations with less snowpack than higher elevations with deep snowpack due to larger areas and higher degree day values at middle elevations. Using average daily air temperature fails to capture melt events that may have occurred during the afternoons at higher elevations. Snow cover analyses in Chapter 3 indicated that the majority of snowmelt runoff is generated from higher elevations in the Cache la Poudre basin. This suggests that the SRM did not capture the magnitude of snowmelt from higher elevations, and more accurate representation of spatial variability in snowmelt runoff with SRM would likely require assigning different runoff coefficients to each elevation zone. In addition, the SRM does not partition runoff into groundwater and surface water components (i.e., the model does not represent the physical processes that govern runoff generation). Rather, the model treats the entire runoff process conceptually, enabling representation of snowmelt runoff with minimal parameter requirements.

Snowmelt and precipitation events did not increase runoff during hydrograph recession, as the SRM generally produced a smooth receding limb devoid of noise (Figures D.1 to D.14). This suggests that runoff simulations were most sensitive to runoff coefficients during hydrograph rise and to recession coefficients during hydrograph recession. As $(1 - k)$ is the proportion of daily meltwater that immediately appears as

runoff, recession coefficients decreased during hydrograph rise and increased during hydrograph recession (Figure 4.5), resembling the shape of an inverse hydrograph.

The SRM simulated seasonal hydrographs with good performance ($NSCE > 0.9$) for all years in the initial model trial (Table 4.4). Calibrating runoff and recession coefficients for individual seasons produced relatively accurate simulations of snowmelt runoff despite variability in precipitation, temperature, and snow cover depletion between years. The good model performance may be partially attributed to the procedure used to generate naturalized flow records. The 7-day moving average used for naturalized flow records produced relatively smooth hydrographs devoid of noise. When calibrated to this smoothed naturalized hydrograph, SRM can reproduce the dominant snowmelt runoff signal for every season, suggesting that this relatively simple model successfully captures the important processes that produce discharge in the Cache la Poudre basin.

The model's ability to simulate seasonal hydrographs across a range of years using a standard set of parameters was evaluated in the second trial. For the second trial, model performance decreased for all years when compared to the first trial. However, model performance was still good ($NSCE > 0.85$) in four of seven years and fair ($NSCE > 0.7$) in six of seven years using the standard set of parameters (Table 4.6). Two years, 2002 and 2005, serve as examples demonstrating sources of variability in model performance when using standard parameters for every year. In 2002, although the shape of the hydrograph was captured, runoff was significantly overestimated in the second model trial (Figure 4.6). Annual water yield for 2002 at the Canyon Mouth was the lowest recorded in 127 years of record. The substantial overestimation of runoff for the 2002 simulation was due to runoff coefficients that were too large. This suggests that

median parameter values should produce reasonably accurate simulations of seasonal streamflow in average WYs. However, a standard set of parameters may significantly overestimate runoff in particularly dry years similar to 2002. As no years with above average runoff were observed during the study period, model performance in wetter years using a standard set of parameters is uncertain.

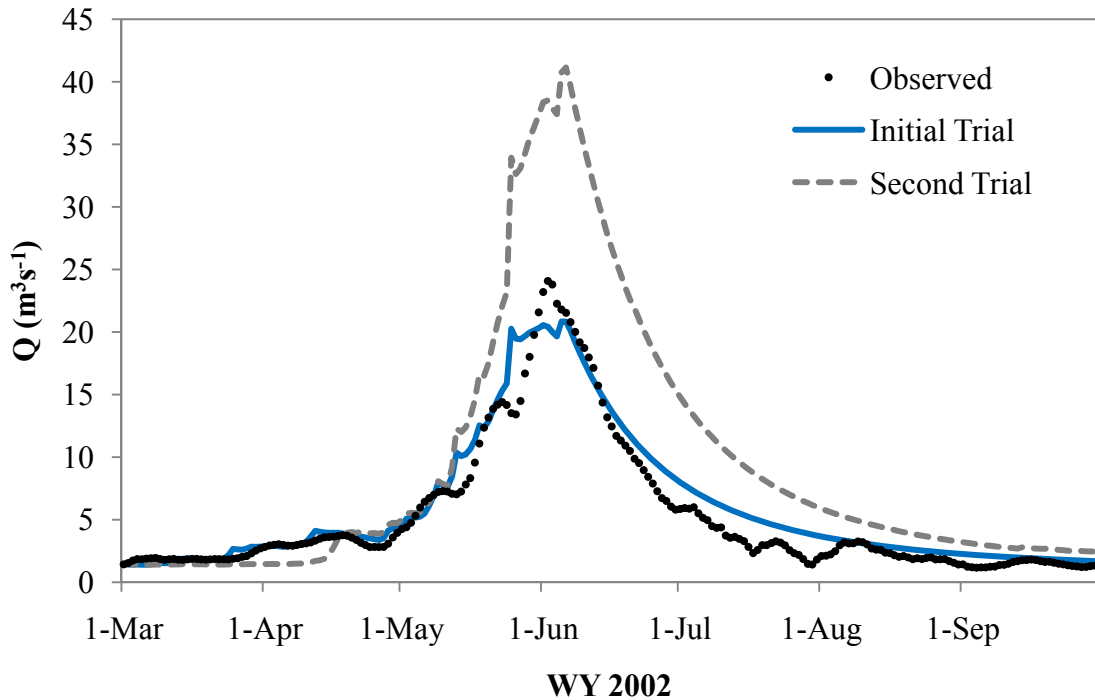


Figure 4.6. Comparison of observed and simulated hydrographs at the Canyon Mouth for the two model trials during the 2002 snowmelt season.

In contrast to 2002, 2005 was an average year for runoff at the Canyon Mouth (Figure 1.1). For 2005, the model produced accurate results in both the initial trial (NSCE = 0.97; $D_v = 1.0$) and second trial (NSCE = 0.88; $D_v = -0.4$). Although the model accurately captured the volume of runoff using the median set of parameters, the shape of the hydrograph was poorly represented (Figure 4.7). Three distinct peaks were observed in the 2005 naturalized hydrograph. The SRM captured two of these peaks in the initial

trial, but only simulated one peak in the second trial that was approximately 25% larger than the observed peak (Figure 4.7). Although the volume of runoff was accurately simulated with the median set of parameters in 2005, the timing and magnitude of peak flow was not captured. Results from 2002 and 2005 demonstrate that the model is highly sensitive to the value of runoff coefficients, so inappropriate selection of runoff coefficients may cause significant over- or under-estimation of runoff volume and timing.

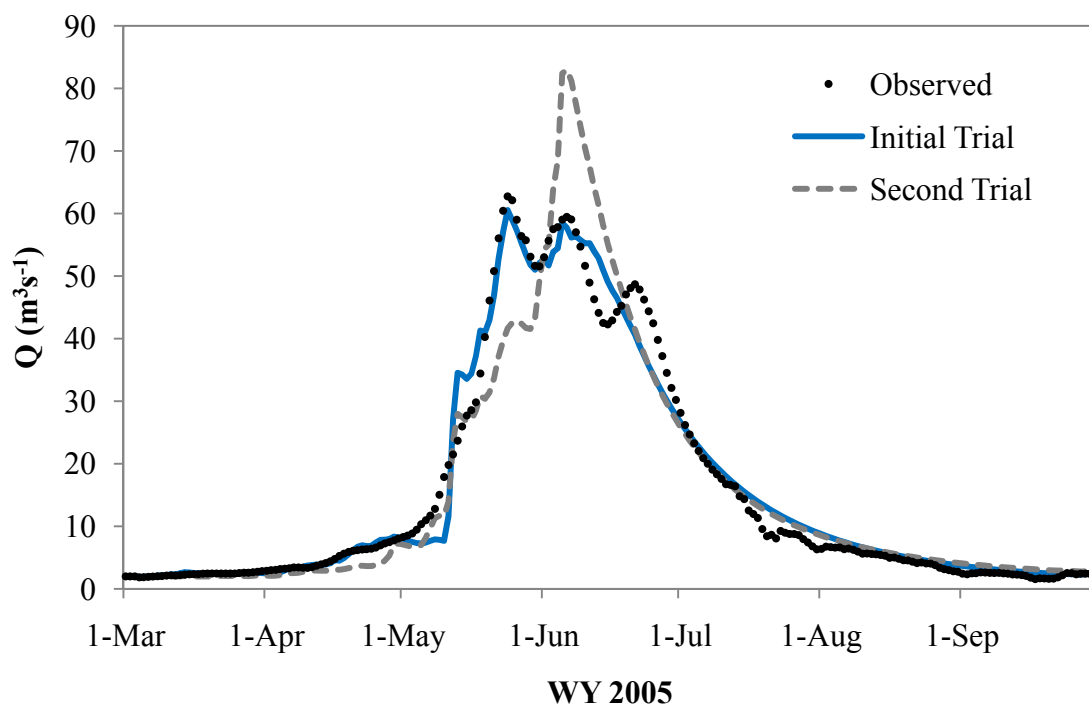


Figure 4.7. Comparison of observed and simulated hydrographs at the Canyon Mouth for the two model trials during the 2005 snowmelt season.

Future research will test whether SRM is a suitable model structure for flow forecasting in the Cache la Poudre basin. Model trials for the thesis were not divided into calibration and verification subsets due to the limited number of years included in the study period. Future work will use 2007-2009 to test model performance on a dataset that was not utilized during model calibration. These preliminary calibration results suggest

the model has potential, but appropriate selection of runoff coefficients and input data will be necessary to take the SRM from simulation to forecasting mode. Future selection of runoff coefficients could be improved by identifying relationships to hydrologic variables, such as SWE. Forecasts of input variables (precipitation, temperature, and snow cover depletion) for each elevation zone will also be necessary to generate streamflow forecasts with the SRM. Other model configurations could also be tested to identify optimum combinations of model subunits. For example, the basin could be partitioned into a network of sub-basins and each sub-basin divided into elevation zones. This form of subdivision would enable accounting for greater spatial variability in precipitation and snow cover.

4.5 CONCLUSIONS

The SRM was used to simulate hydrographs for the Cache la Poudre River at the Canyon Mouth during the snowmelt season from 2000-2006. Two trials were used to evaluate model performance. For the initial trial, runoff and recession coefficients were calibrated for each year generating a range of parameter values. To evaluate model sensitivity to a standard set of parameters, the median values for runoff and recession coefficients from the initial trial were used for all simulations in the second trial. The SRM simulated seasonal hydrographs with good performance in the initial model trial ($NSCE > 0.9$), suggesting that the structure of this model is well-suited for simulating discharge in the Cache la Poudre basin. Although model performance decreased for all years in the second trial, the SRM produced satisfactory results ($NSCE > 0.7$) in six of the seven years using median parameters values from the initial trial. This suggests that

the SRM could be used to generate seasonal streamflow forecasts given appropriate selection of parameter values and input variables. Future research is focused on developing relationships between hydrologic variables and SRM parameters to inform selection of runoff and recession coefficients.

CHAPTER 5: CONCLUSIONS

This study was undertaken to analyze how variability in runoff production in the Cache la Poudre basin relates to climate. The objectives of this thesis were to: (1) develop a naturalized flow record for the Cache la Poudre River and determine the effects of flow modification on the magnitude and timing of discharge; (2) analyze relationships between snow cover distributions and naturalized discharge to identify important areas for runoff production; and (3) evaluate the ability of the Snowmelt Runoff Model (SRM) to simulate seasonal hydrographs at a daily time step for the Cache la Poudre River.

Flow modification reduced discharge at the Canyon Mouth at both annual and seasonal time scales for the study period. The amount of water diverted from the river during 2000-2006 was over double that of foreign water inputs from trans-basin diversions. The net effect of reservoir operations on discharge varied seasonally and led to both increased and decreased flows at the Canyon Mouth. Reservoir operations generally decreased flow during hydrograph rise and increased flow during hydrograph recession. The combined effects of diversions, foreign water, and reservoir operations led to a shift in hydrograph timing by as much as two weeks, according to hydrograph quantiles. Shifts in streamflow timing of this magnitude could easily mask any trends in runoff response caused by climate changes in basins with modified drainage networks such as the Cache la Poudre.

The mountain snowpack that generates streamflow can have high spatial variability. In basins like the Cache la Poudre, point snow measurements may be insufficient for determining climate-induced changes in snowmelt and runoff. Snow covered area (SCA) is an easily observable snow variable that can characterize snowpack properties at a range of spatial scales. This makes it a useful addition to long-term hydro-climate monitoring networks, as it can supplement sparsely distributed point-scale snow measurements. The MODIS-derived SCA products provide a means to monitor the snowpack at a range of elevations to determine spatial variability in climate sensitivity. In the Cache la Poudre basin, middle elevations (2680 to 3042 m) exhibited the strongest correlation between snow depletion and hydrograph rise, which suggests that monitoring snow cover at these elevations could aid in streamflow forecasting. Analysis of snow cover probability and PRISM datasets confirm that a small portion of the watershed at or above this middle elevation zone generates the majority of snowmelt runoff for the Cache la Poudre River. Investigating the relationship between snow cover and discharge for different stream gauges over a range of elevations and scales could further characterize spatial variability in snowmelt runoff, particularly for the area at or above the mid-elevation transition zone. Due to the influence of elevation on precipitation and snowmelt in mountainous regions, snow measurements should be collected along elevation gradients that include both high elevations with deep snowpack and transitional zones at middle elevations to improve runoff prediction in snowmelt dominated basins.

To test how the distributed SCA data could aid in snowmelt runoff prediction, the Snowmelt Runoff Model (SRM) was used to simulate hydrographs for the Cache la Poudre River at the Canyon Mouth during the snowmelt season from 2000-2006. Two

trials were used to evaluate model performance. Runoff and recession coefficients were calibrated for each year in the initial trial generating a range of parameter values. To evaluate model sensitivity to a standard set of parameters, median values for runoff and recession coefficients from the initial trial were used for all simulations in a second simulation trial. The SRM simulated seasonal hydrographs with good model performance ($NSCE > 0.9$) for all years in initial model trial. Although model performance decreased for all simulations in the second trial, the SRM produced fair results ($NSCE > 0.7$) in six of the seven years using the median parameters values. This suggests that the SRM could be used to generate seasonal streamflow forecasts given appropriate selection of parameter values and input variables. When the SRM was assigned spatially uniform parameter values, more runoff was generated from middle elevations below the deep snowpack at higher elevations that generates the majority of snowmelt runoff. Future research will test methods of assigning spatially variable parameters to examine whether the SRM can reproduce spatial patterns in runoff providing a stronger link between this conceptual model and the physical processes that govern snowmelt.

The analyses in this thesis point to the utility of snow cover data and the Snowmelt Runoff Model in representing runoff generation in the Cache la Poudre basin. Because analyses were restricted to the 2000-2006 study period, when both naturalized flow and MODIS snow cover data could be obtained, results likely do not capture the total range of hydrologic behavior possible for the Cache la Poudre basin. All but one of years analyzed had below average snowpack, and five of the seven years had below average annual water yield. None of years included in the study period would be considered “good” years for annual water yield. In addition, the uncertainty regarding

accuracy of naturalized flow records and lack of real time snow cover data could limit application of the SRM in the Cache la Poudre basin. However, continued monitoring and analysis of snow cover should further elucidate variability in relationships between snow cover and snowmelt runoff for a range of hydrological and climatic conditions, and quantify uncertainty in snowmelt simulations and forecasts with the SRM.

In the Cache la Poudre, snowmelt runoff during the study period was generated from a small portion of the basin located from middle to high elevations. Land use activities and natural disturbances, such as fire or infestation, in this area could affect snow accumulation and melt, thereby altering snowmelt runoff and water yields. Future research in the basin could use snow cover data to characterize snow behavior in areas with different land uses to help distinguish between climate and land cover controls on snowpack variability. In other basins, snow cover data may also prove to be a useful data source, particularly in areas without *in situ* monitoring. Probability of snow datasets provide a means to analyze general snow distribution patterns and identify additional sites for *in situ* snowpack monitoring. The rather simple and empirical Snowmelt Runoff Model can simulate snowmelt runoff fairly successfully using snow cover and temperature as the major driving variables. These conclusions all point to the utility of snow cover data for both monitoring snowpack characteristics and modeling snowmelt runoff in mountain basins. Therefore, long term snow cover datasets would be advantageous for water resources management and planning in snowmelt dominated basins.

REFERENCES

- Andreadis, K.M., and D.P. Lettenmaier. 2006. Assimilating remotely sensed snow observations into a macroscale hydrology model. *Advances in Water Resources* 29: 872-886.
- Bales, R.C., N.P. Molotch, T.H. Painter, M.D. Dettinger, R. Rice, and J. Dozier. 2006. Mountain hydrology of the western United States. *Water Resources Research* 42: W08432, doi: 10.1029/2005WR004387.
- Balk, B., and K. Elder. 2000. Combining binary decision tree and geostatistical methods to estimate snow distribution in a mountain watershed. *Water Resources Research* 36: 13-26.
- Barnett, T.P., D.W. Pierce, H.G. Hidalgo, C. Bonfils, B.D. Santer, T. Das, G. Bala, A.W. Wood, T. Nozawa, A.A. Mirin, and M.D. Dettinger. 2008. Human-induced changes in the hydrology of the western United States. *Science* 319: 1080-1083.
- Clark, M.P., A.G. Slater, A.P. Barrett, L.E. Hay, G.J. McCabe, B. Rajagopalan, and G.H. Leavesley. 2006. Assimilation of snow covered area information into hydrologic and land surface models. *Advances in Water Resources* 29: 1209-1221.
- Cline, D.W., R.C. Bales, and J. Dozier. 1998. Estimating the spatial distribution of snow in mountain basins using remote sensing and energy balance modeling. *Water Resources Research* 34(5): 1275-1285.
- Dingman, S.L. 2002. Snow and snowmelt. In *Physical Hydrology*: 166-219. Long Grove, Illinois: Waveland Press, Inc.
- Doesken, N.J., and A. Judson. 1996. *The Snow Booklet: A Guide to the Science, Climatology, and Measurement of Snow in the United States*. Department of Atmospheric Sciences, Colorado State University, Fort Collins, CO.
- Dozier, J., and T.H. Painter. 2004. Multispectral and hyperspectral remote sensing of alpine snow properties. *Annual Review of Earth and Planetary Sciences* 32: 465-494. doi: 10.1146/annurev.earth.32.101802.120404.

- Dressler, K.A., G.H. Leavesley, R.C. Bales, and S.R. Fassnacht. 2006. Evaluation of gridded snow water equivalent and satellite snow cover products for mountain basins in a hydrologic model. *Hydrological Processes* 20: 673-688.
- Fassnacht, S.R., K.A. Dressler, and R.C. Bales. 2003. Snow water equivalent interpolation for the Colorado River Basin from snow telemetry (SNOTEL) data. *Water Resources Research* 39(8): 1208, doi:10.1029/2002WR001512.
- Ferguson, R.I. 1999. Snowmelt runoff models. *Progress in Physical Geography* 23(2): 205-227.
- Gómez-Landesa, E., and A. Rango. 2002. Operational snowmelt runoff forecasting in the Spanish Pyrenees using the snowmelt runoff model. *Hydrological Processes* 16: 1583-1591.
- Hall, D.K., G.A. Riggs, and V.V. Salomonson. 2006, updated weekly. MODIS/Terra snow cover 8-day L3 global 500m grid V005, 14-Mar-2000 to 10-June-2006. Boulder, Colorado USA: National Snow and Ice Data Center. Digital media.
- Hawkins, T.W. 2006. Parameterization of the Snowmelt Runoff Model for the Salt-Verde system, Arizona during drought conditions. *Journal of the Arizona-Nevada Academy of Science* 38(2): 66-73.
- Jain, S., and U. Lall. 2000. Magnitude and timing of annual maximum floods: Trends and large-scale climatic associations for the Blacksmith Fork River, Utah. *Water Resources Research* 36(12): 3641-3651.
- Knowles, P., M.D. Dettinger, and D.R. Cayan. 2006, Trends in snowfall versus rainfall in the western United States. *Journal of Climate*. 19: 4545-4559.
- Lee, S., A.G. Klein, and T.M. Over. 2005. A comparison of MODIS and NOHRSC snow-cover products from simulating streamflow using the Snowmelt Runoff Model. *Hydrological Processes* 19: 2951-2972.
- Liston, G.E. 1999. Interrelationships among snow distribution, snowmelt, and snow cover depletion: implications for atmospheric, hydrologic, and ecologic modeling. *Journal of Applied Meteorology* 38: 1474-1487.
- Martinec, J. 1975. Snowmelt-runoff model for stream flow forecasts. *Nordic Hydrology* 6: 145-154.
- Martinec, J., and A. Rango. 1986. Parameter values for snowmelt runoff modeling. *Journal of Hydrology* 84: 197-219.

- Martinec, J., A. Rango, and R. Roberts. 2007. Snowmelt Runoff Model User's Manual, Updated Edition 2007, WinSRM Version 1.11. USDA Jornada Experimental Range, New Mexico State University, Las Cruces, NM 88003, U.S.A.
- Maurer, E.P., J.D. Rhoads, R.O. Dubayah, and D.P. Lettenmaier. 2003. Evaluation of the snow-cover area data product from MODIS. *Hydrological Processes* 17: 59-71.
- McGuire, M., A.W. Wood, A.F. Hamlet, D.P. Lettenmaier. 2006. Use of satellite data for streamflow and reservoir storage forecasts in the Snake River basin. *Journal of Water Resources Planning and Management* 132(2): 97-110.
- Microsoft (Internet). 2009. Solver uses generalized reduced gradient algorithm, © 2009. Cited 13-Jul-2009. Available at <http://support.microsoft.com/kb/82890>.
- Molotch, N.P., and S.A. Margulis. 2008. Estimating the distribution of snow water equivalent using remotely sensed snow cover data and a spatially distributed snowmelt model: A multi-resolution, multi-sensor comparison. *Advances in Water Resources* 31: 1503-1514.
- Moore, J.N., J.T. Harper, and M.C. Greenwood. 2007. Significance of trends toward earlier snowmelt runoff, Columbia and Missouri Basin headwaters, western United States. *Geophysical Research Letters* 34(L16402). doi10.1029/2007GL031022.
- Mote, P.W., A.F. Hamlet, M.P. Clark, and D.P. Lettenmaier. 2005. Declining mountain snowpack in western North America. *Bulletin of the American Meteorological Society* 86(1): 39-49. doi: 10.1175/BAMS-86-1-39.
- Nagler, T., H. Rott, P. Malcher, and F. Müller. 2008. Assimilation of meteorological and remote sensing data for snowmelt runoff forecasting. *Remote Sensing of Environment* 112: 1408-1420.
- Rango, A., and V. van Katwijk. 1990. Development and testing of a snowmelt-runoff forecasting technique. *Water Resources Bulletin* 26(1): 135-144.
- Rango, A., and J. Martinec. 1995. Revisiting the degree-day method for snowmelt computations. *Water Resources Bulletin* 31(4): 657-669.
- Rees, W.G. 2006. Chapter 5: Remote sensing of snow cover, in *Remote Sensing of Snow and Ice*: pp.137-156. Taylor & Francis Group, Boca Raton, Florida.
- Regonda, S.K., B. Rajagopalan, M. Clark, and J. Pitlick. 2005. Seasonal cycle shifts in hydroclimatology over the western United States. *Journal of Climate* 18: 372-384.
- Rood, S.B., J. Pan, K.M. Gill, C.G. Franks, G.M. Samuelson, and A. Sheperd. 2008. Declining summer flows of Rocky Mountain rivers: changing seasonal hydrology and

- probable impacts on floodplain forests. *Journal of Hydrology* 349: 397-410. doi: 10.1016/j.jhydrol.2007.11.012.
- Seidel, K., and J. Martinec. 2004. *Remote Sensing in Snow Hydrology: Runoff Modelling, Effect of Climate Change*: 150 pp. Praxis Publishing Ltd, Chichester, UK.
- Singh, V.P., and D.A. Woolhiser. 2002. Mathematical modeling of watershed hydrology. *Journal of Hydrologic Engineering* 7(4): 270-292.
- Smith, R.S., R.A. Scherer, and D.A. Dobson. 2008. Snow cover extent during spring snowmelt in the south-central interior of British Columbia. *BC Journal of Ecosystems and Management* 9: 57-70.
- Soncini-Sessa, R., and M. Volta. 2005. One-year long runoff forecast by a single snowpack evaluation. *Hydrological Processes* 19: 1419-1430.
- Stewart, I.T., D.R. Cayan, and M.D. Dettinger. 2004. Changes in snowmelt runoff timing in western North America under a 'Business as Usual' climate change scenario. *Climate Change* 62: 217-232.
- Stewart, I.T., D.R. Cayan, and M.D. Dettinger. 2005. Changes toward earlier streamflow timing across western North America. *Journal of Climate* 18: 1136-1155.
- Stewart, I.T. 2009. Changes in snowpack and snowmelt runoff for key mountain regions. *Hydrological Processes* 23: 78-94.
- Tekeli, A.E., Z. Akyurek, A.A. Sorman, A. Sensoy, and A.U. Sorman. 2005. Using MODIS snow cover maps in modeling snowmelt runoff process in the eastern part of Turkey. *Remote Sensing of Environment* 97: 216-230.
- van Katwijk, V.F., A. Rango, and A.E. Childress. 1993. Effects of simulated climate change on snowmelt runoff modeling in selected basins. *Water Resources Bulletin* 29: 755-766.
- Zhou, X., H. Xie, and J.M.H. Hendrickx. 2005. Statistical evaluation of remotely sensed snow-cover products with constraints from streamflow and SNOTEL measurements. *Remote Sensing and the Environment* 94: 214-231.

APPENDIX A: HYDROLOGIC DATASET

The compilation and analysis of a hydrologic dataset for the Cache la Poudre was necessary for completion of this thesis. The dataset includes spatial (Table A.1), temporal (Table A.2), and spatiotemporal data (Table A.3). Spatial data were derived using ArcGIS 9.3 or downloaded and incorporated into the GIS dataset. Hydrometric and meteorological data were obtained from a variety of sources. Streamflow data were obtained from the US Geological Survey (USGS), Colorado Division of Water Resources (CDWR), and Northern Colorado Water Conservancy District (NCWCD). Precipitation and temperature data were obtained from the National Resources Conservation Service (NRCS) and the National Climatic Data Center (NCDC).

Moderate Resolution Imaging Spectroradiometer (MODIS) snow cover products were downloaded and processed to analyze SCA depletion within the Cache la Poudre basin during the snowmelt season. Due to the limited availability of the MODIS snow covered area product, which became operational in 2000, the temporal dataset was condensed to water years (WY) 2000-2006 for all analyses, with the water year beginning October 1 and ending September 30. Land cover, elevation, and PRISM-derived precipitation for the Cache la Poudre basin are shown in Figure A.1, A.2, and A.3, respectively.

Table A.1. Spatial data obtained for compilation of the Cache la Poudre hydrologic dataset.

| Description | Source |
|--|--|
| Digital Elevation Model (DEM) | USGS EROS Data Center http://edc.usgs.gov |
| Basin and sub-basin boundaries | Derived from DEM in ArcGIS 9.3 |
| Hydrology raster datasets: flow direction, flow accumulation, sink-filled DEM, and sinks | Derived with Hydrology Tools in ArcGIS 9.3 |
| Stream networks | (1) Derived from DEM in ArcGIS 9.3 (2) USGS National Hydrography Dataset http://nhd.usgs.gov/ |
| Water bodies | USGS National Hydrography Dataset http://nhd.usgs.gov/ |
| National Land Cover Dataset 2001 | USGS Land Cover Institute http://landcover.usgs.gov |
| National Cooperative Soil Survey | NRCS http://soils.usda.gov/survey/geography/ |
| Roads: local, major, and highways | Colorado Department of Transportation (CDOT) http://www.dot.state.co.us |
| Cities, counties, and state boundaries | USGS Seamless Data Distribution Center http://seamless.usgs.gov |
| SNOTEL site locations | NRCS http://www.wcc.nrcs.usda.gov/snow/ |
| Stream gauge locations | USGS http://waterdata.usgs.gov/nwis/sw |

Table A.2. Temporal data obtained for compilation of the Cache la Poudre hydrologic dataset. Parentheses indicate period of record.

| Description | Source |
|--|---|
| Average daily discharge for: | USGS |
| <ul style="list-style-type: none"> • South Fork Cache la Poudre River near Rustic (1956-1979) • South Fork Cache la Poudre River near Eggers (1929-1931) • Fall Creek near Rustic (1960-1973) • Cache la Poudre River near Log Cabin (1909-1931) • Cache la Poudre River near Rustic (1956-1968) • Cache la Poudre River at Chambers Lake Outlet (1929-1931) • Cache la Poudre River above Boxelder Creek near Timnath (1979-Present) • Cache la Poudre River at Fort Collins (1975-Present) • North Fork Cache la Poudre River at Livermore (1986-Present) • North Fork Cache la Poudre River below Halligan Reservoir (1998-Present) • Joe Wright Creek below Joe Wright Reservoir (1978-Present) • Joe Wright Creek above Joe Wright Reservoir (1978-Present) • Cache la Poudre River at Canyon Mouth (1881-Present) | http://waterdata.usgs.gov/nwis/sw ; CDWR http://water.state.co.us/pubs/datasearch.asp |
| Un-depleted monthly discharge for: | NCWCD |
| <ul style="list-style-type: none"> • Cache la Poudre River at Canyon Mouth (1950-2007) | |
| Un-depleted daily discharge for: | CDWR and NCWCD |
| <ul style="list-style-type: none"> • Cache la Poudre River at Canyon Mouth (2000-2006) | |
| Daily snow water equivalent, cumulative precipitation, average temperature, minimum temperature, and maximum temperature for: | NRCS |
| <ul style="list-style-type: none"> • Joe Wright SNOTEL Site (1978-Present) • Deadman Hill SNOTEL Site (1978-Present) • Lake Irene SNOTEL Site (1978-Present) • Willow Park SNOTEL Site (1979-Present) | http://www.wcc.nrcs.usda.gov/snow |

| | |
|---|---|
| Daily precipitation, average temperature, minimum temperature, and maximum temperature for: | NCDC http://www.ncdc.noaa.gov/oa/ncdc.html |
| <ul style="list-style-type: none"> • Hourglass COOP Station (1988-Present) • Fort Collins COOP Station (1937-Present) • Buckhorn Mountain 1e COOP Station (1988-Present) • Rustic 9wsw COOP Station (1991-Present) • Virginia Dale 7 ENE COOP Station (1995-Present) | |

Table A.3. Spatiotemporal data obtained for compilation of the Cache la Poudre hydrologic dataset.

| Description | Source |
|--|---|
| MODIS/Terra 8-day Maximum Snow Extent (i.e. snow covered area) from mid-March through June (2000-2006) | EOS Data Gateway http://nsidc.org/~imswww/pub/imswelcome/index.html |
| Parameter-elevation Regressions on Independent Slopes Model (PRISM) datasets for average annual precipitation, monthly precipitation, and average, maximum, and minimum annual temperature | U.S. Department of Agriculture (USDA) Geospatial Gateway http://datagateway.nrcs.usda.gov/GatewayHome.html |
| Probability of snow and cloud for the snowmelt season (i.e., all 90 images used in analyses from 2000-2006), each year in the study period, and as a time series at 8-day intervals | Derived from 8-day MODIS images in ArcGIS 9.3 |

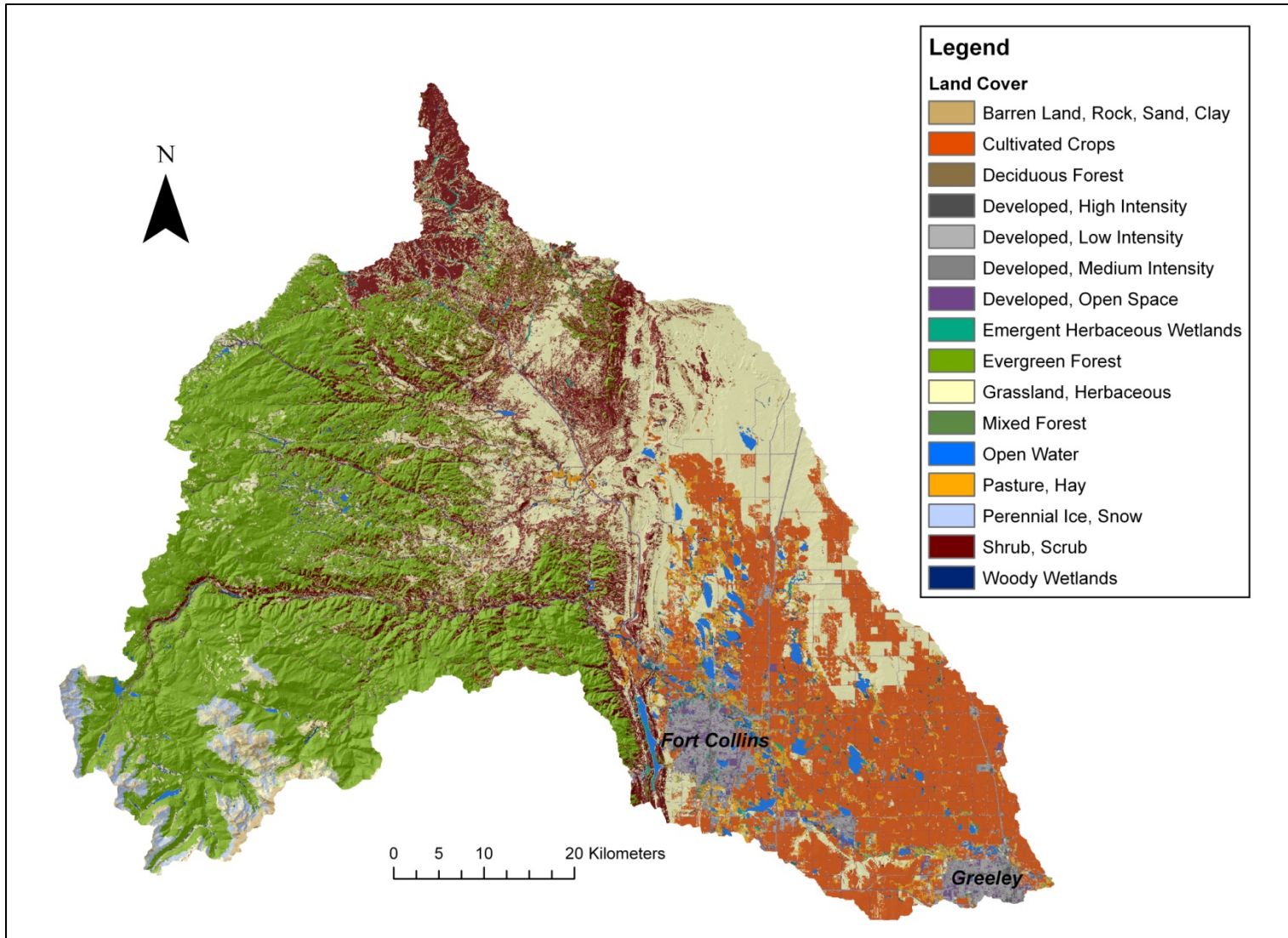


Figure A.1. Land cover for the Cache la Poudre basin derived from 2001 National Land Cover Dataset (NLCD).

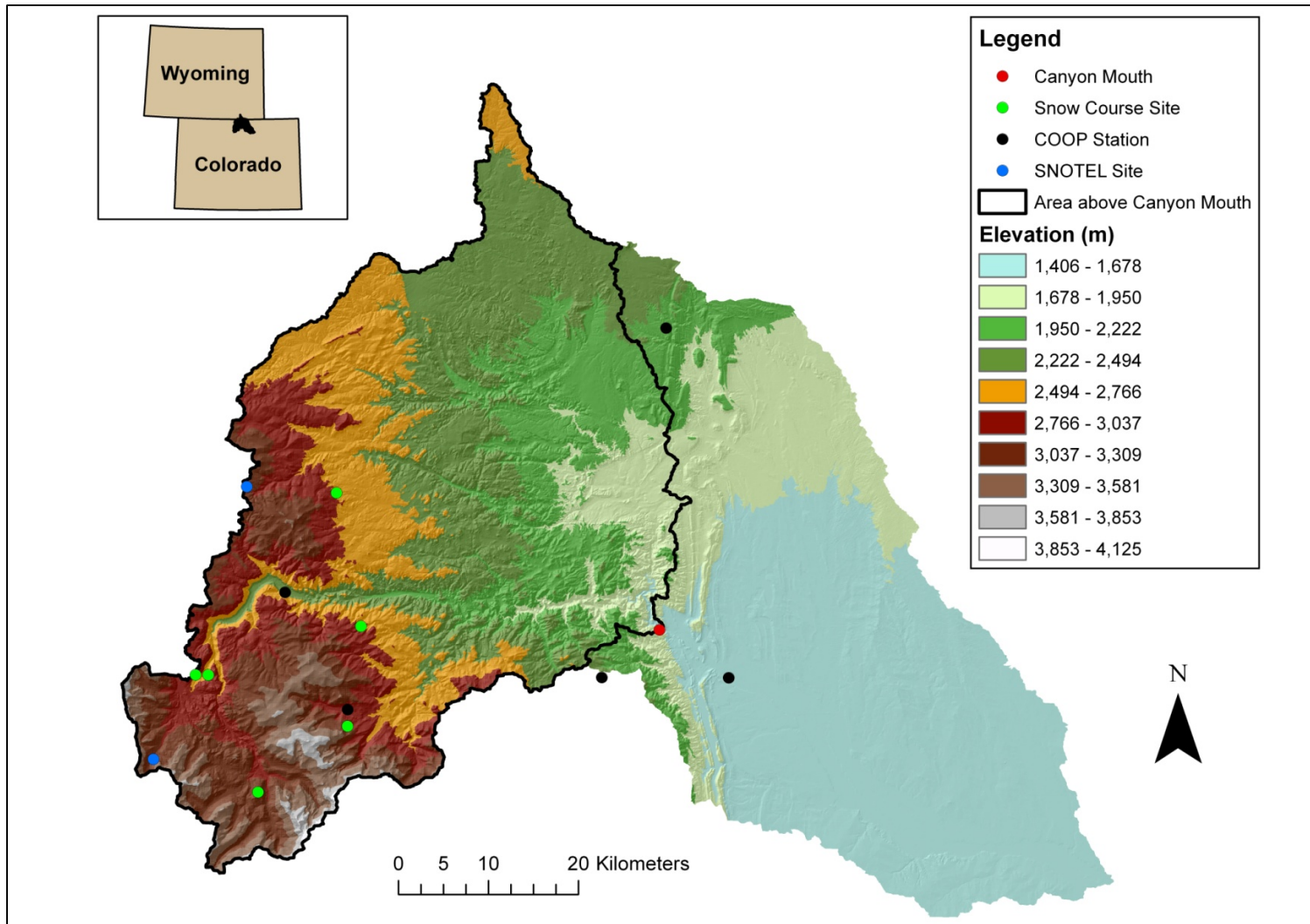


Figure A.2. Elevation for the Cache la Poudre basin derived from a digital elevation model (DEM) including meteorological stations, snow courses, and the Canyon Mouth stream gauge.

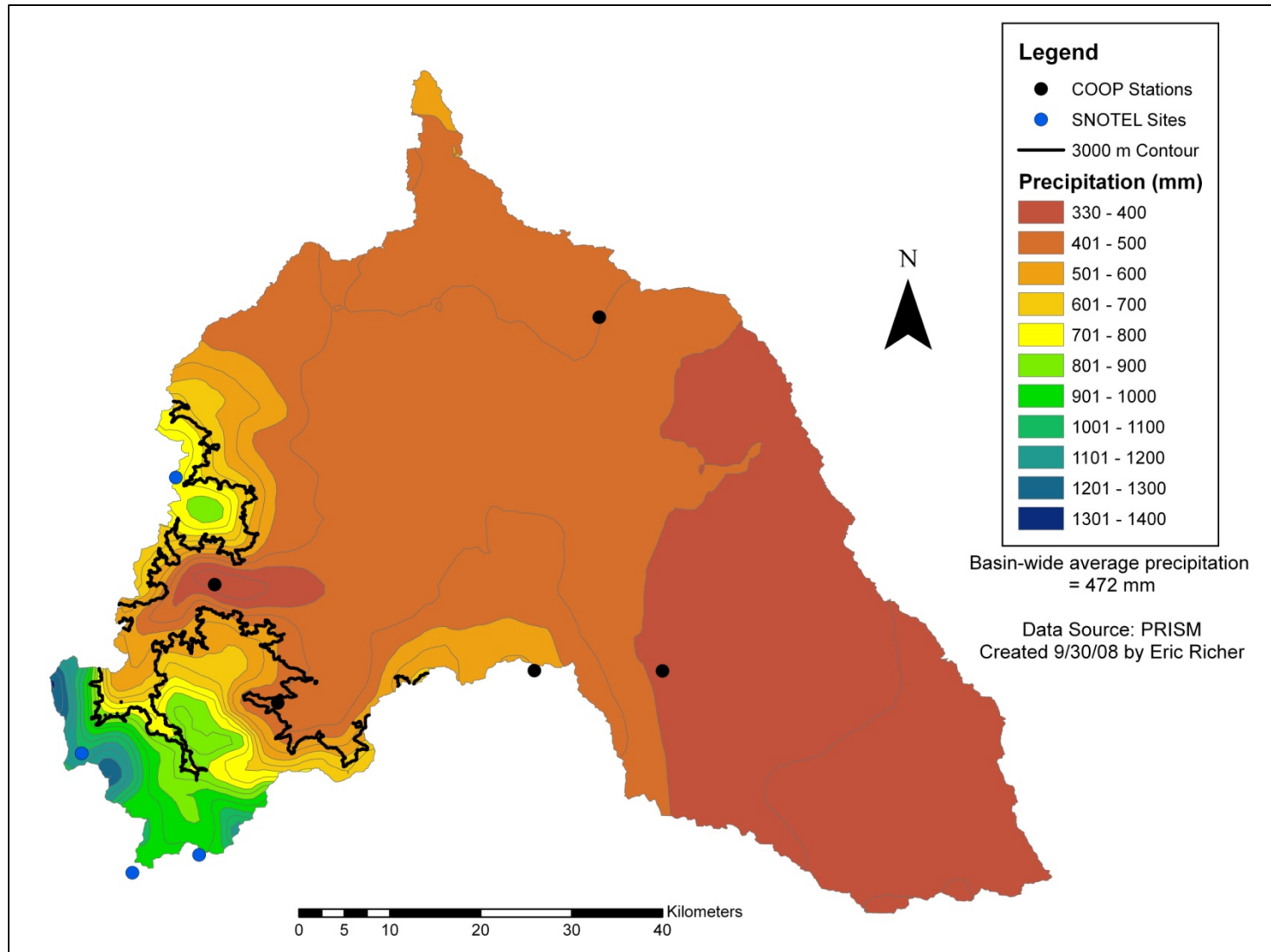


Figure A.3. PRISM derived average annual precipitation for the Cache la Poudre basin: 1971-2001.

APPENDIX B: FLOW MODIFICATION

Table B.1. Comprehensive list of flow modification structures located above the Canyon Mouth.

| ID # | Name | Water Source | Type | Description | Use | Latitude | Longitude | Total Vol (AF) | Total Rate (cfs) | Owner |
|------|--------------------------------------|-----------------------|----------|-------------|-----|-----------|-------------|----------------|------------------|---------------------------------|
| 4609 | Rawah Ditch 1 | Cache la Poudre River | Ditch | Diversion | F | | | | | Water Supply and Storage Co |
| 905 | North Poudre Supply Canal | Cache la Poudre River | Ditch | Diversion | A | 40.691242 | -105.255761 | | 8620.842 | North Poudre Irrigation Co |
| 907 | Poudre Valley Canal | Cache la Poudre River | Ditch | Diversion | A | 40.670699 | -105.226863 | | 6422.052 | Poudre Valley Canal Co |
| 1006 | E.P. Collins No 2 | Ravine | Ditch | Diversion | U | 40.956003 | -105.689662 | | 7.5 | Van Warning |
| 1005 | E.P. Collins No 1 | Sheep Creek | Ditch | Diversion | U | 40.946394 | -105.709918 | | 6.5 | Van Warning |
| 994 | North Poudre Canal | NFCLP River | Ditch | Diversion | A | 40.842289 | -105.289662 | | 3709.222 | North Poudre Irrigation Co |
| 995 | William Calloway Ditch No 1 | NFCLP River | Ditch | Diversion | A | 40.833339 | -105.282311 | | 17.05 | Judson Land and Cattle Co |
| 996 | William Calloway Ditch No 2 | NFCLP River | Ditch | Diversion | A | | | | 4.94 | Koch Angus Ranch & ETAL |
| 997 | Chase Ditch | NFCLP River | Ditch | Diversion | A | 40.822666 | -105.277395 | | 10.705 | Al Johnson |
| 815 | JD Wagner Ditch 1 | Rabbit Creek | Ditch | Diversion | U | 40.846909 | -105.341393 | | 2.5 | Colorado Division of Wildlife |
| 1233 | Middle Fork Rabbit Creek Ditch 2 | Rabbit Creek | Ditch | Diversion | U | 40.824838 | -105.353161 | | 2.5 | no information |
| 1234 | Middle Fork Rabbit Creek Ditch 1 | Rabbit Creek | Ditch | Diversion | U | 40.82303 | -105.358062 | | 2.5 | no information |
| 1030 | Rabbit Creek Ditch | Rabbit Creek | Ditch | Diversion | U | 40.809809 | -105.2894 | | 8 | Judson Land and Cattle Co |
| 1042 | North Pine Ditch | North Pine Creek | Ditch | Diversion | U | 40.808613 | -105.648925 | | 65 | Red Feather Lakes St |
| 1037 | Emerson Brothers Ditches | Lone Pine Creek | Ditch | Diversion | I | 40.775771 | -105.333735 | | 29.88 | Ed Hansen |
| 1038 | Burnham Emerson Ditch | Lone Pine Creek | Ditch | Diversion | A | 40.790152 | -105.334357 | | 26 | Ed Hansen |
| 1039 | Mitchell Weymouth Ditch 2 | Lone Pine Creek | Ditch | Diversion | A | 40.794283 | -105.309832 | | 35.27 | Ed Hansen |
| 1040 | Mitchell Weymouth Ditch 1 | Lone Pine Creek | Ditch | Diversion | A | 40.794331 | -105.30002 | | 17.35 | Ed Hansen |
| 1041 | Weltzer-Weymouth Ditch | Lone Pine Creek | Ditch | Diversion | A | 40.794297 | -105.290427 | | 13.37 | Wetzler, Mitchell #2, B&E Ditch |
| 1051 | Peery Ditch No 1 | South Pine Creek | Ditch | Diversion | A | 40.783197 | -105.616476 | | 3.5 | no information |
| 1050 | Peery Ditch No 2 | South Pine Creek | Ditch | Diversion | A | 40.780754 | -105.622704 | | 3.5 | no information |
| 959 | Bellaire Lake Reservoir Feeder Ditch | Elkhorn Creek | Ditch | Diversion | U | 40.76297 | -105.647349 | | | Division of Wildlife |
| 1052 | South Pine Supply Ditch | South Pine Creek | Ditch | Diversion | U | 40.785985 | -105.598584 | | | Division of Wildlife |
| 906 | Fort Collins Pipeline | Cache la Poudre River | Pipeline | Diversion | A | 40.704921 | -105.247914 | | 502.094 | City of Fort Collins |

| ID # | Name | Water Source | Type | Description | Use | Latitude | Longitude | Total Vol (AF) | Total Rate (cfs) | Owner |
|-------------|----------------------------------|-----------------------|-----------|---------------|-----|-----------|-------------|----------------|------------------|-----------------------------|
| 4601 | Grand River Ditch | Long Draw Creek | Ditch | Foreign Water | A | | | | | Water Supply and Storage Co |
| 4602 | Cameron Pass Ditch | Joe Wright Creek | Ditch | Foreign Water | A | | | | | Water Supply and Storage Co |
| 4603 | Michigan Ditch | Joe Wright Creek | Ditch | Foreign Water | A | | | | | City of Fort Collins |
| 4605 | Skyline Ditch | Joe Wright Creek | Ditch | Foreign Water | A | | | | | Water Supply and Storage Co |
| 4606 | Bob Creek Ditch | Roaring Creek | Ditch | Foreign Water | A | | | | | City of Greely |
| 4607 | Columbine Ditch | NFCLP River | Ditch | Foreign Water | I | | | | | City of Greely |
| 4608 | Deadman Ditch | Sheep Creek | Ditch | Foreign Water | A | | | | | Divide Reservoir and Canal |
| 4604 | Wilson Supply Ditch | Sheep Creek | Ditch | Foreign Water | A | | | | | Divide Reservoir and Canal |
| 4600 | Laramie-Poudre Tunnel | Cache la Poudre River | Pipeline | Foreign Water | A | | | | | Water Supply and Storage Co |
| 500 3676 | Sand Creek Ditch | Transbasin Water | Ditch | Foreign Water | F | 40.931672 | -105.785183 | | | District 76 Ditch |
| | Long Draw Reservoir | Long Draw Creek | Reservoir | Reservoir | A | 40.50159 | -105.772026 | 10801 | | Water Supply and Storage Co |
| 3677 | Peterson Lake Reservoir | Unnamed Creek | Reservoir | Reservoir | A | 40.559791 | -105.793404 | 1251.9 | | City of Greely |
| 3678 | Joe Wright Reservoir | Joe Wright Creek | Reservoir | Reservoir | A | 40.559781 | -105.86932 | 7957.78 | | City of Fort Collins |
| 3679 | Chambers Lake Reservoir | Joe Wright Creek | Reservoir | Reservoir | A | 40.602821 | -105.843772 | 8854 | | Water Supply and Storage Co |
| 3683 | Barnes Meadow Reservoir | Barnes Meadow Creek | Reservoir | Reservoir | A | 40.602802 | -105.836472 | 2348.8 | | City of Greely |
| 3684 | Twin Lakes Reservoir | Unnamed creek | Reservoir | Reservoir | A | 40.561664 | -105.576165 | 278 | | City of Greely |
| 3686 | Comanche Reservoir | Big Beaver Creek | Reservoir | Reservoir | A | 40.585425 | -105.645183 | 2629 | | City of Greely |
| 3720 | Hourglass Reservoir (Big Beaver) | Big Beaver Creek | Reservoir | Reservoir | A | 40.582099 | -105.630827 | 1588 | | City of Greely |
| 3814 | Panhandle Reservoir | Panhandle Creek | Reservoir | Reservoir | A | | | 1017 | | no information |
| 3726 | Worster Reservoir | Sheep Creek | Reservoir | Reservoir | A | 40.943732 | -105.713526 | 3747 | | Worster Reservoir Co |
| 3712 | Hallagan Reservoir | NFCLP River | Reservoir | Reservoir | A | 40.878322 | -105.336882 | 46278 | 5692.842 | North Poudre Irrigation Co |
| 3722 | Erie Lake | North Pine Creek | Reservoir | Reservoir | A | 40.820815 | -105.624472 | 86 | | Red Feather Lakes St |
| 3807 | Mitchell Lake 6 | North Pine Creek | Reservoir | Reservoir | A | 40.805654 | -105.603112 | 32.13 | | Red Feather Lakes St |
| 3714 | Apache Lake | North Pine Creek | Reservoir | Reservoir | A | 40.807517 | -105.595842 | 109.11 | | no information |
| 3819 | Nokomis Lake | North Pine Creek | Reservoir | Reservoir | A | 40.8182 | -105.586428 | | | Red Feather Lakes St |

| ID # | Name | Water Source | Type | Description | Use | Latitude | Longitude | Total Vol (AF) | Total Rate (cfs) | Owner |
|------|-----------------------------|------------------|-----------|-------------|-----|-----------|-------------|----------------|------------------|--------------------------|
| 3808 | Mitchell Lake 1 | North Pine Creek | Reservoir | Reservoir | A | 40.802155 | -105.593457 | 760 | | Red Feather Lakes St |
| 3810 | Mitchell Lake 3 | North Pine Creek | Reservoir | Reservoir | A | 40.794866 | -105.576756 | 115 | | Red Feather Park Assoc |
| 3809 | Mitchell Lake 2 | North Pine Creek | Reservoir | Reservoir | A | 40.798485 | -105.579155 | 106 | | Red Feather Lakes St |
| 3723 | Snake Lake | North Pine Creek | Reservoir | Reservoir | A | 40.796485 | -105.555283 | 121 | | Red Feather Lk Str Assoc |
| 3724 | Deer Lake | North Pine Creek | Reservoir | Reservoir | A | 40.803737 | -105.56726 | 88 | | Red Feather Lakes St |
| 3745 | Dowdy Lake Reservoir | South Pine Creek | Reservoir | Reservoir | A | 40.800036 | -105.55769 | 1059 | | Division of Wildlife |
| 3412 | Fox Acres Reservoir No 1 | North Pine Creek | Reservoir | Reservoir | A | 40.802962 | -105.575601 | 91.60001 | 30 | Campbell Development |
| 3413 | Fox Acres Reservoir No 2 | North Pine Creek | Reservoir | Reservoir | A | 40.802962 | -105.575601 | 194.9 | 30 | Campbell Development |
| 3414 | Fox Acres Reservoir No 3 | North Pine Creek | Reservoir | Reservoir | A | 40.810674 | -105.558047 | 225.1 | 28 | Campbell Development |
| 3411 | South Fox Acres Reservoir | North Pine Creek | Reservoir | Reservoir | A | 40.802962 | -105.575601 | 16.3 | 36 | Campbell Development |
| 3415 | Lower Fox Acres Reservoir | North Pine Creek | Reservoir | Reservoir | A | 40.810627 | -105.555681 | 130.89 | 30 | Campbell Development |
| 3416 | Upper Fox Acres Reservoir 3 | North Pine Creek | Reservoir | Reservoir | A | 40.809001 | -105.560246 | 23.94 | 30 | Campbell Development |
| 3417 | Fox Acres West Lake | North Pine Creek | Reservoir | Reservoir | A | 40.803881 | -105.57917 | 19.96 | 30 | Campbell Development |
| 3418 | Mirror Lake | North Pine Creek | Reservoir | Reservoir | A | 40.810726 | -105.560412 | 70.33 | 32 | Campbell Development |
| 3419 | Robinson Draw Lake | North Pine Creek | Reservoir | Reservoir | A | 40.809189 | -105.569729 | 40.84 | 30 | Campbell Development |
| 3420 | Lake 15 | North Pine Creek | Reservoir | Reservoir | A | 40.809136 | -105.564972 | 5.47 | 30 | Campbell Development |
| 3424 | Deer Lake No 2 | North Pine Creek | Reservoir | Reservoir | A | 40.809084 | -105.562629 | 24.98 | 39.5 | Campbell Development |
| 3425 | Middle Letitia Lake | North Pine Creek | Reservoir | Reservoir | A | 40.805479 | -105.564882 | 19.37 | 30 | Campbell Development |
| 3426 | Upper Letitia Lake | North Pine Creek | Reservoir | Reservoir | A | 40.805479 | -105.564882 | 17.4 | 30 | Campbell Development |
| 3427 | Lower Letitia Lake | North Pine Creek | Reservoir | Reservoir | A | 40.807352 | -105.564908 | 28.96 | 30 | Campbell Development |
| 3687 | Bellaire Lake Reservoir | Elkhorn Creek | Reservoir | Reservoir | A | 40.773654 | -105.620401 | 69 | | Division of Wildlife |
| 3429 | West R of 'South 60' R | South Pine Creek | Reservoir | Reservoir | A | 40.787727 | -105.605782 | 11.06 | 30 | Campbell Development |
| 3430 | Middle R of 'South 60' R | South Pine Creek | Reservoir | Reservoir | A | 40.789515 | -105.605745 | 12.34 | 30 | Campbell Development |
| 3431 | East R of 'South 60' R | South Pine Creek | Reservoir | Reservoir | A | 40.789532 | -105.603325 | 7.99 | 30 | Campbell Development |
| 3754 | Twin Lakes (aka West Lake) | South Pine Creek | Reservoir | Reservoir | A | 40.791223 | -105.564843 | 195 | | Division of Wildlife |
| 3718 | Parvin Lake | South Pine Creek | Reservoir | Reservoir | A | 40.792823 | -105.545924 | 1321 | | Division of Wildlife |
| 3713 | Milton Seaman Reservoir | NFCLP River | Reservoir | Reservoir | A | 40.706055 | -105.235328 | 15000 | 4752.61 | City of Greeley |

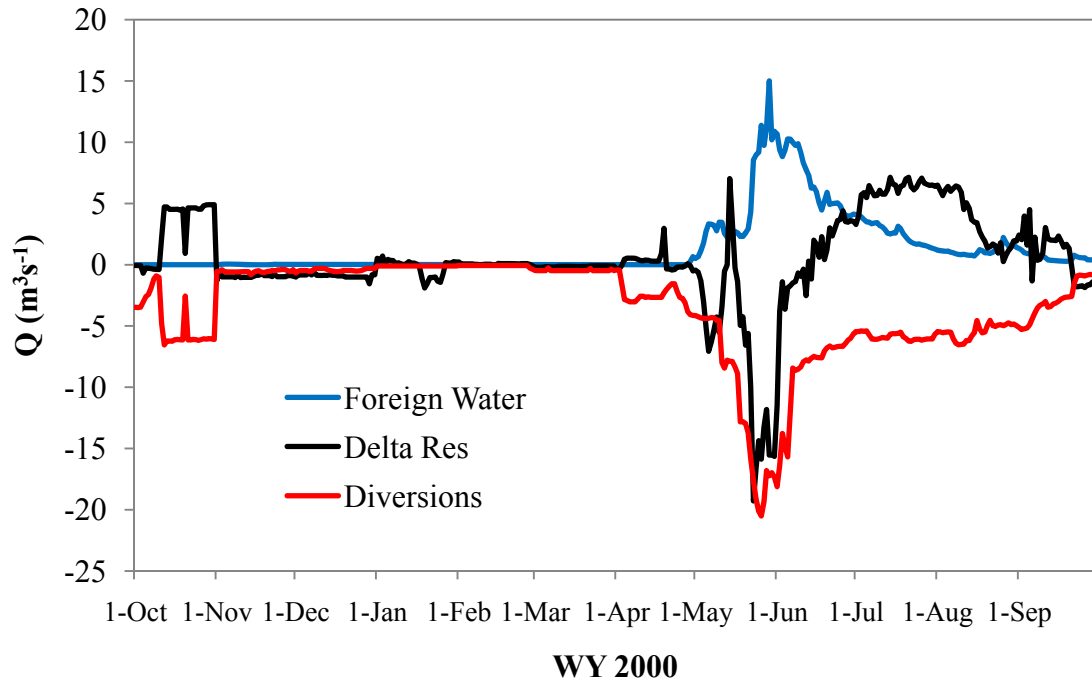


Figure B.1. Daily flow modification including foreign water inputs, change in reservoir storage, and diversions for the Cache la Poudre River: WY 2000.

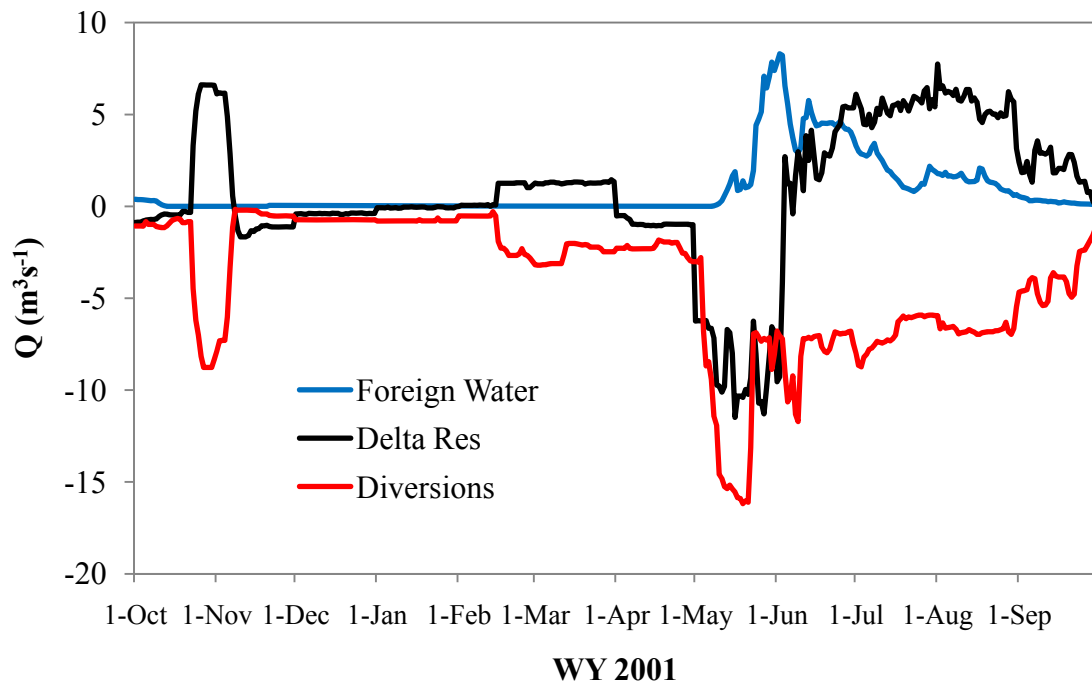


Figure B.2. Daily flow modification including foreign water inputs, change in reservoir storage, and diversions for the Cache la Poudre River: WY 2001.

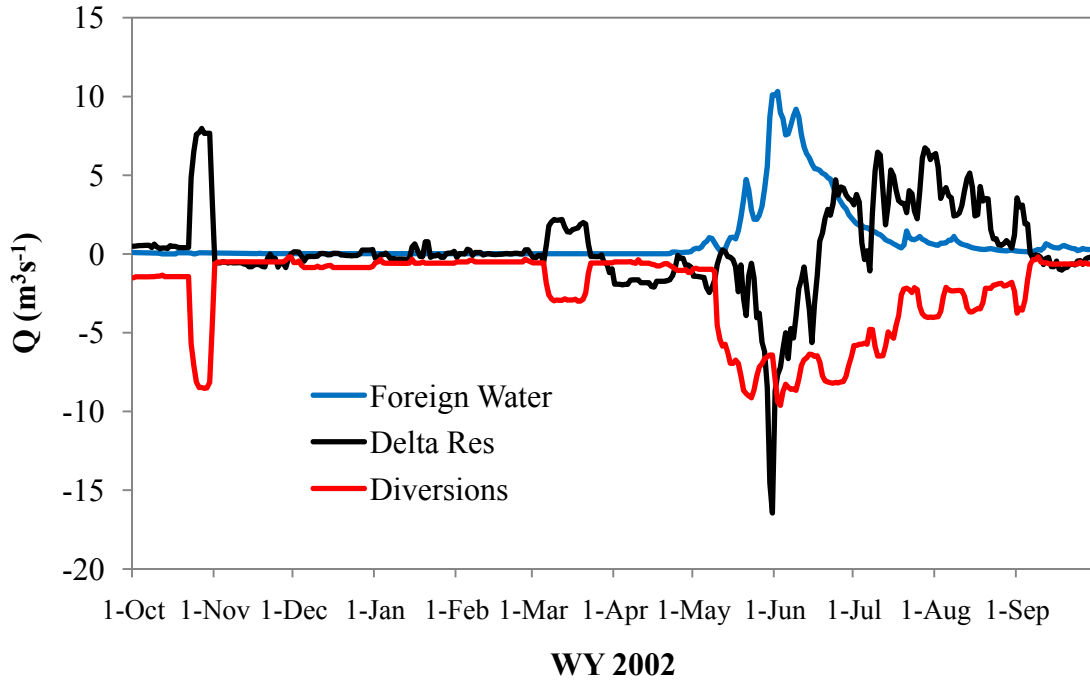


Figure B.3. Daily flow modification including foreign water inputs, change in reservoir storage, and diversions for the Cache la Poudre River: WY 2002.

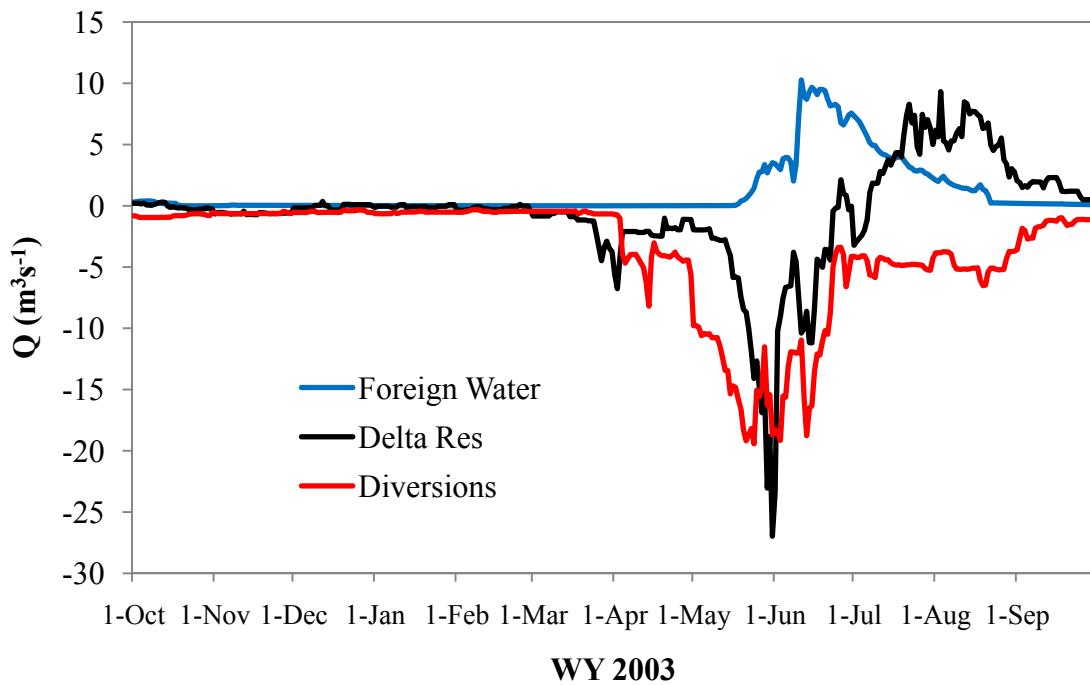


Figure B.4. Daily flow modification including foreign water inputs, change in reservoir storage, and diversions for the Cache la Poudre River: WY 2003.

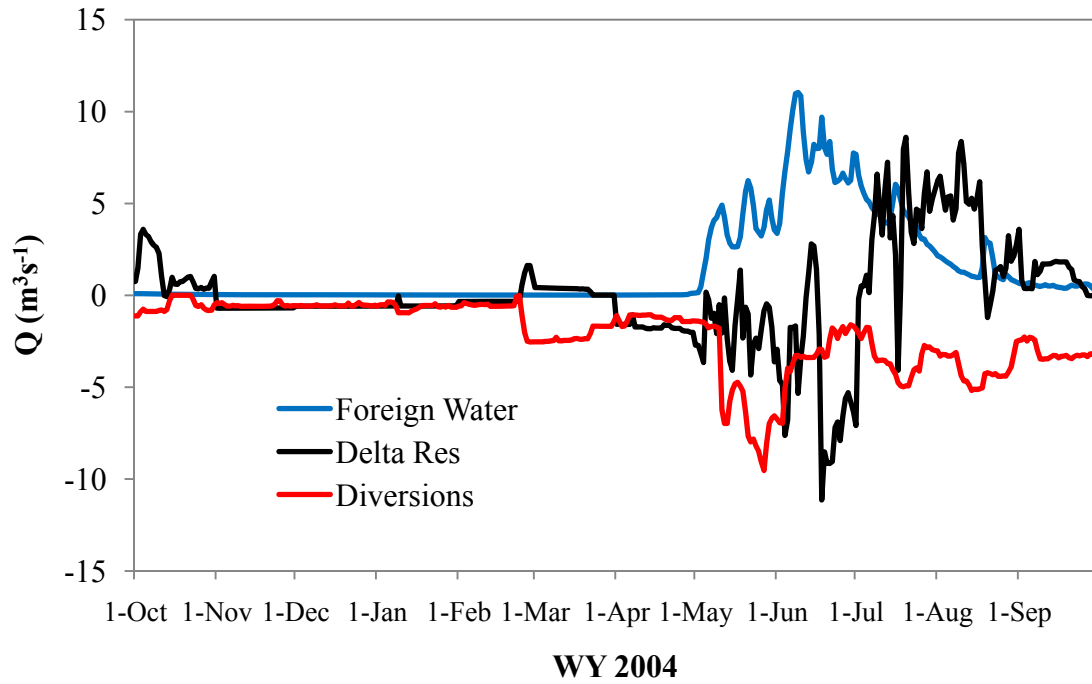


Figure B.5. Daily flow modification including foreign water inputs, change in reservoir storage, and diversions for the Cache la Poudre River: WY 2004.

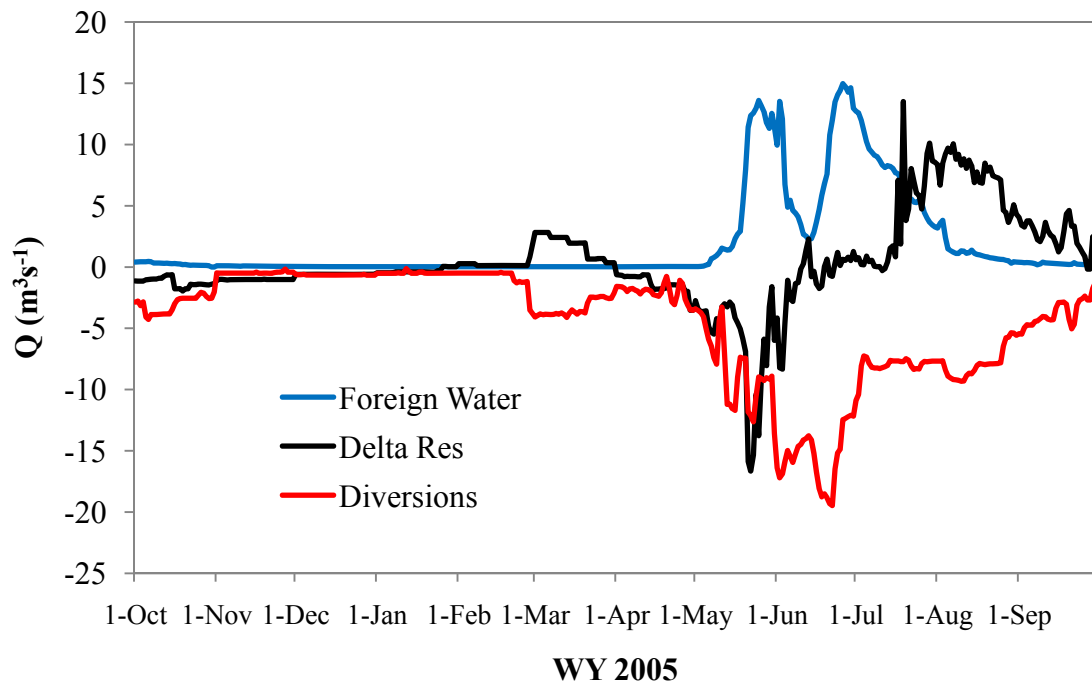


Figure B.6. Daily flow modification including foreign water inputs, change in reservoir storage, and diversions for the Cache la Poudre River: WY 2005.

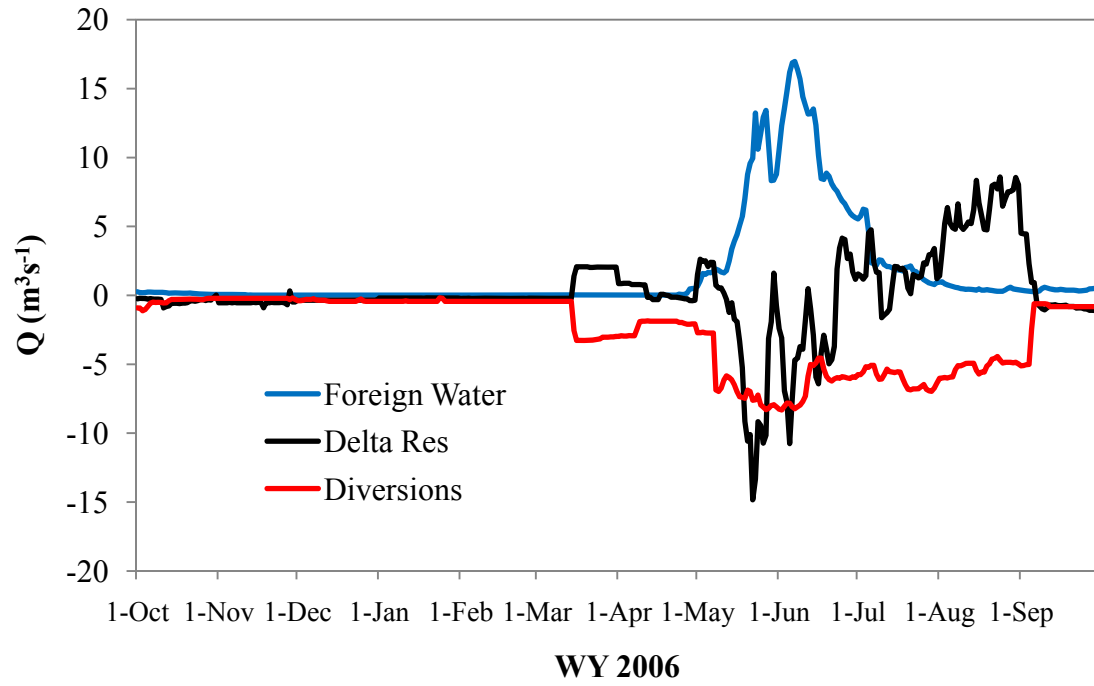


Figure B.7. Daily flow modification including foreign water inputs, change in reservoir storage, and diversions for the Cache la Poudre River: WY 2006.

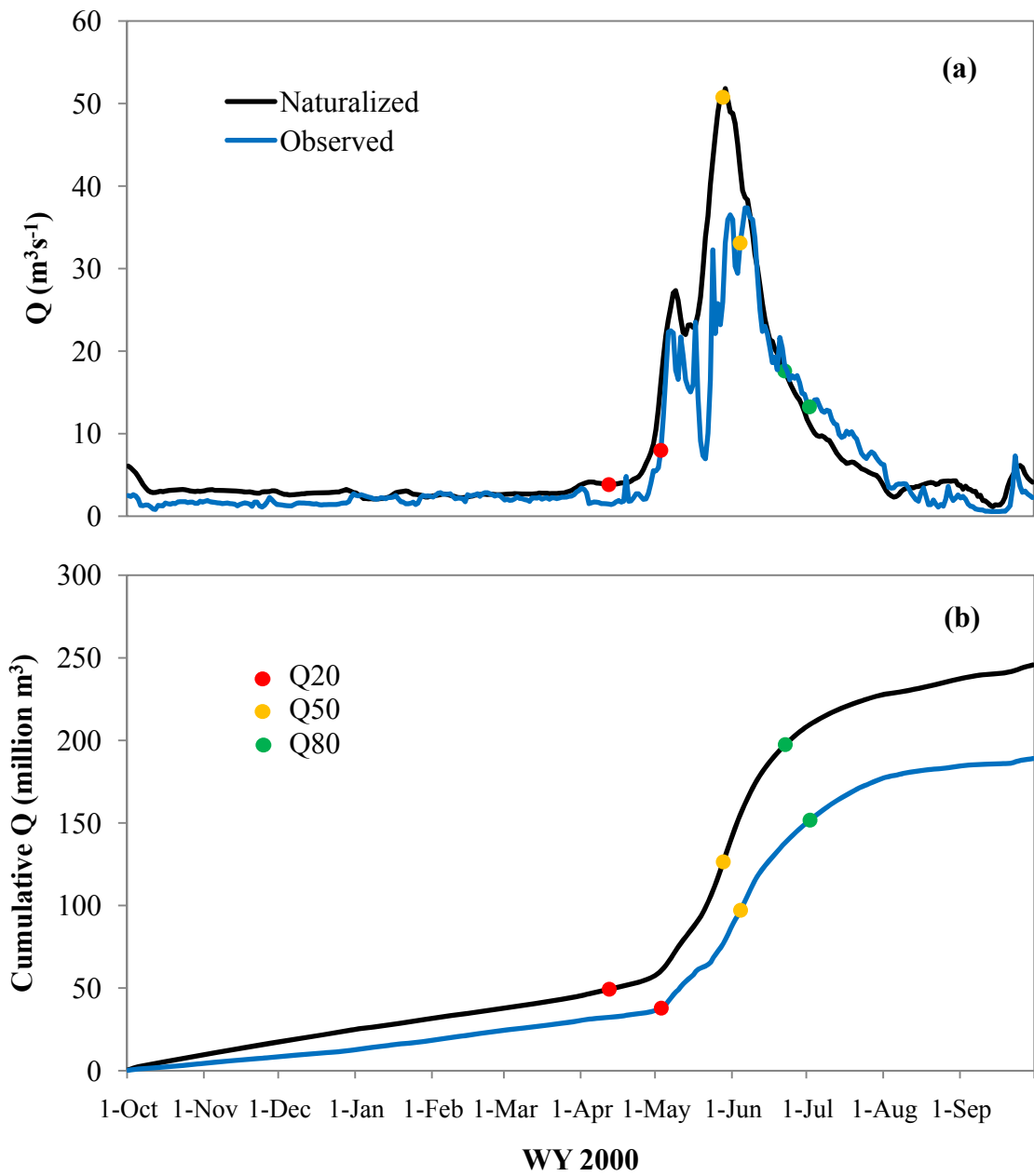


Figure B.8. Naturalized and observed (a) hydrographs and (b) cumulative discharge curves showing timing of 20th, 50th, and 80th (i.e., Q20, Q50, and Q80) flow percentiles for the Cache la Poudre River at the Canyon Mouth: WY 2000.

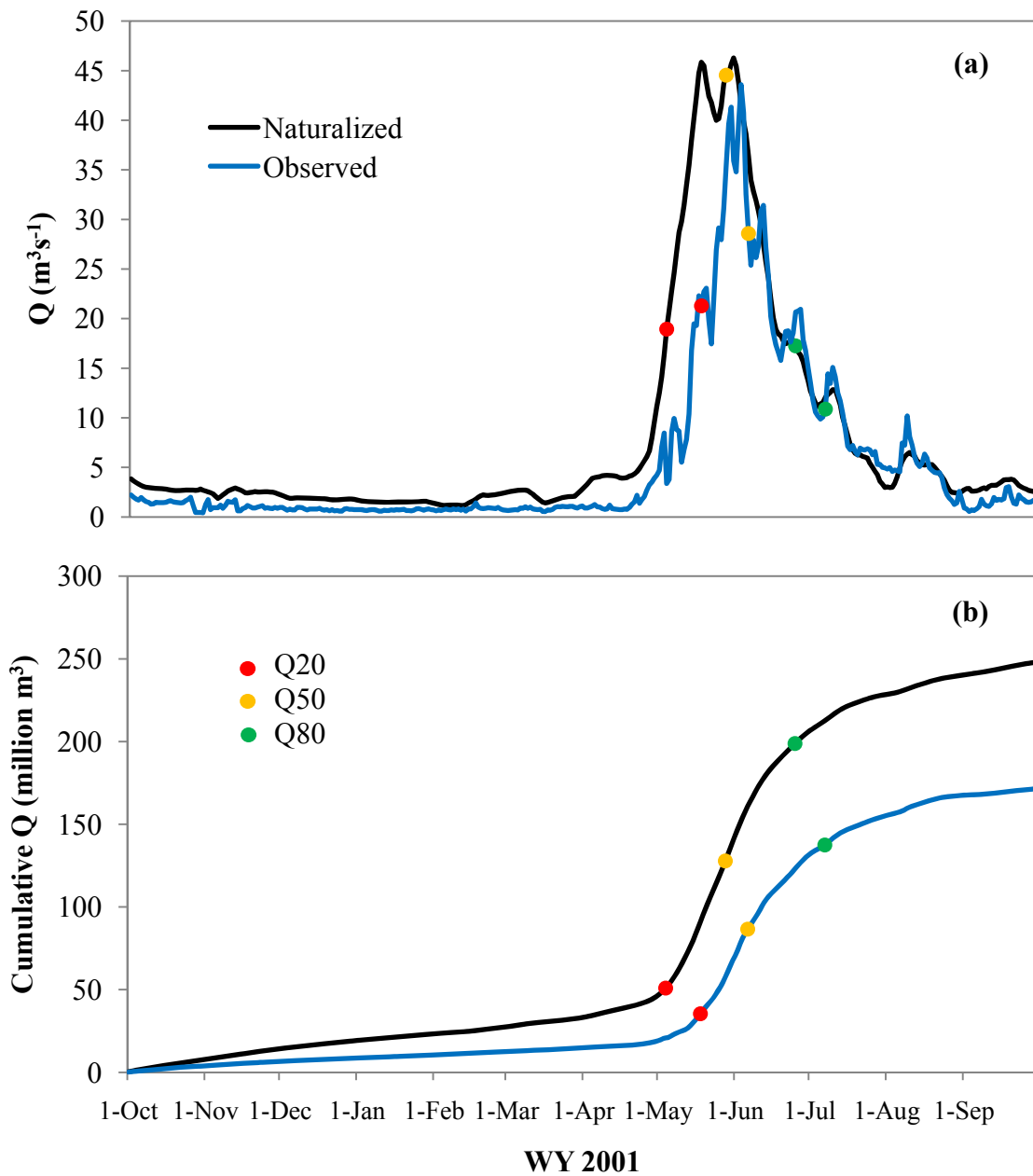


Figure B.9. Naturalized and observed (a) hydrographs and (b) cumulative discharge curves showing timing of 20th, 50th, and 80th (i.e., Q20, Q50, and Q80) flow percentiles for the Cache la Poudre River at the Canyon Mouth: WY 2001.

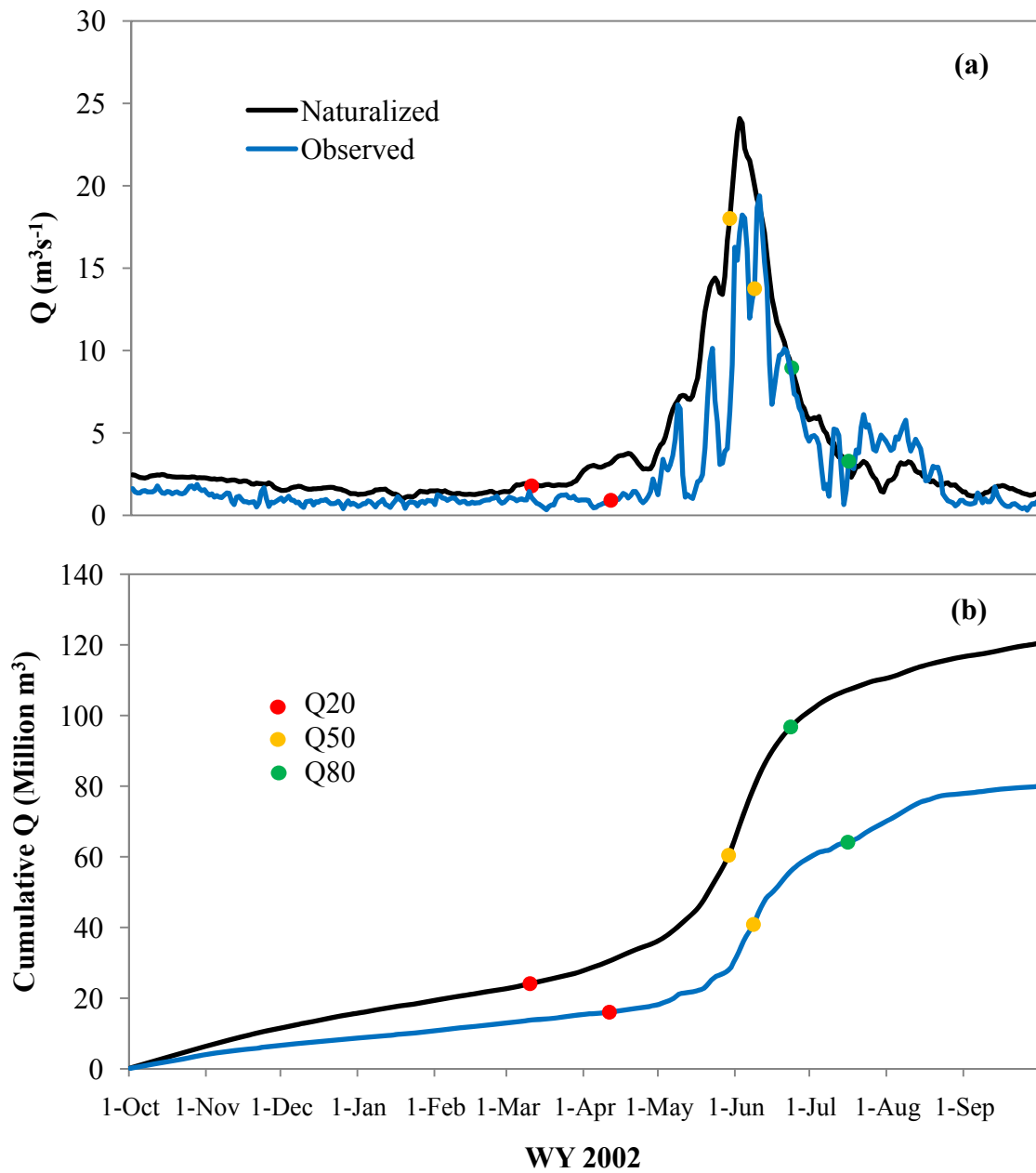


Figure B.10. Naturalized and observed (a) hydrographs and (b) cumulative discharge curves showing timing of 20th, 50th, and 80th (i.e., Q20, Q50, and Q80) flow percentiles for the Cache la Poudre River at the Canyon Mouth: WY 2002.

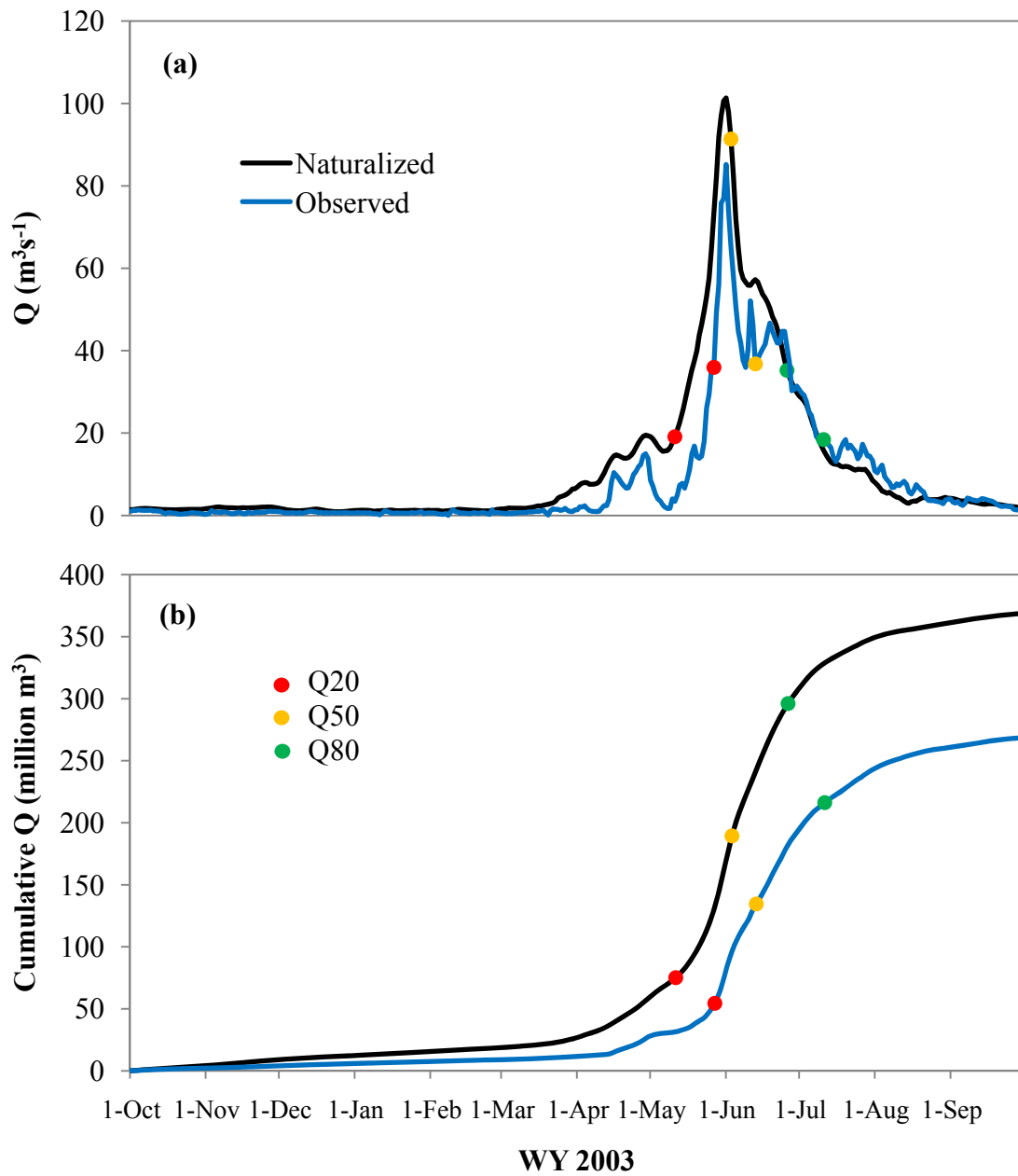


Figure B.11. Naturalized and observed (a) hydrographs and (b) cumulative discharge curves showing timing of 20th, 50th, and 80th (i.e., Q20, Q50, and Q80) flow percentiles for the Cache la Poudre River at the Canyon Mouth: WY 2003.

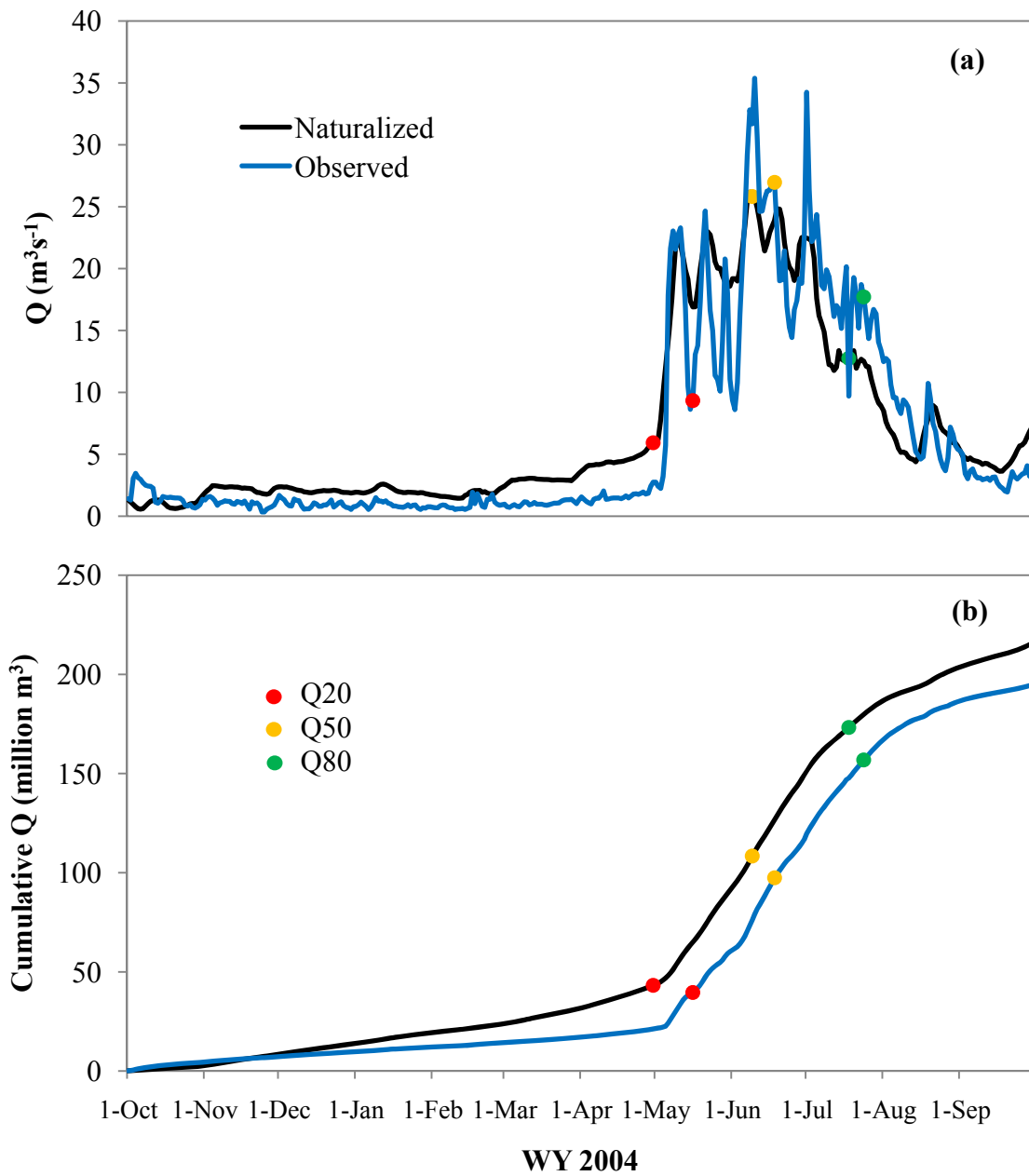


Figure B.12. Naturalized and observed (a) hydrographs and (b) cumulative discharge curves showing timing of 20th, 50th, and 80th (i.e., Q20, Q50, and Q80) flow percentiles for the Cache la Poudre River at the Canyon Mouth: WY 2004.

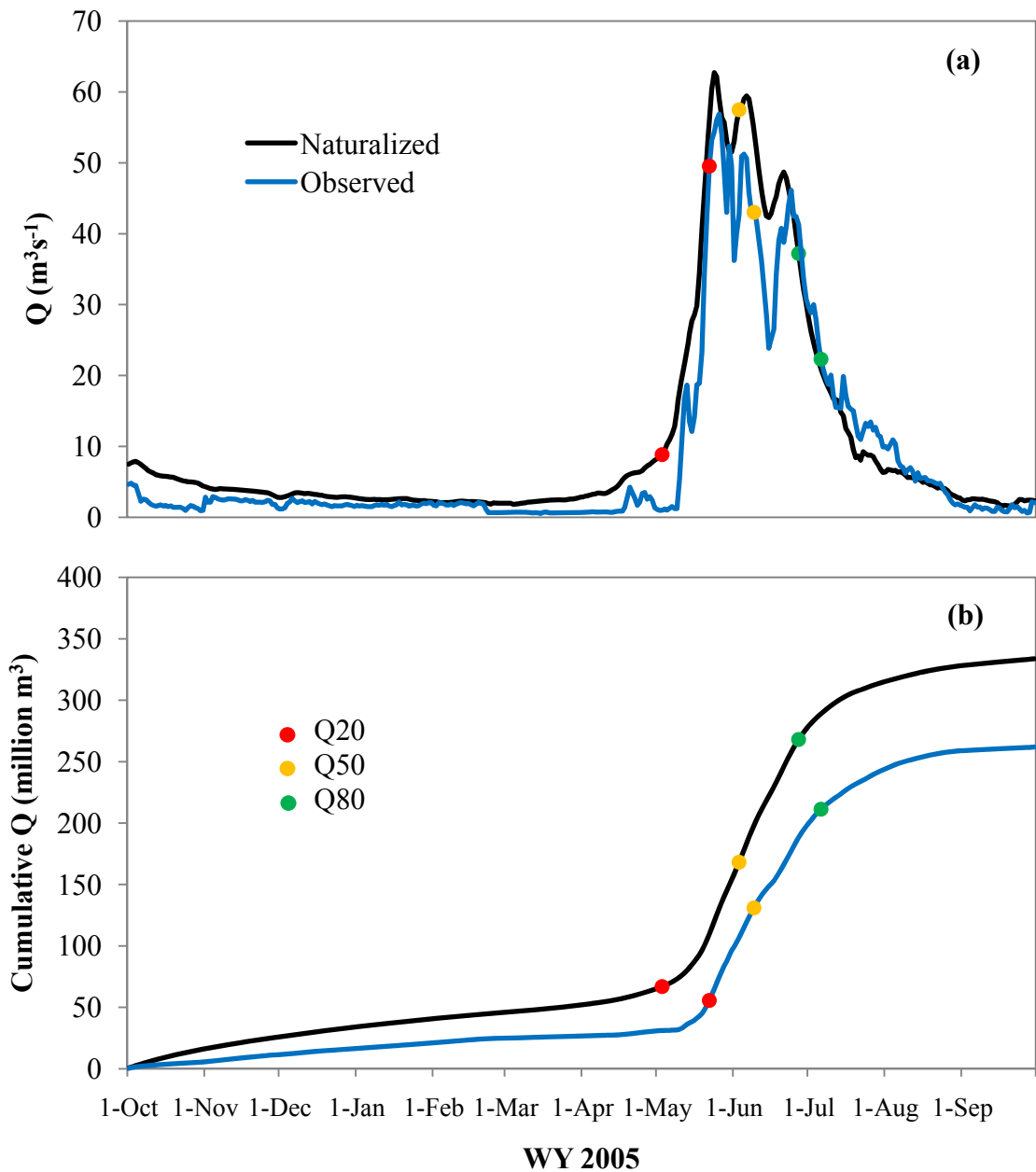


Figure B.13. Naturalized and observed (a) hydrographs and (b) cumulative discharge curves showing timing of 20th, 50th, and 80th (i.e., Q20, Q50, and Q80) flow percentiles for the Cache la Poudre River at the Canyon Mouth: WY 2005.

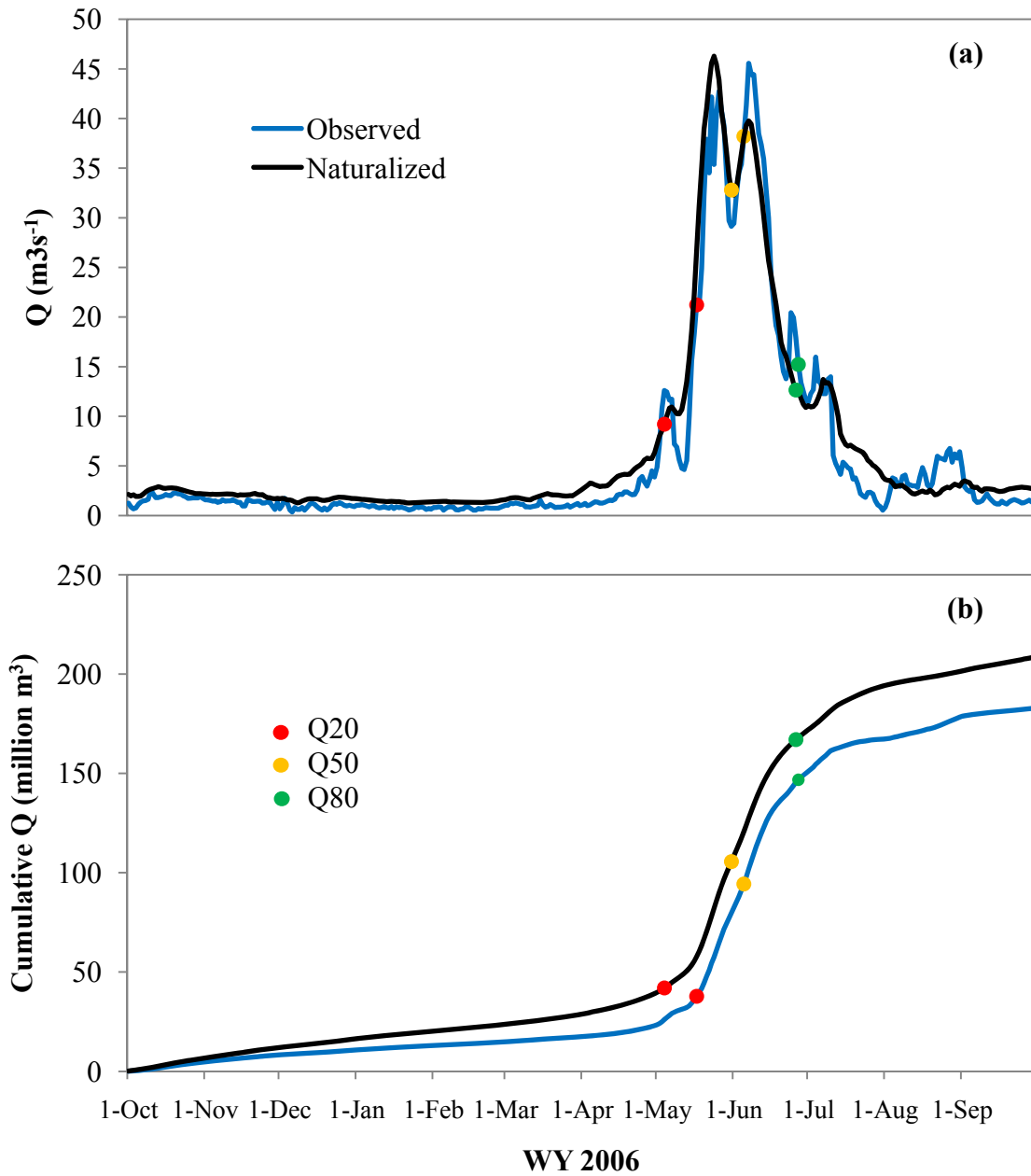


Figure B.14. Naturalized and observed (a) hydrographs and (b) cumulative discharge curves showing timing of 20th, 50th, and 80th (i.e., Q20, Q50, and Q80) flow percentiles for the Cache la Poudre River at the Canyon Mouth: WY 2006.

APPENDIX C: SNOW COVERED AREA

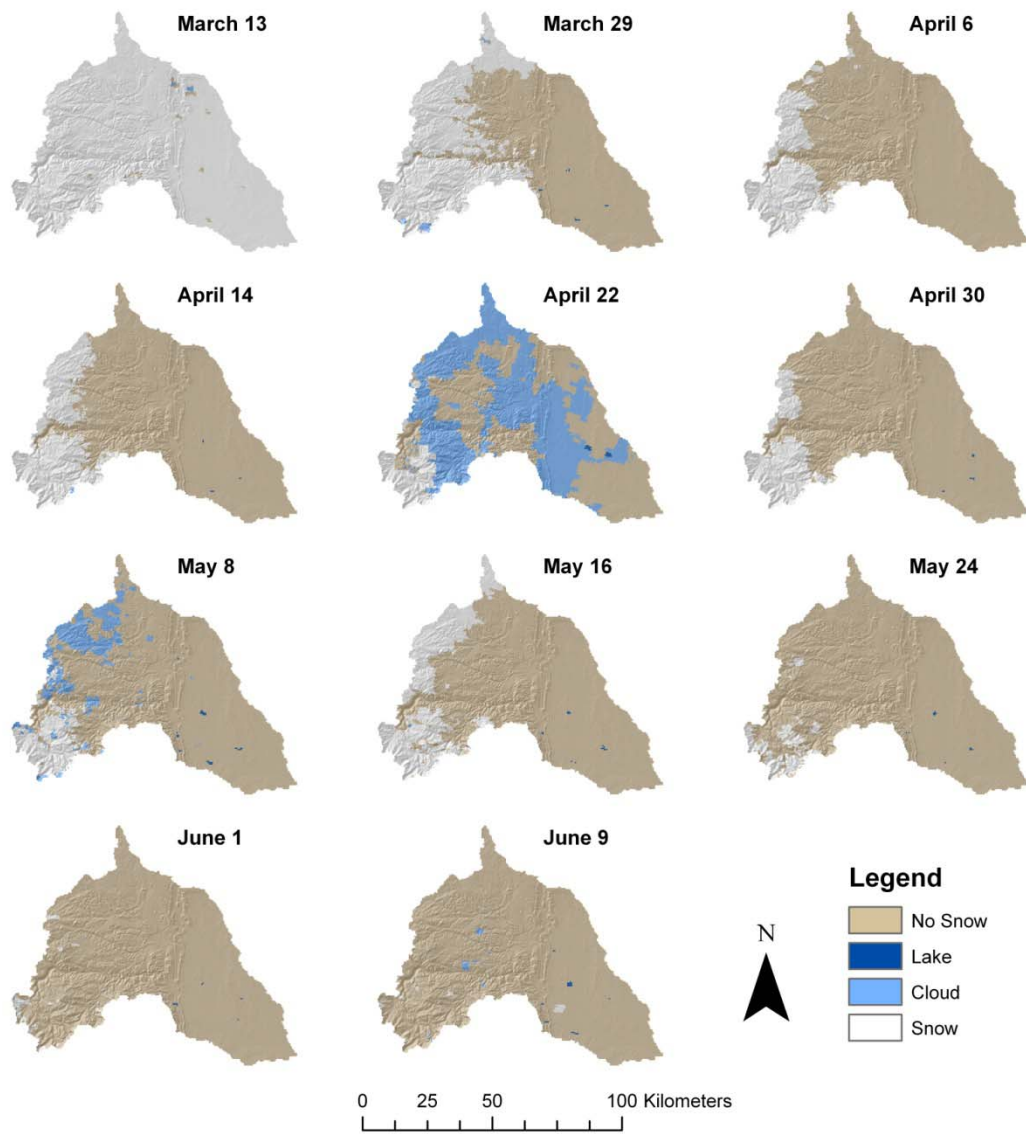


Figure C.1. MODIS 8-day SCA images used in analyses for the 2000 snowmelt season in the Cache la Poudre basin.

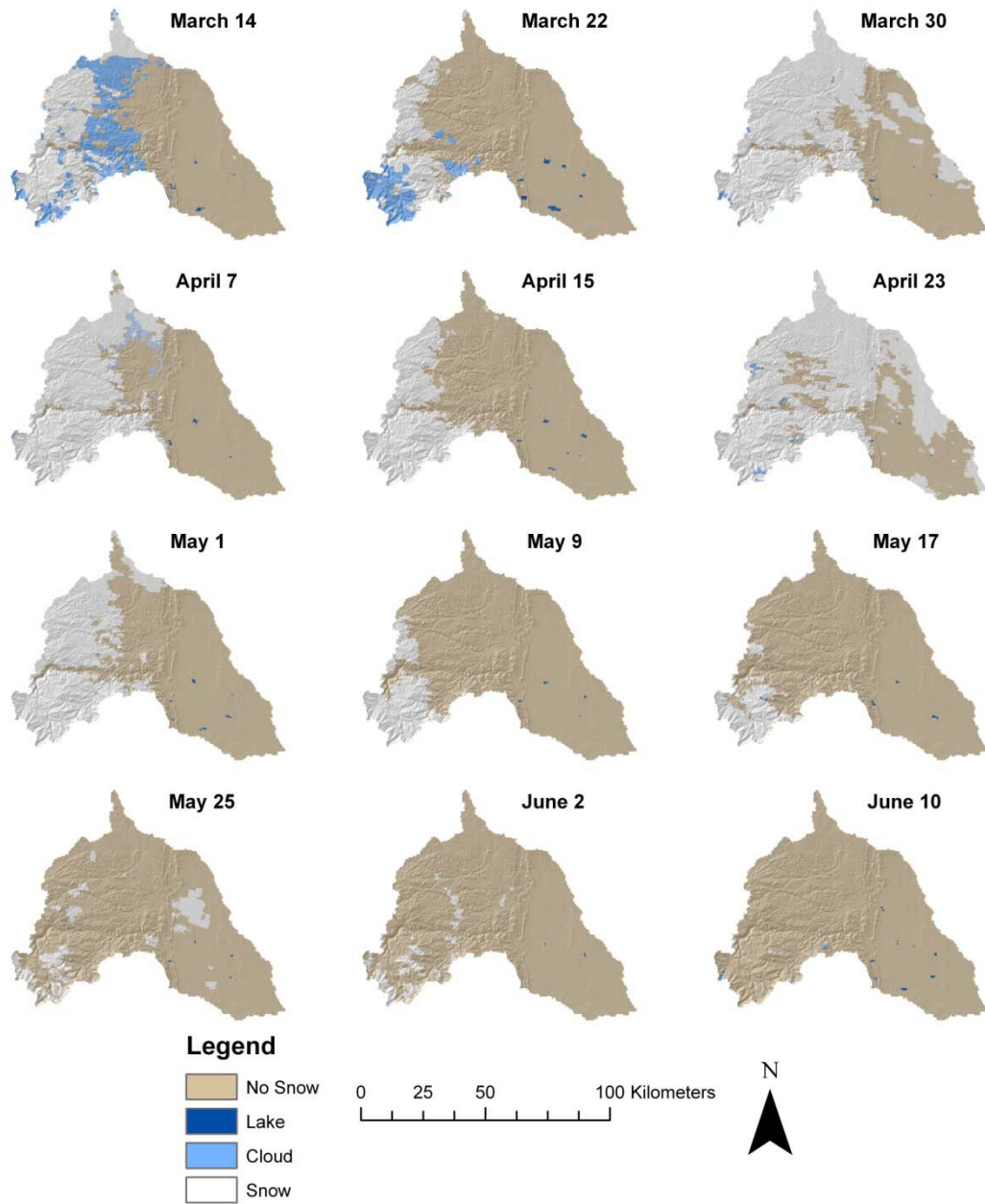


Figure C.2. MODIS 8-day SCA images used in analyses for the 2001 snowmelt season in the Cache la Poudre basin.

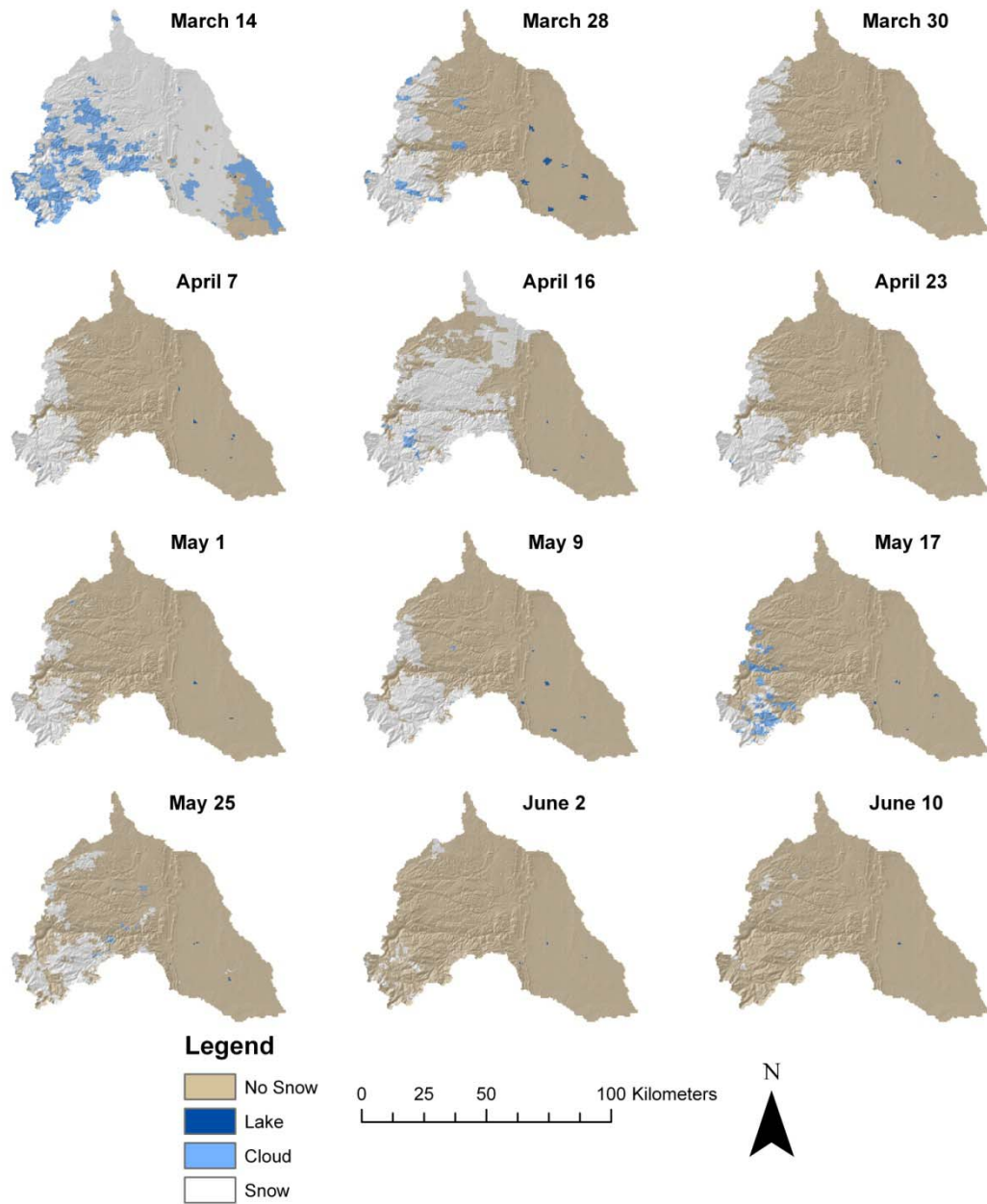


Figure C.3. MODIS 8-day SCA images used in analyses for the 2002 snowmelt season in the Cache la Poudre basin.

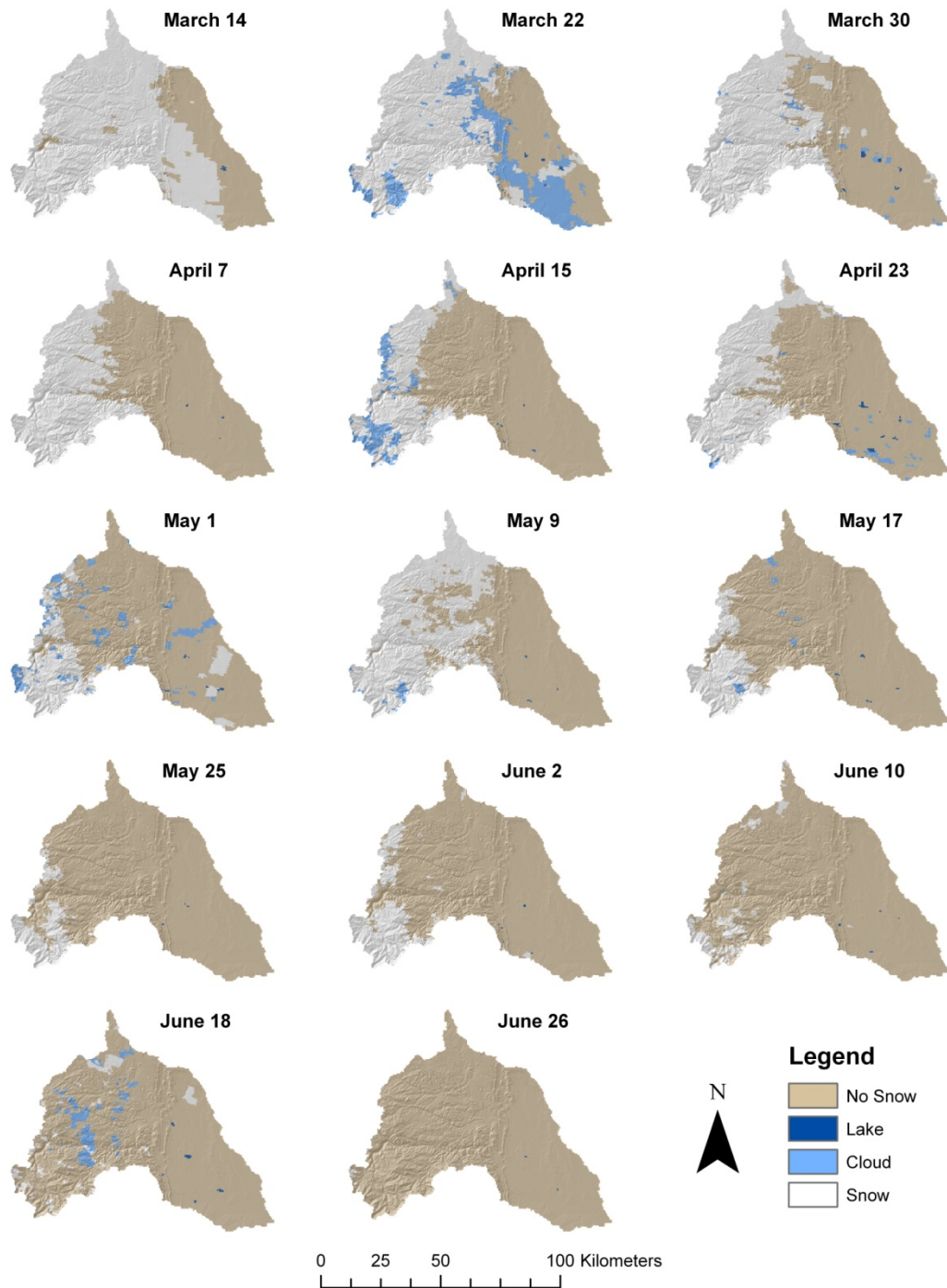


Figure C.4. MODIS 8-day SCA images used in analyses for the 2003 snowmelt season in the Cache la Poudre basin.

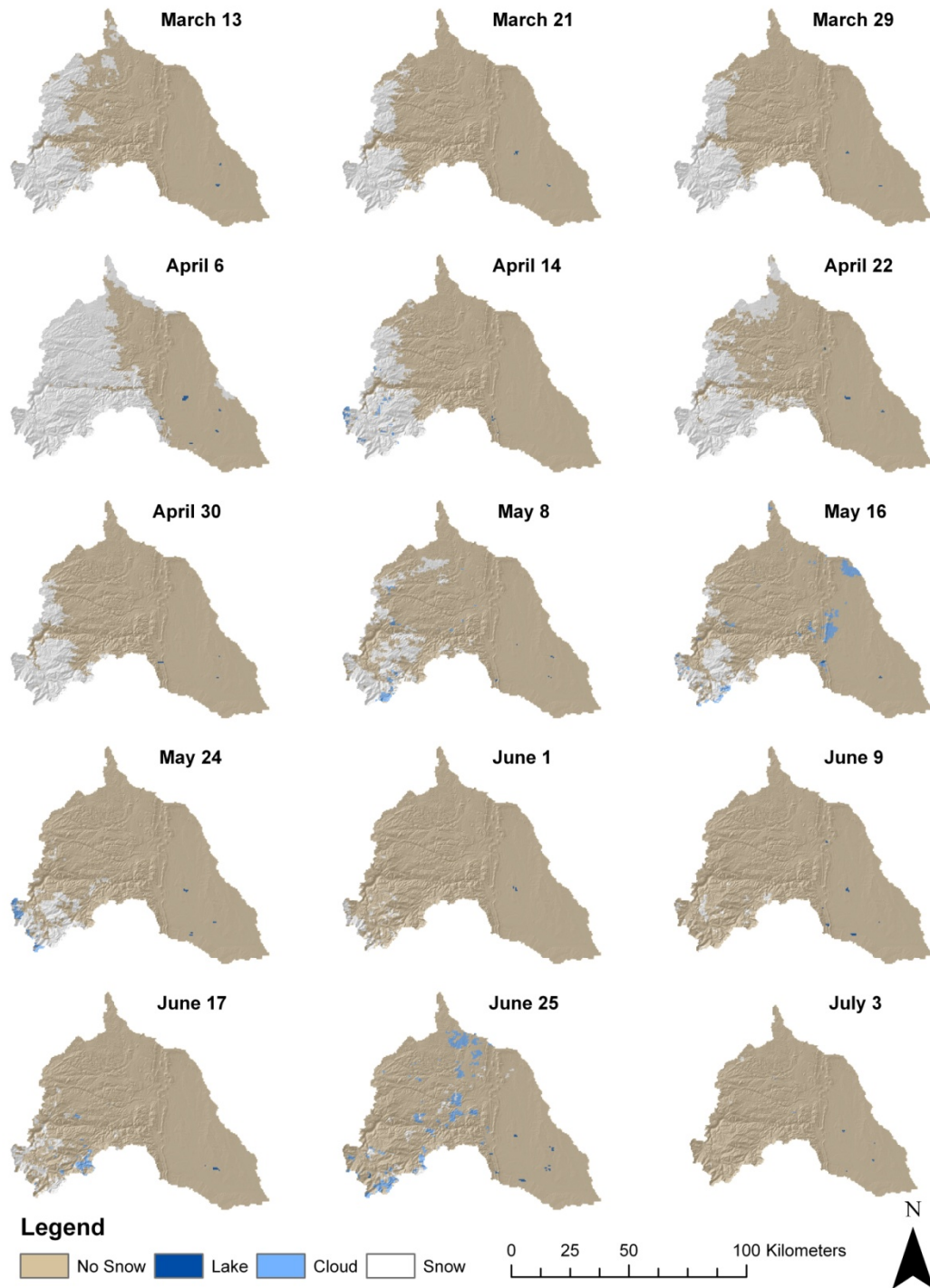


Figure C.5. MODIS 8-day SCA images used in analyses for the 2004 snowmelt season in the Cache la Poudre basin.

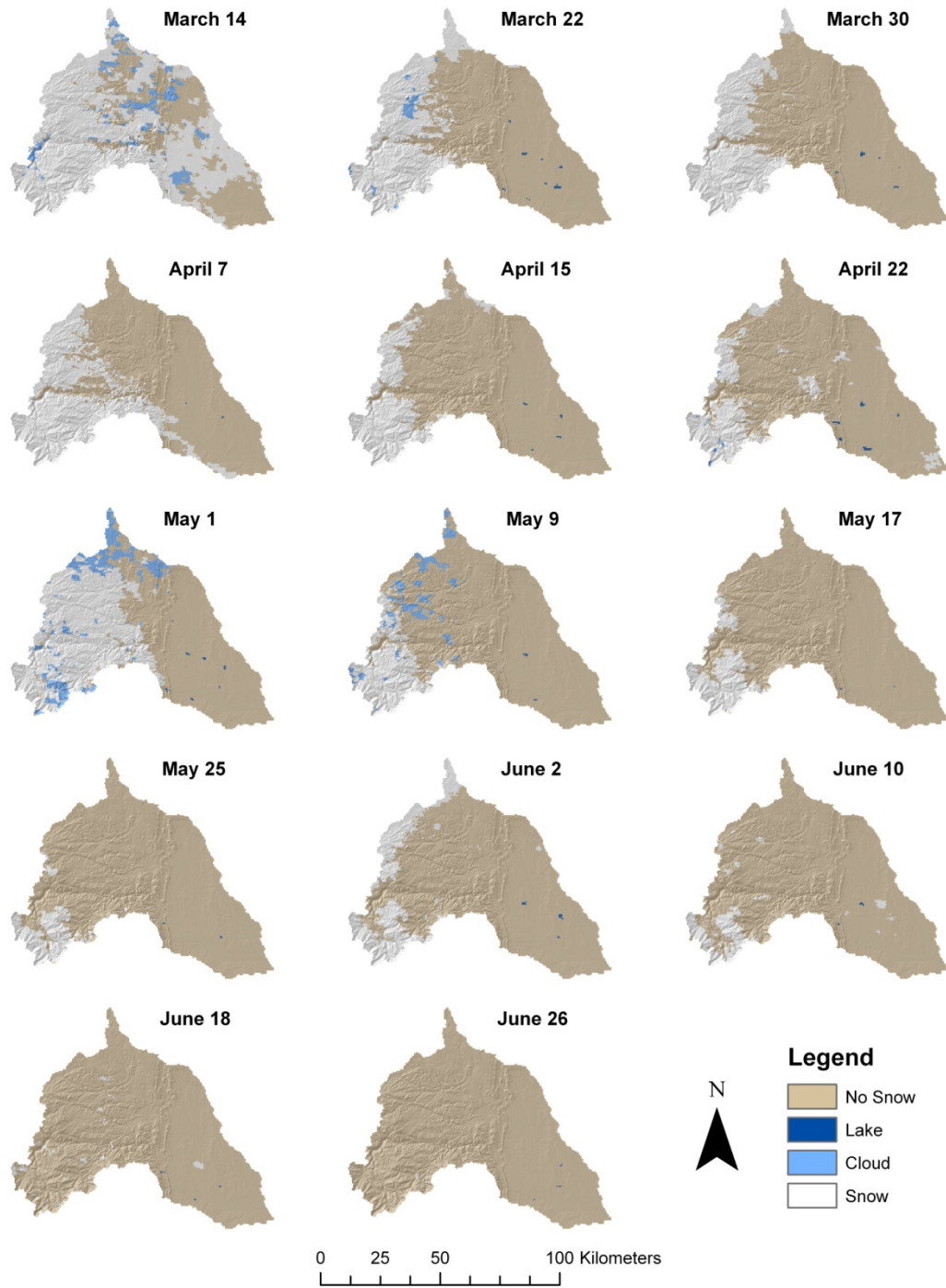


Figure C.6. MODIS 8-day SCA images used in analyses for the 2005 snowmelt season in the Cache la Poudre basin.

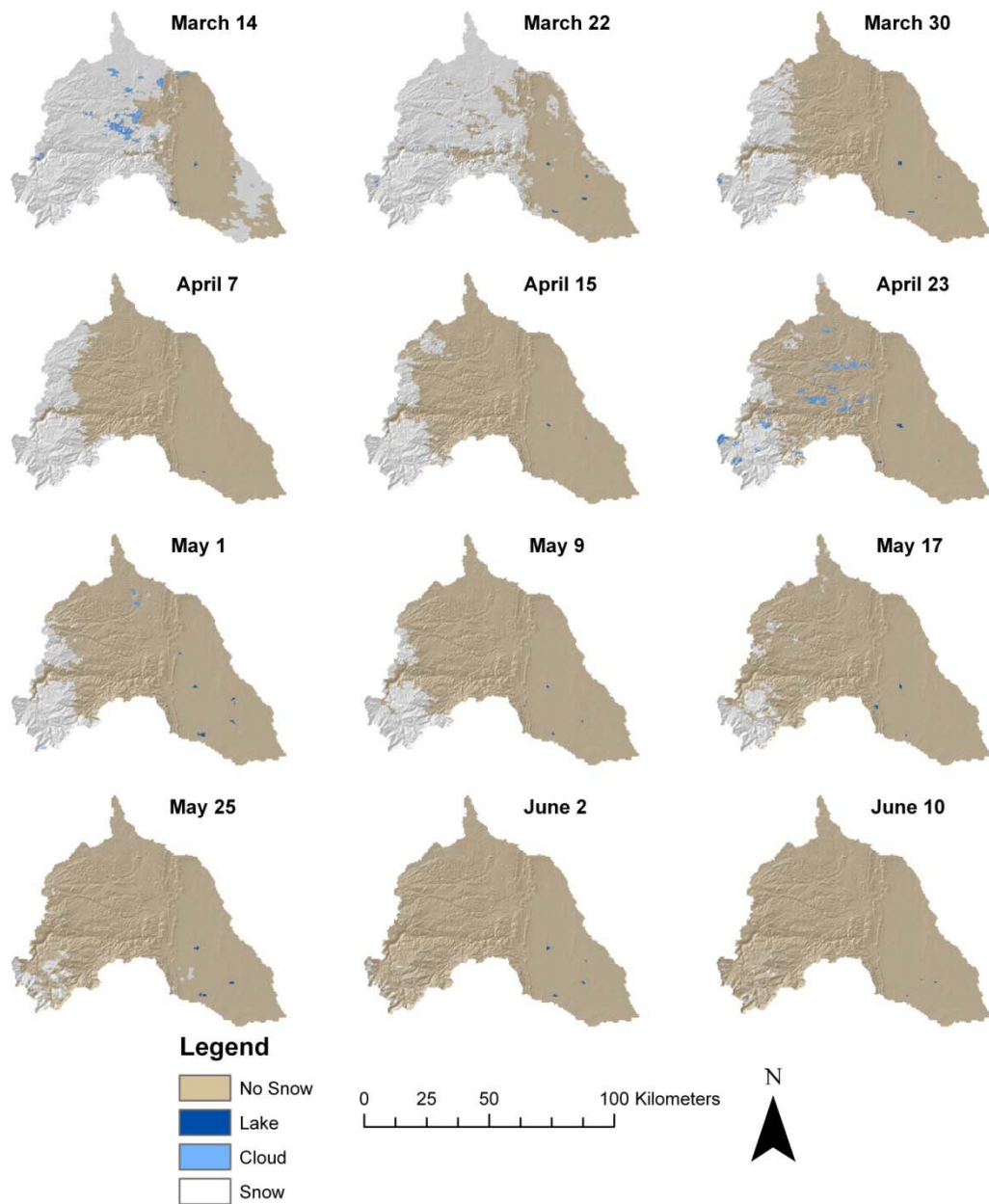


Figure C.7. MODIS 8-day SCA images used in analyses for the 2006 snowmelt season in the Cache la Poudre basin.

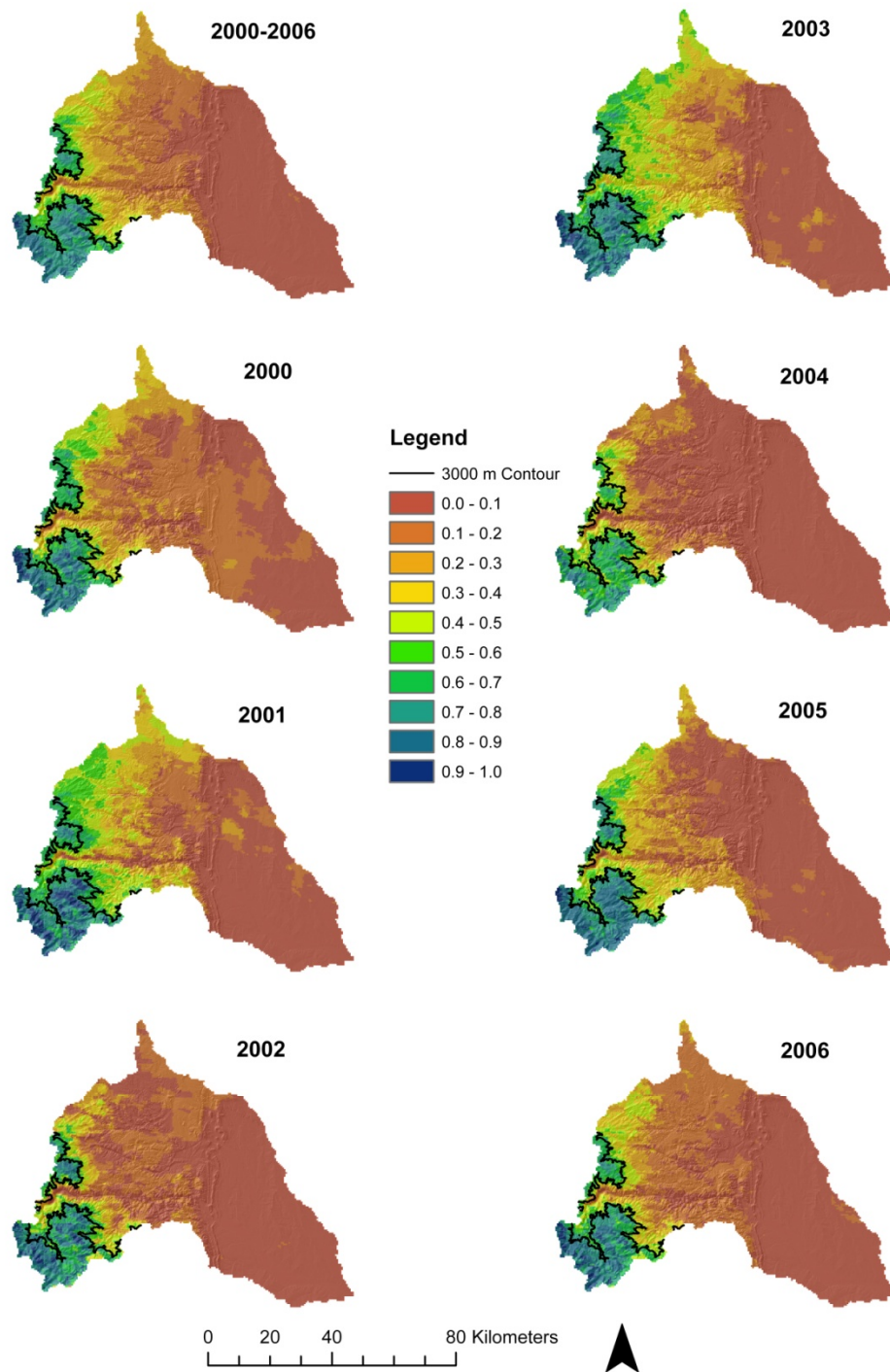


Figure C.8. Probability of snow during the snowmelt season within the Cache la Poudre basin for the entire dataset of 90 images (2000-2006) and each year.

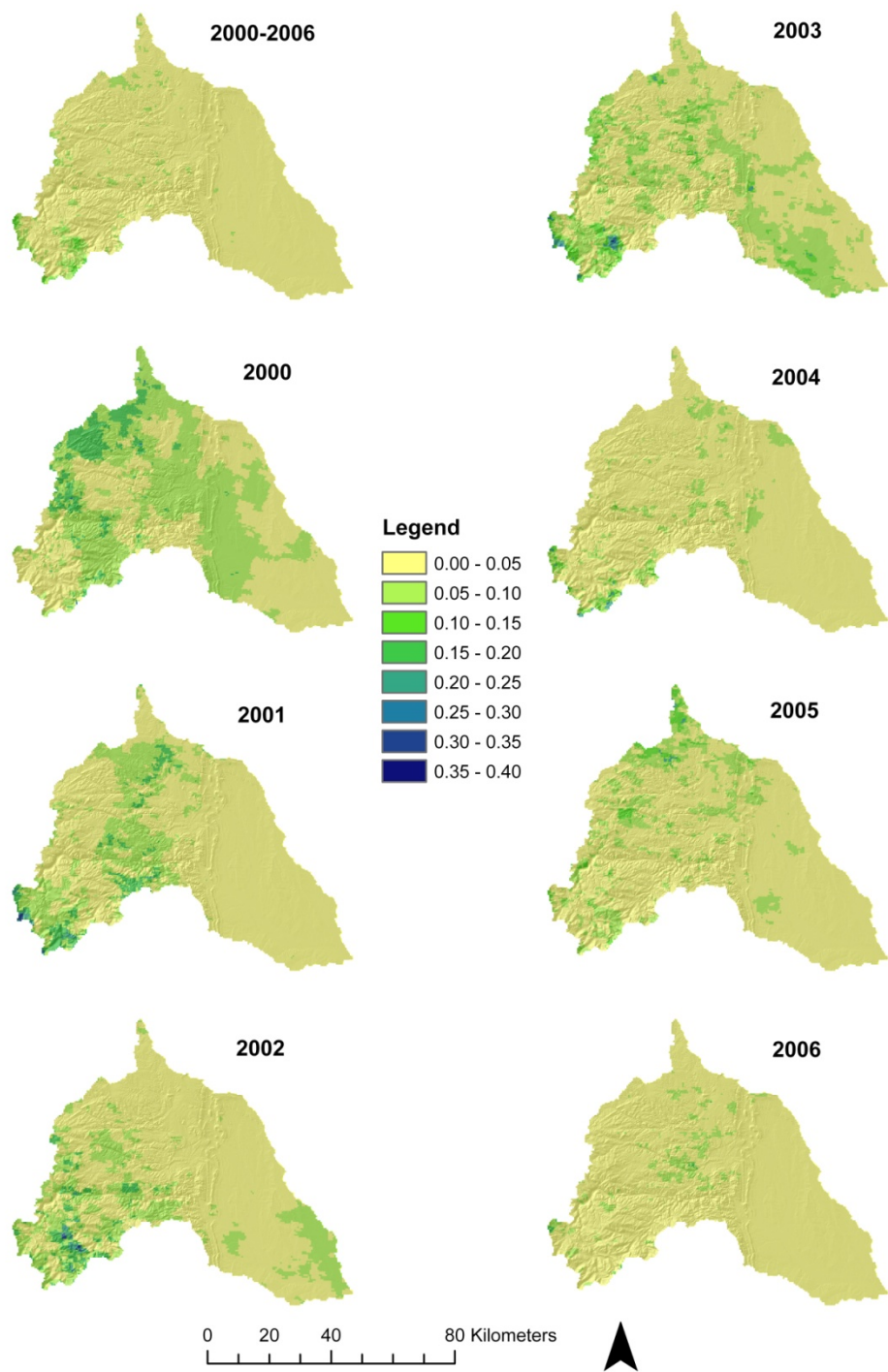


Figure C.9. Probability of cloud during the snowmelt season within the Cache la Poudre basin for the entire dataset of 90 images (2000-2006) and each year.

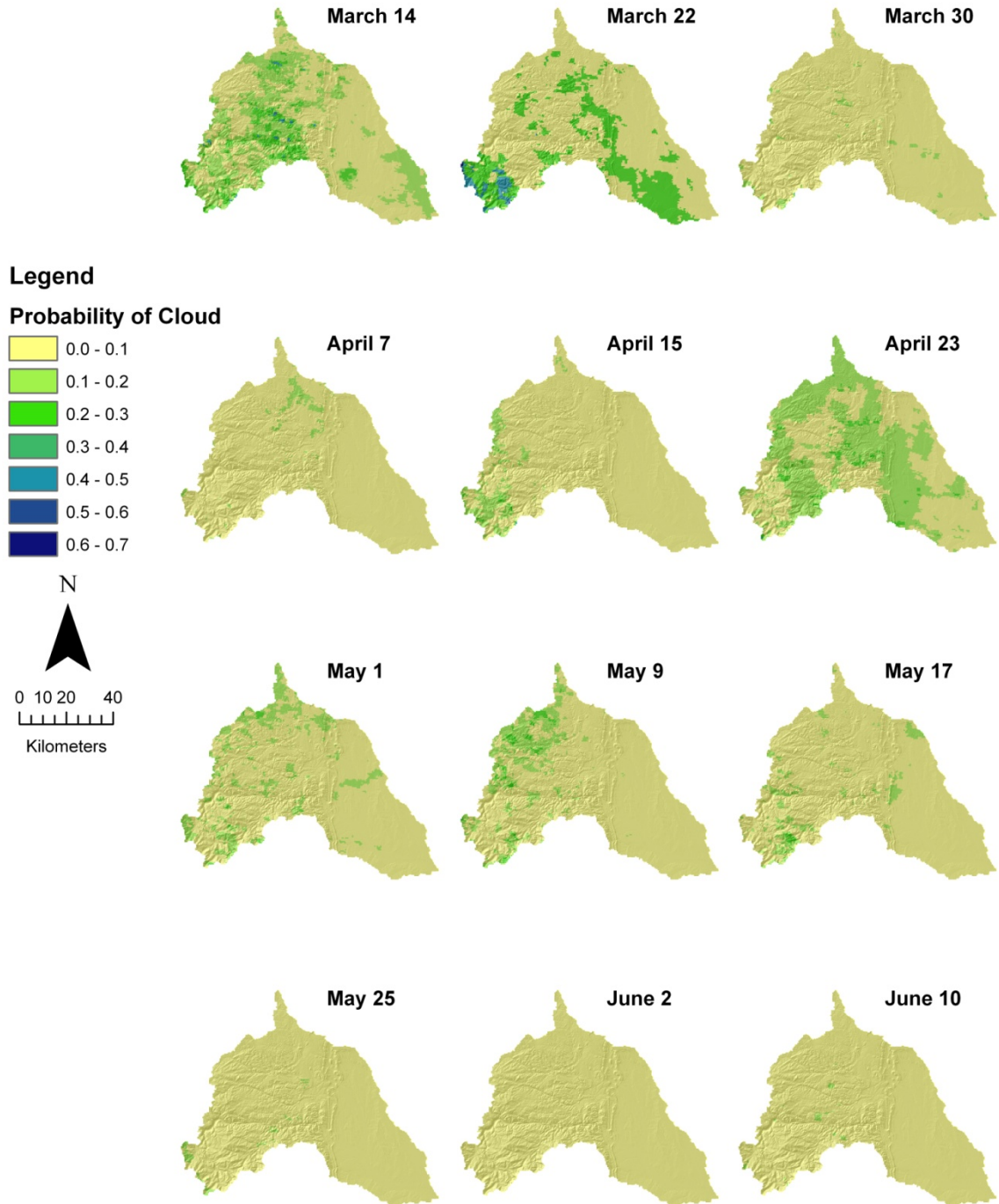


Figure C.10. Probability of cloud time series derived from MODIS 8-day images showing likelihood of cloud impairment for the Cache la Poudre basin during the snowmelt season. For each date, probabilities are calculated using images from 2000-2006.

APPENDIX D: SNOWMELT RUNOFF MODEL

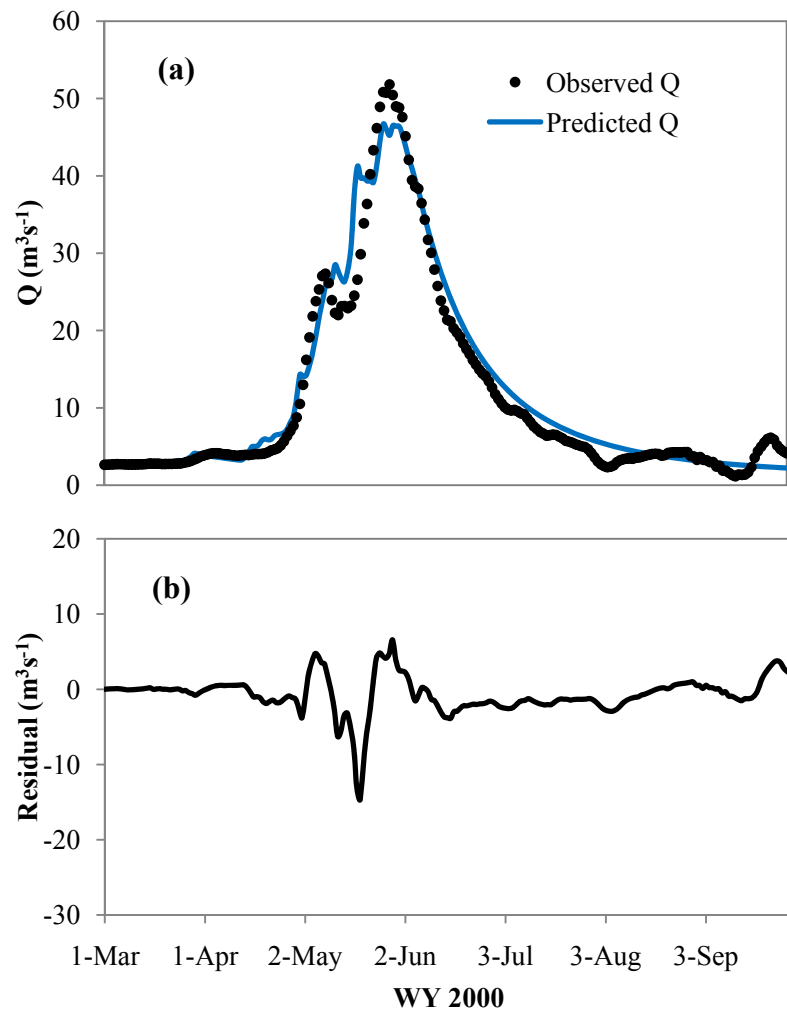


Figure D.1. Results from initial SRM trial (a) comparing observed and predicted hydrographs and (b) daily residuals for the 2000 snowmelt season.

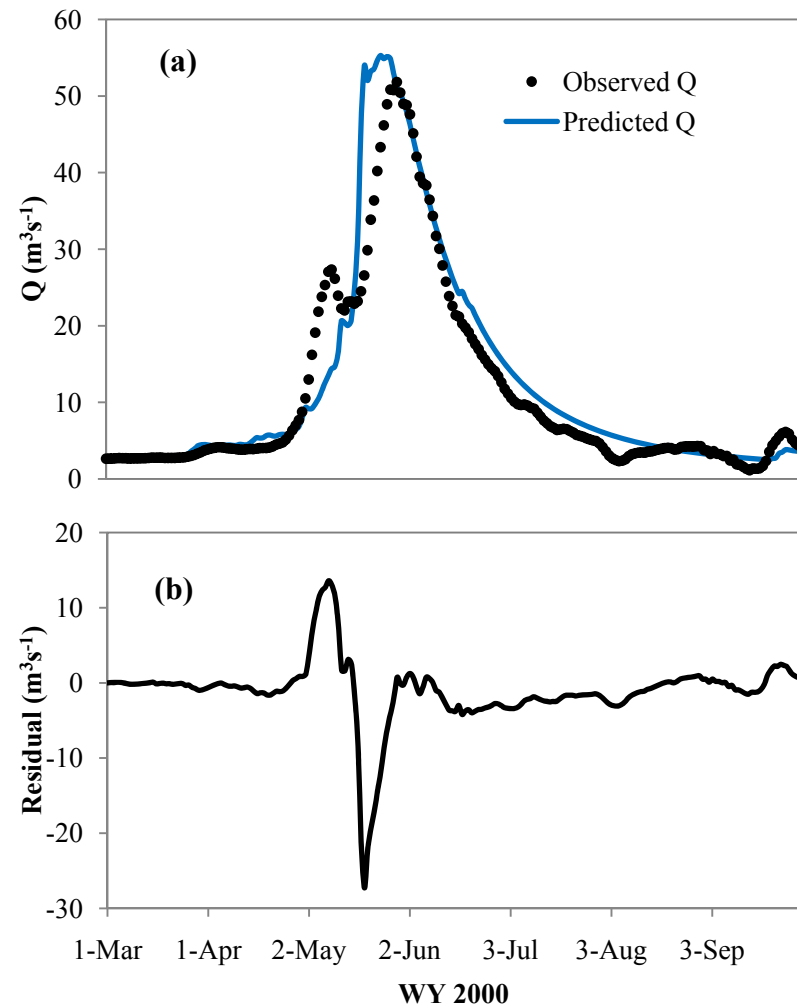


Figure D.2. Results from second SRM trial (a) comparing observed and predicted hydrographs and (b) daily residuals for the 2000 snowmelt season.

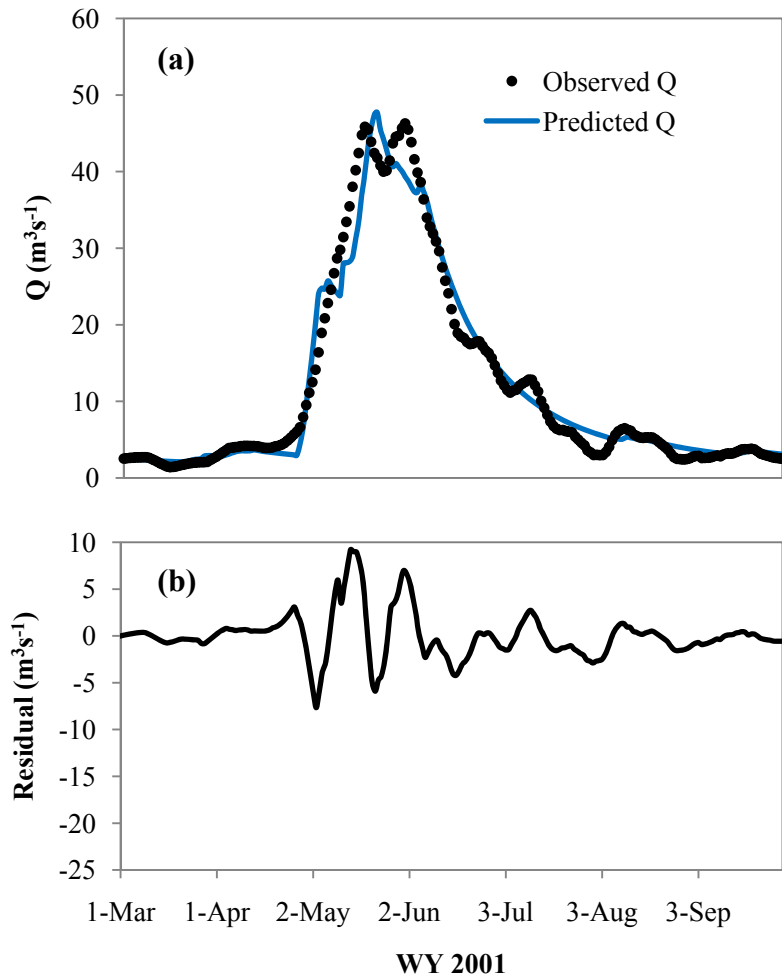


Figure D.3. Results from initial SRM trial (a) comparing observed and predicted hydrographs and (b) daily residuals for the 2001 snowmelt season.

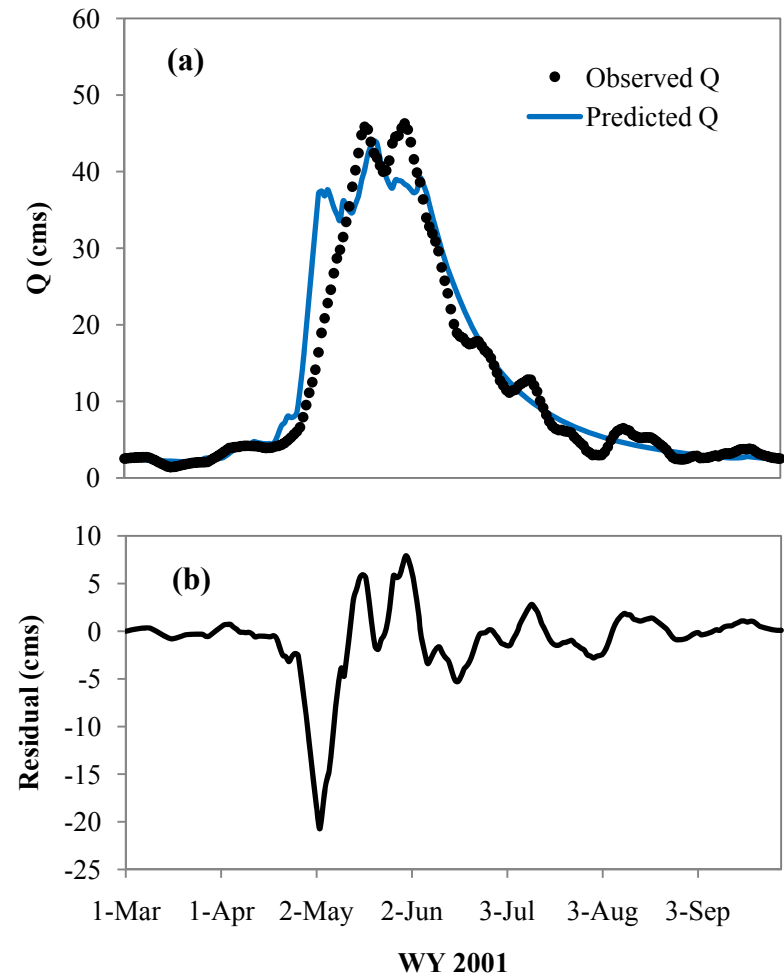


Figure D.4. Results from second SRM trial (a) comparing observed and predicted hydrographs and (b) daily residuals for the 2001 snowmelt season.

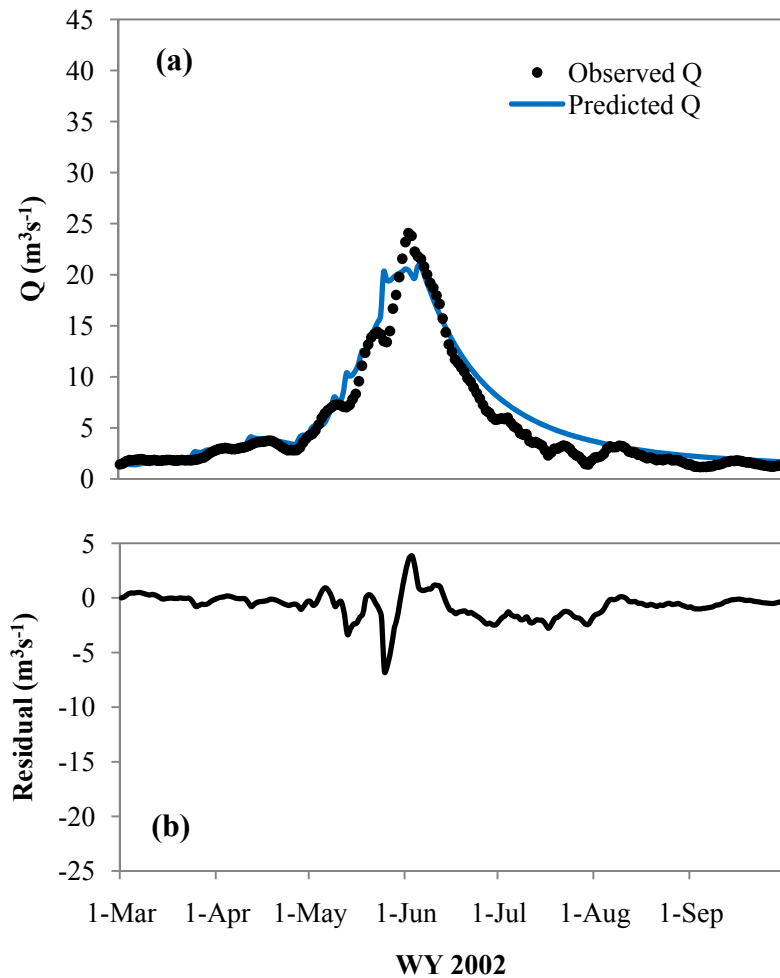


Figure D.5. Results from initial SRM trial (a) comparing observed and predicted hydrographs and (b) daily residuals for the 2002 snowmelt season.

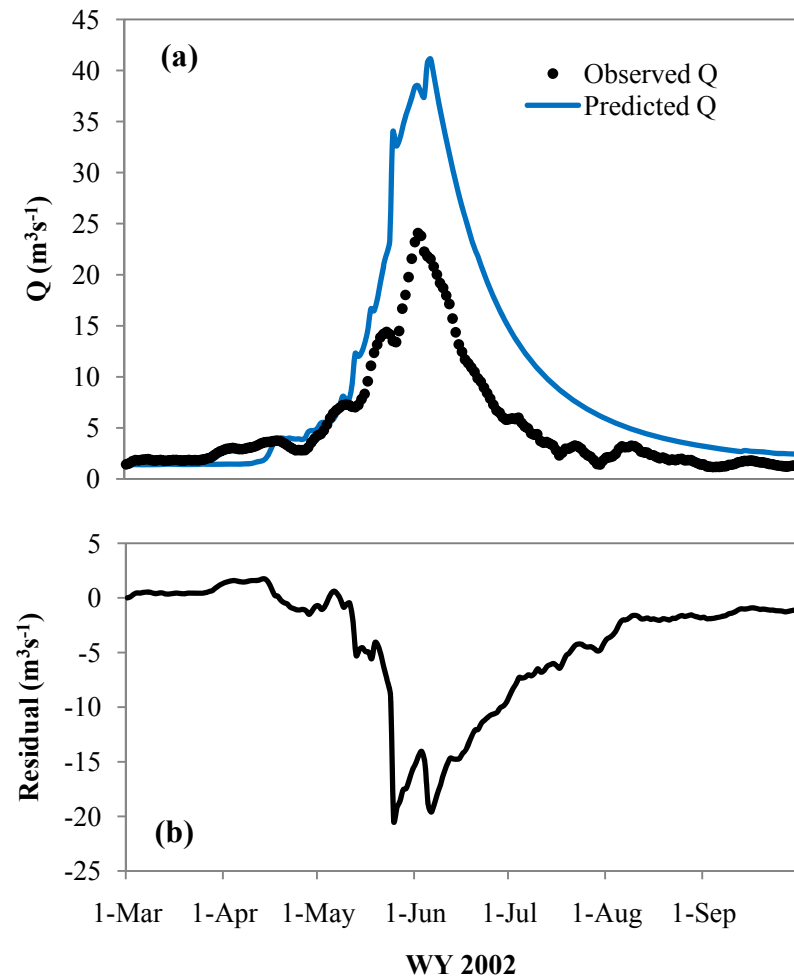


Figure D.6. Results from second SRM trial (a) comparing observed and predicted hydrographs and (b) daily residuals for the 2002 snowmelt season.

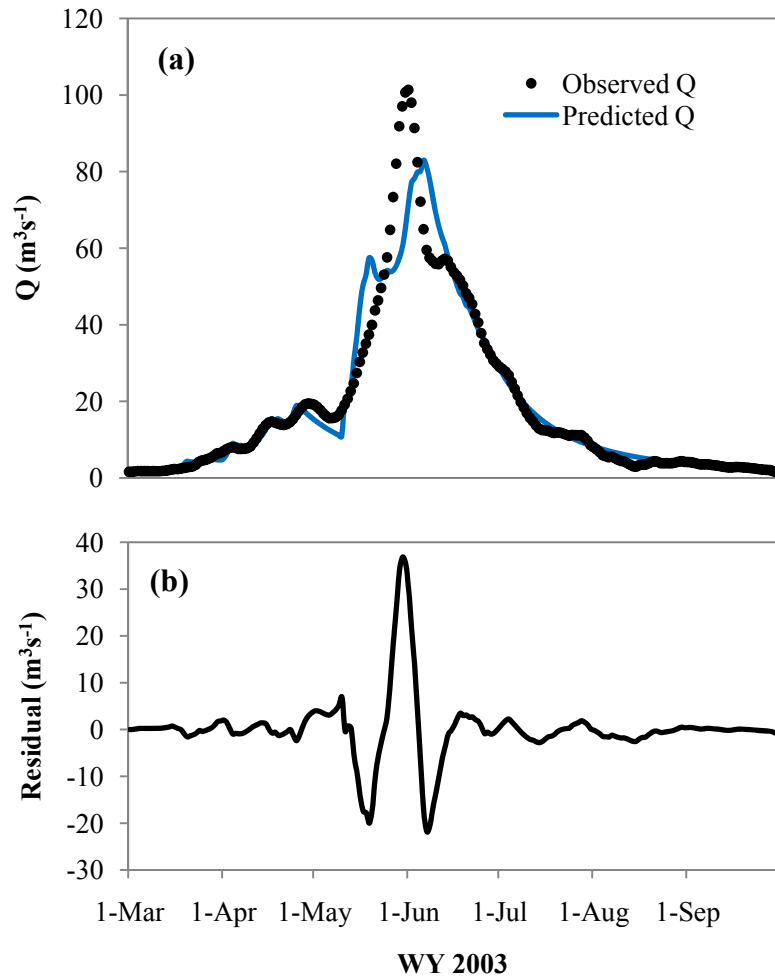


Figure D.7. Results from initial SRM trial (a) comparing observed and predicted hydrographs and (b) daily residuals for the 2003 snowmelt season.

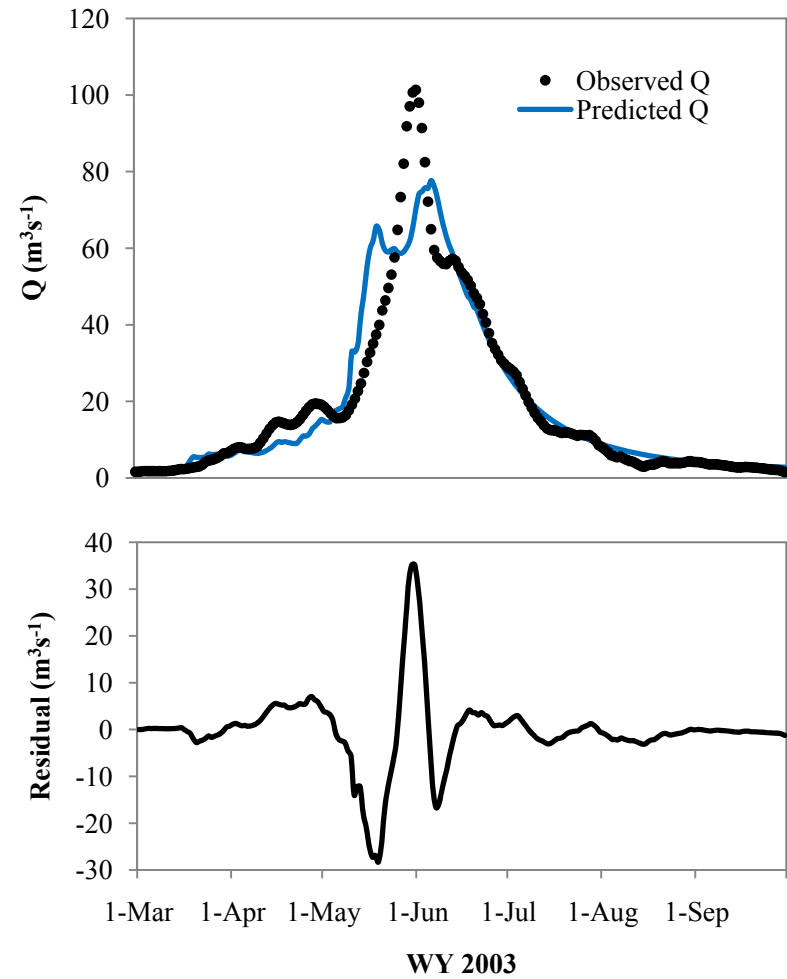


Figure D.8. Results from second SRM trial (a) comparing observed and predicted hydrographs and (b) daily residuals for the 2003 snowmelt season.

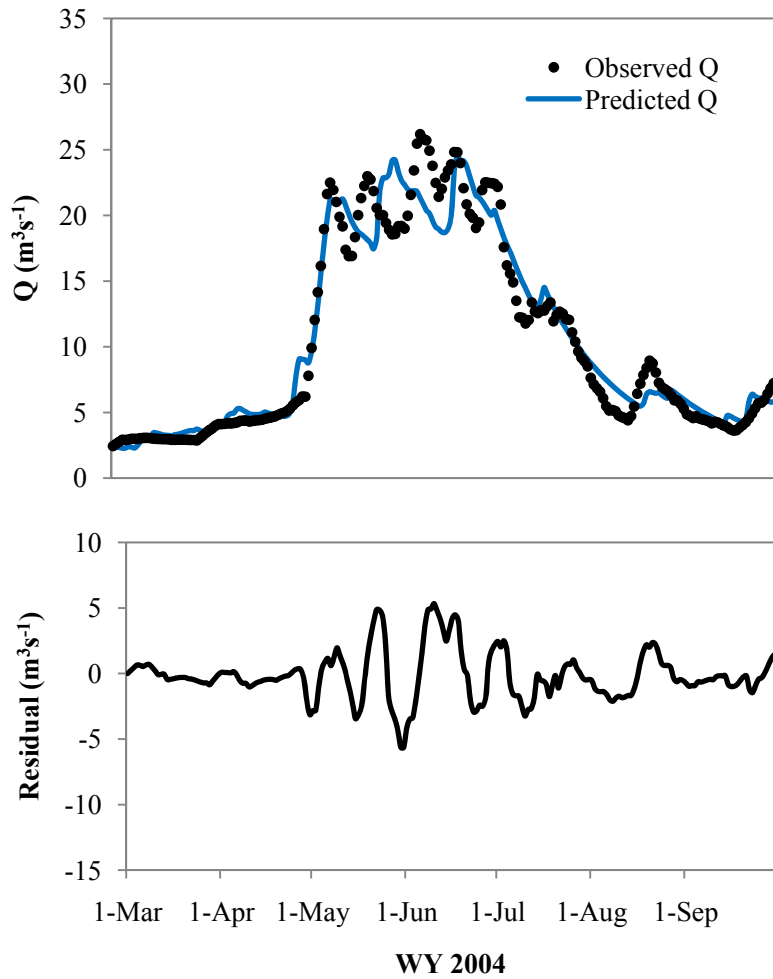


Figure D.9. Results from initial SRM trial (a) comparing observed and predicted hydrographs and (b) daily residuals for the 2004 snowmelt season.

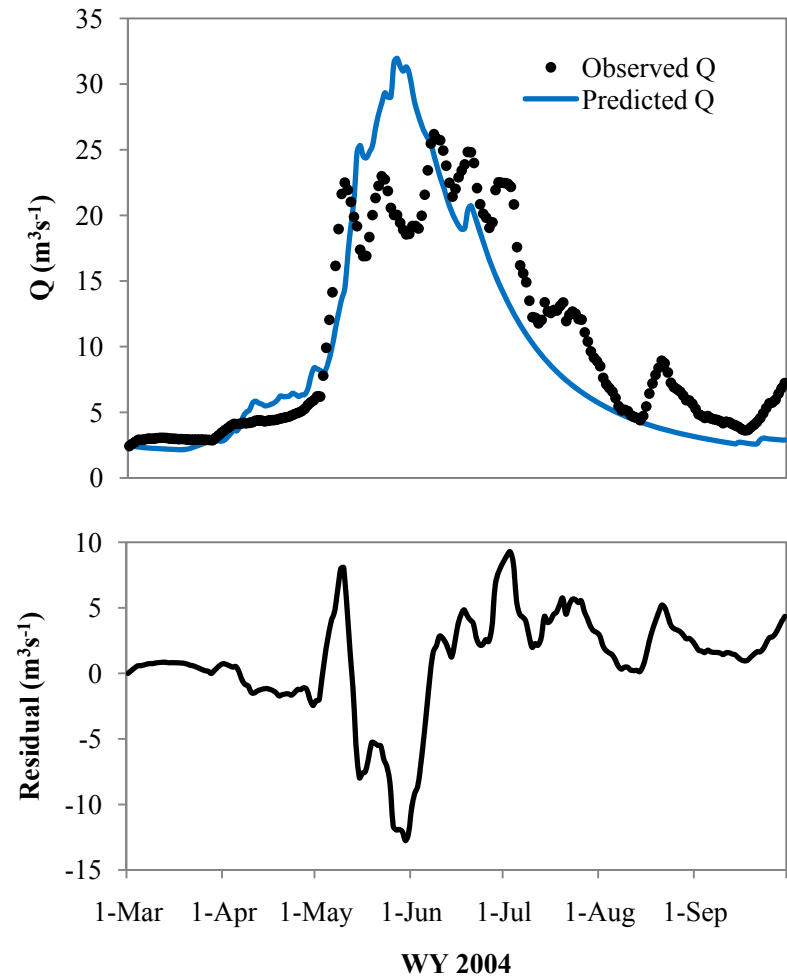


Figure D.10. Results from second SRM trial (a) comparing observed and predicted hydrographs and (b) daily residuals for the 2004 snowmelt season.

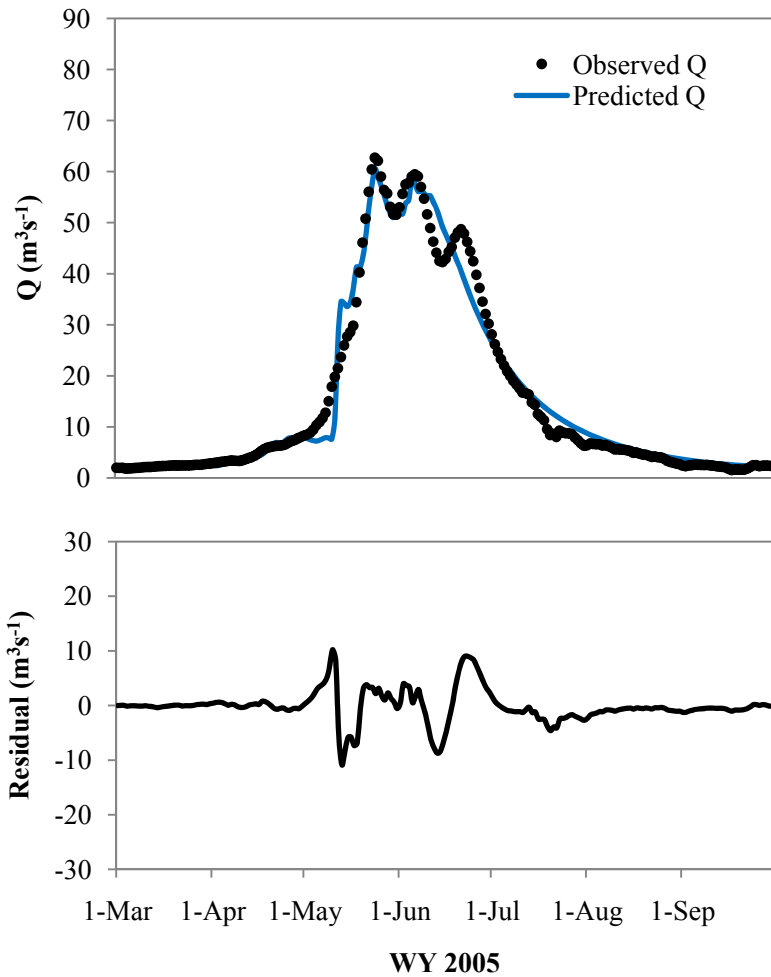


Figure D.11. Results from initial SRM trial (a) comparing observed and predicted hydrographs and (b) daily residuals for the 2005 snowmelt season.

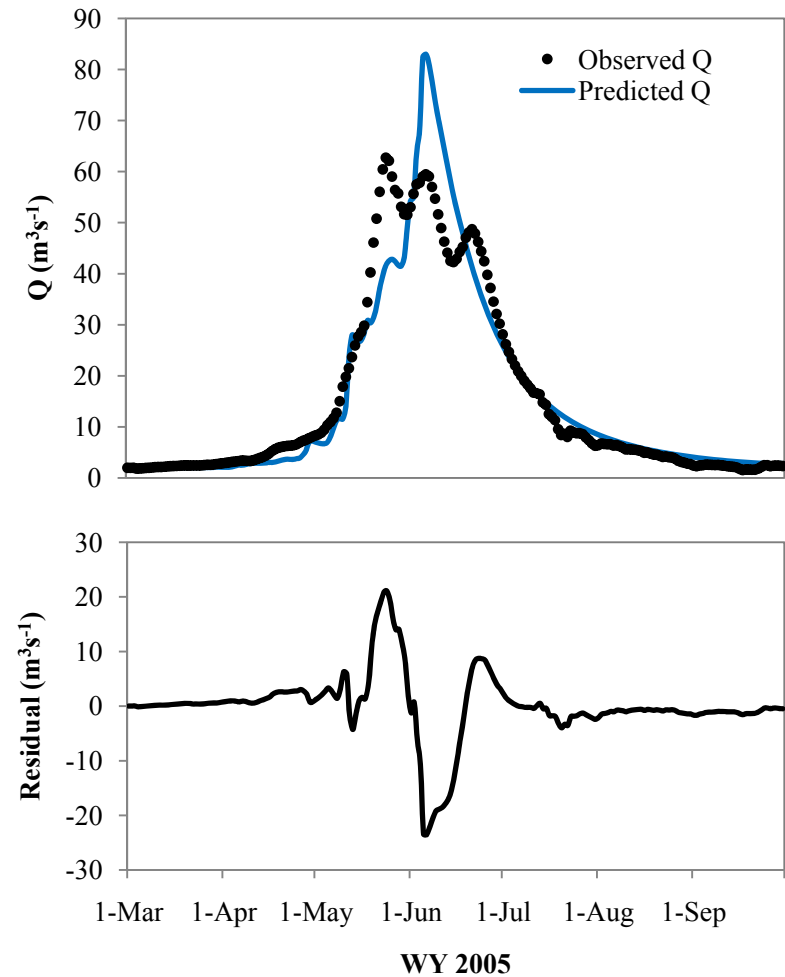


Figure D.12. Results from second SRM trial (a) comparing observed and predicted hydrographs and (b) daily residuals for the 2005 snowmelt season.

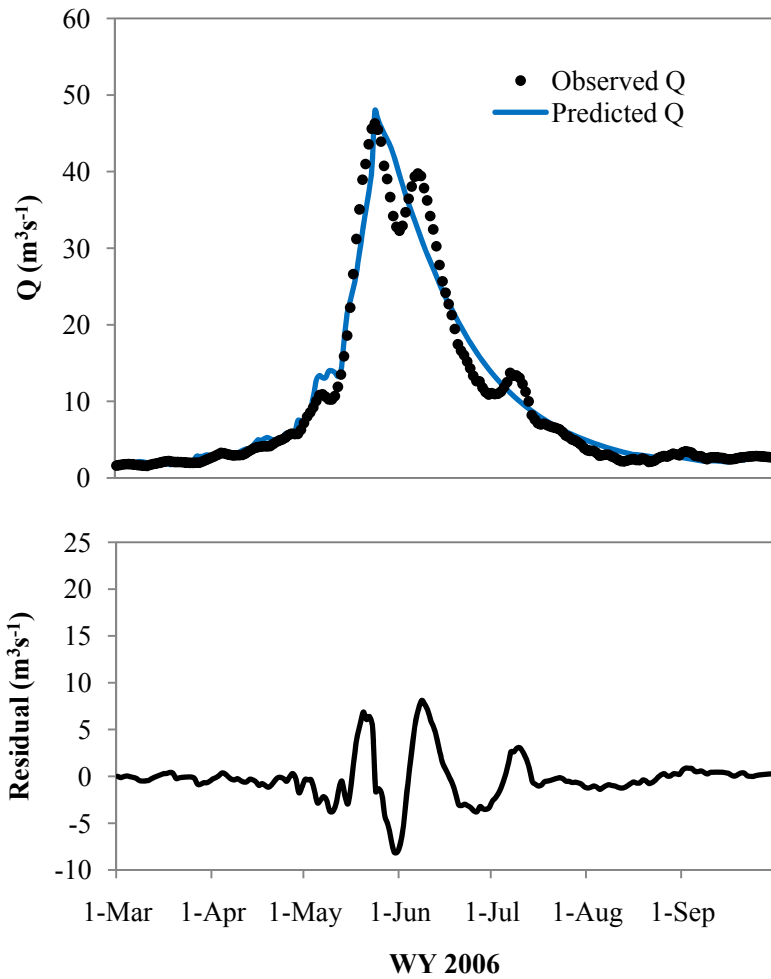


Figure D.13. Results from initial SRM trial (a) comparing observed and predicted hydrographs and (b) daily residuals for the 2006 snowmelt season.

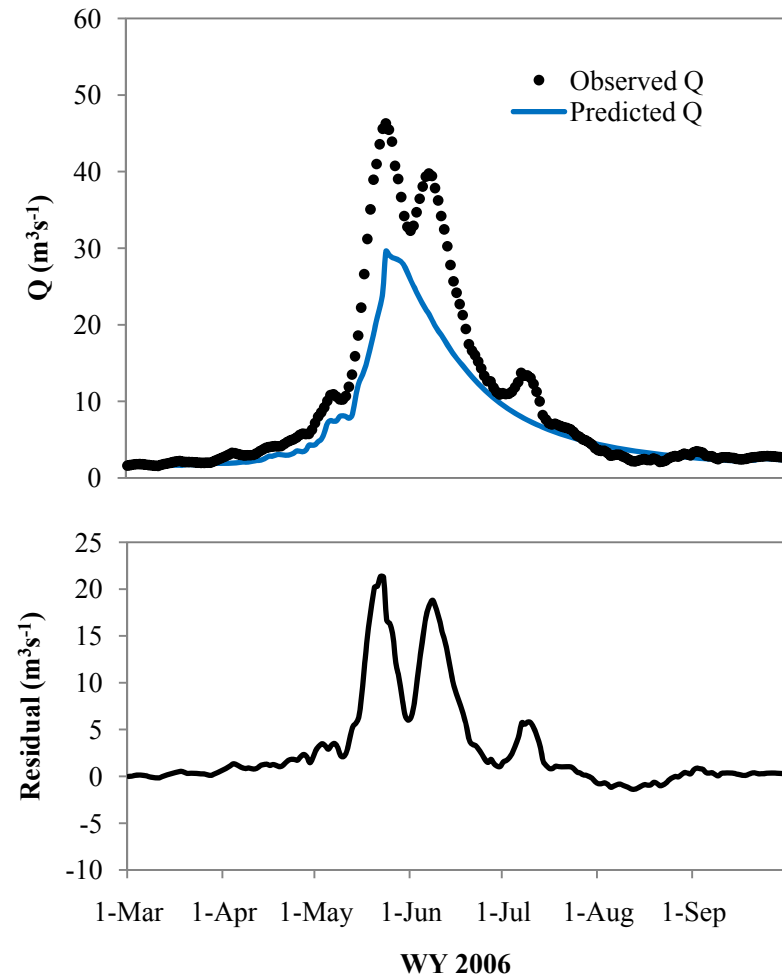


Figure D.14. Results from second SRM trial (a) comparing observed and predicted hydrographs and (b) daily residuals for the 2006 snowmelt season.